8-BS

AN EXPERIMENTAL AND THEORETICAL ANALYSIS OF DIVERTER SYSTEM PERFORMANCE

A Dissertation

Submitted to the Graduate Faculty of the
Louisiana State University and
Agricultural and Mechanical College
in partial fulfillment of the
requirements for the degree of
Doctor of Philosophy

in

The Department of Petroleum Engineering

by
Frederick E. Beck
B.S., Louisiana State University, 1981
M.S., Louisiana State University, 1984
December 1986

TABLE OF CONTENTS

LIST OF TABLES

ABSTRACT

Diverter systems, used as an alternate means of well control while drilling surface hole, have a demonstrated history of failure. Of particular interest in this dissertation are failures related to excessive backpressure, such as mechanical failure of surface equipment or the loss of the rig due to foundation collapse. Critical flow effects, neglected by current design practices, are shown both experimentally and theoretically to have a significant effect on backpressure. Critical flow is modeled by quantifying exit pressures and by including fluid acceleration pressure losses in backpressure calculations.

"Systems analysis" of diverter operations is developed and applied to a field example, proving its effectiveness as a design method. In addition to incorporating critical flow effects, this analysis also considers wellbore and reservoir performance. Computer programs and calculation methods developed to perform the systems analysis are discussed. Design procedures culminate in a method by which diverter vent line diameter, conductor depth, and drilling depth are related to identify a safe interval over which to operate the diverter system.

CHAPTER I

INTRODUCTION

1.1. Introduction

Conventional well control methods require surface casing to be set to sufficient depth to protect shallow formations with low fracture resistance from the high pressures associated with shutting in the well and pumping out a kick. However, in many young sedimentary basins, such as offshore Gulf of Mexico, there is a substantial risk of encountering shallow gas-bearing zones before surface casing is set (Baird (1976), Lukkien (1982)). If a gas kick were taken in one of these zones, conventional well control methods would fracture unprotected shallow sediments, allowing high pressure fluids to broach to the surface around the conductor casing or through the sediments.

In areas where shallow gas is likely to be encountered, a diverter system provides an alternate means of well control while the surface hole is being drilled. The diverter system permits the well to be flowed, rather than shut-in, by safely routing flowing formation fluids away from the rig and rig personnel. Successful diverter operations should provide enough time to safely evacuate personnel from the rig. In addition, the diverter system should allow the flowing formation to subside by depletion or by sediments collapsing into and plugging the wellbore ("bridging over"), permitting normal drilling operations to be resumed. The magnitude of economic, environmental, and personnel losses is strongly dependent upon the success or failure of the diverter operations. It is therefore

imperative that the diverter system be designed, maintained and operated to insure successful diverter operations.

1.2. Definition of a Diverter System

A diverter system consists of four components. These are the annular preventer, the diverter (or vent) line, valves (along with their control mechanisms), and the conductor casing (Figure 1.1).

The purpose of the annular preventer is to stop the upward flow of fluids in the wellbore annulus and to divert the flow into the diverter vent line. Annular type blowout preventers are used for this function.

The diverter vent line is a large diameter steel pipe connected to the well below the annular preventer to carry fluids away from the rig. The line is normally sloped downward away from the well to prevent plugging. Historically, diameters have ranged in size from 4 in. to 16 in., and current regulations set 6 in. as a minimum diameter. Two lines are generally installed and oriented so that the flow can be directed downwind by opening or closing the valves in the line. The lengths of the lines are determined by the dimensions of the rig.

Valves are located on the diverter line to close the system during normal drilling operations. The minimum diameter of the valves should be no less than the diameter of the vent line to prevent the valve from acting as a choke. Valves are usually remote controlled, and must open before the annular preventer is closed.

The conductor pipe stabilizes the wellbore in the soft and unconsolidated shallow sediments. The diameter of the conductor pipe

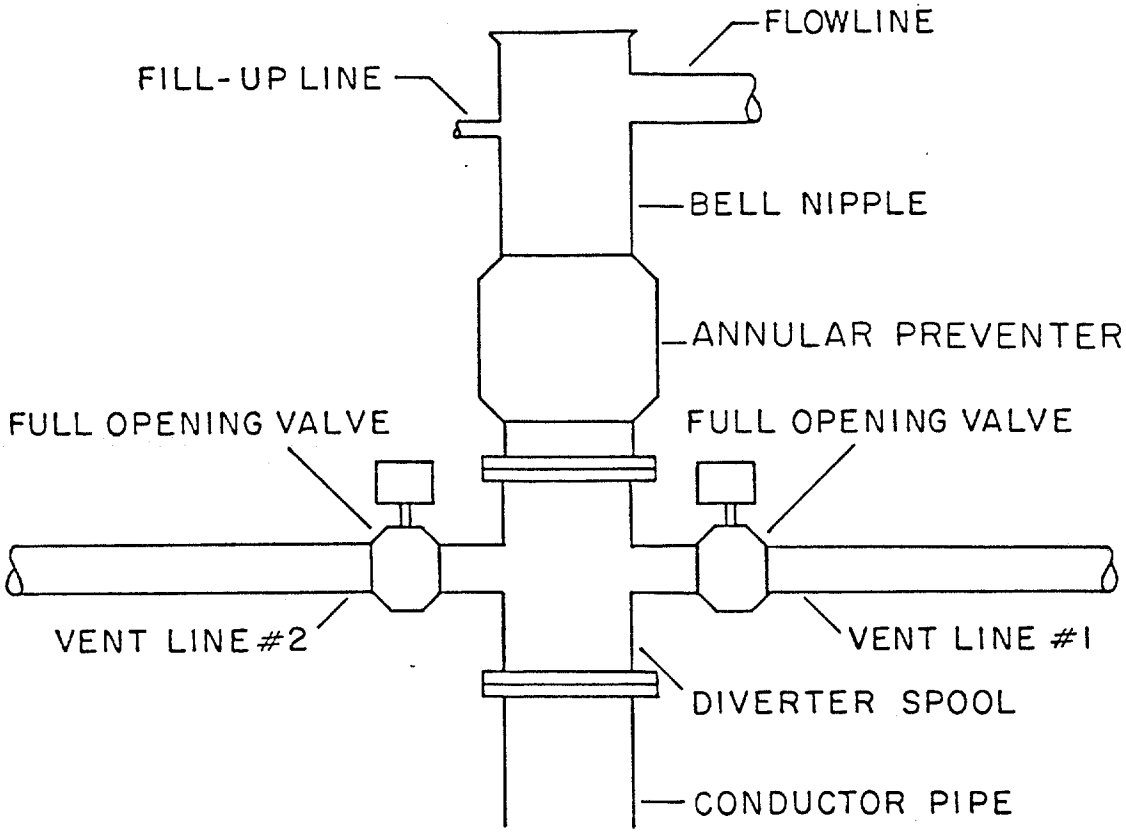

Figure 1.1 Components of a Diverter System

is based on the requirements of the well. The depth to which the conductor is set is somewhat arbitrary, and is often determined by regulatory agencies. Schuh (1979) suggested that the conductor be set down to the 10 ppg fracture depth to insure mud returns. The size of the annular preventer used in the diverter system is governed by the conductor pipe diameter.

1.3. History of Diverter Usage

The Minerals Management Service (MMS) began requiring diverter systems to be installed on drilling rigs operating in Federal waters in 1975, and events of diverter usage can be traced to 1965 (personal comm., MMS, 1985). Diverter systems are also used in state offshore waters and onshore inland waters, marshes, and lang rigs. Through 1983, 27 diverter usage events have been documented by the MMS in the Gulf of Mexico, of which two-thirds were considered unsuccessful. This extremely high failure rate indicates a need to review the various methods by which diverters have failed in order to pinpoint areas in need of further study.

1.4. Methods of Failure

1.4.1. Valves

One common mode of diverter system failure is the malfunction of the valve system. If the valve system fails to open before the annular preventer closes, all of the previously mentioned problems associated with conventional well control are encountered. If the diverter system is designed for low surface operating pressures (i.e. below 500 psia), the system can fail to

contain the well. Valve system failures are most often, if not always, associated with poor maintenance or improper operation.

1.4.2. Erosion

Formation fluids flowing at very high rates and carrying large amounts of sand can quickly erode elbows and valves located in the diverter system. In several instances erosion has been the primary cause of diverter system failure, and warrants serious investigation. Studies have been conducted on the erosion resistance of various elbows (Rohleder, 1985), and at least one additional study is being conducted at this time. Current practice is to construct the vent lines as straight as possible to minimize erosion.

1.4.3. Mechanical Failure

Quite often diverter system failure is caused by the loss of mechanical integrity of the diverter system. Documented cases include leakage of the annular preventer and failure of connections. These failures can be caused by poor quality control during construction or by high backpressure on the system. Proper design and maintenance procedures should eliminate failures caused by high backpressure.

1.4.4. Formation Failure

The most common diverter system failure is the broaching of formations by the high pressures associated with the blowout. The rig foundation is threatened by this mode of failure.

Formation failure is caused by excessive backpressure being placed on the well by the diverter system. Proper design methods should also eliminate this problem.

1.5. Scope of Study

Formation failure and mechanical failure of the diverter system comprise approximately 40 percent of the diverter system failures documented in the Gulf Coast. Both modes of failure are attributed to excessive or high backpressure being placed on the well by the diverter system. It therefore appears that a design method based on an accurate estimation of backpressure would eliminate a large percentage of the failures that have occurred in diverter systems. This study was concerned with developing a design procedure for eliminating diverter system failures caused by excessive backpressure. The study of valve system failure or failures caused by erosion is beyond the scope of this investigation.

1.6. Current Design Methods

Oil or drilling company well control manuals often suggest methods of estimating backpressure to use in sizing the diverter vent line. These methods assume sub-critical flow (atmospheric pressure at the diverter exit) in the diverter line and neglect fluid acceleration effects. Both of these assumptions may lead to significant error in the estimation of the backpressure placed on the well by the diverter. Since high-rate, compressible flow is the result of diverter operations, acceleration effects should be investigated. Critical flow resulting from high flow rates may contribute to the backpressure

on the system. Critical flow occurs when the velocity of the flowing fluid reaches the sonic velocity of that fluid. If critical flow occurs in a diverter line, the point of critical velocity will be the diverter exit and pressure at the diverter exit can exceed atmospheric pressure (Smith and van Ness, p. 461). The magnitude to which critical flow increases exit pressures must be investigated.

1.7. Objectives

The type and frequency of failures seen during diverter operations are an indication of serious flaws in the procedures used to design the diverter system. The correct estimation of the backpressure placed on the well and diverter system during diverter operations is a key factor in many of the cases studied. This dissertation explores the developement of experimentally based procedures to be used in calculating the backpressure placed on a well by a diverter system, with emphasis on methods of predicting critical flow and fluid acceleration effects. A method, employing these procedures, is developed to predict the operating pressures expected during diverter operations in both the diverter system and the well, thus providing design criteria for the diverter system. Finally, an analysis of an actual diverter system failure is performed to demonstrate the applicability of the methods presented.

CHAPTER II

EXPERIMENTAL APPARATUS, PROCEDURES, AND RESULTS

2.1. Objectives

The objective of the experiments performed during this study was to provide an experimental basis for determining whether or not critical flow effects need to be considered when making diverter backpressure calculations. The experiments were designed to provide both qualitative and quantitative information on the critical flow phenomena occurring in a diverter line. It was hypothesized that flow would become critical at the diverter exit, thus forcing the pressure at the exit to increase above atmospheric pressure. Experiments were designed to test this hypothesis qualitatively, and provide quantitative data on the critical velocity of natural gas and gas/water mixtures, as critical velocities govern the magnitude of the increase in the exit pressure. The critical velocity data for the gas/water mixtures is of particular interest. Two-phase critical flow is not a well understood problem, and the experimental work was used to test theories of the critical velocity behavior of two-phase flow. Finally, the experiments provided a basis for calibrating the computational techniques used to model pressure losses during critical flow.

The experimental objectives were partially met by measuring pressure traverses of critical flow in model diverter lines. Critical velocities can be extracted from the data and pressure loss calculations checked against the measured profiles. Pressure was

measured at the diverter exit, thus testing the general theory of flow behavior in diverter lines.

2.2. Experimental Apparatus

An experimental apparatus was designed to simulate flow in a diverter line. Two model diverters were built from 42 ft. sections of 1-in. (0.918 in. inner diameter) and 2-in. (1.937 in. inner diameter) steel line pipe. The small diameter lines were used because of restraints on pressure and flow rate. The models were fully instrumented to record flowing pressures, temperatures, and flow rates. The apparatus allowed flow tests to be conducted for dry gas flow and for the flow of gas/water mixtures. Figure 2.1 is a schematic of the experimental apparatus. Gas was supplied at high pressure and high flow rate at the inlet, with the outlet open to the atmosphere. High pressure gas storage tanks provided methane to the 2-in. line. Natural gas (0.69 gravity, air = 1.0 @ 14.7 psia and 60°F) was supplied to the 1-in. line by a commercial gas pipeline. Water was delivered from mud tanks through Halliburton mud pumps.

2.2.1. Instrumentation

a) Pressure

Sperry-Sun pressure transducers accurate to 1 psi were mounted on the model to measure flowing pressures at the inlet and outlet and up to 4 other locations along the length of the model. The transducers were dead-weight tested to insure accuracy and to provide absolute pressure measurements.

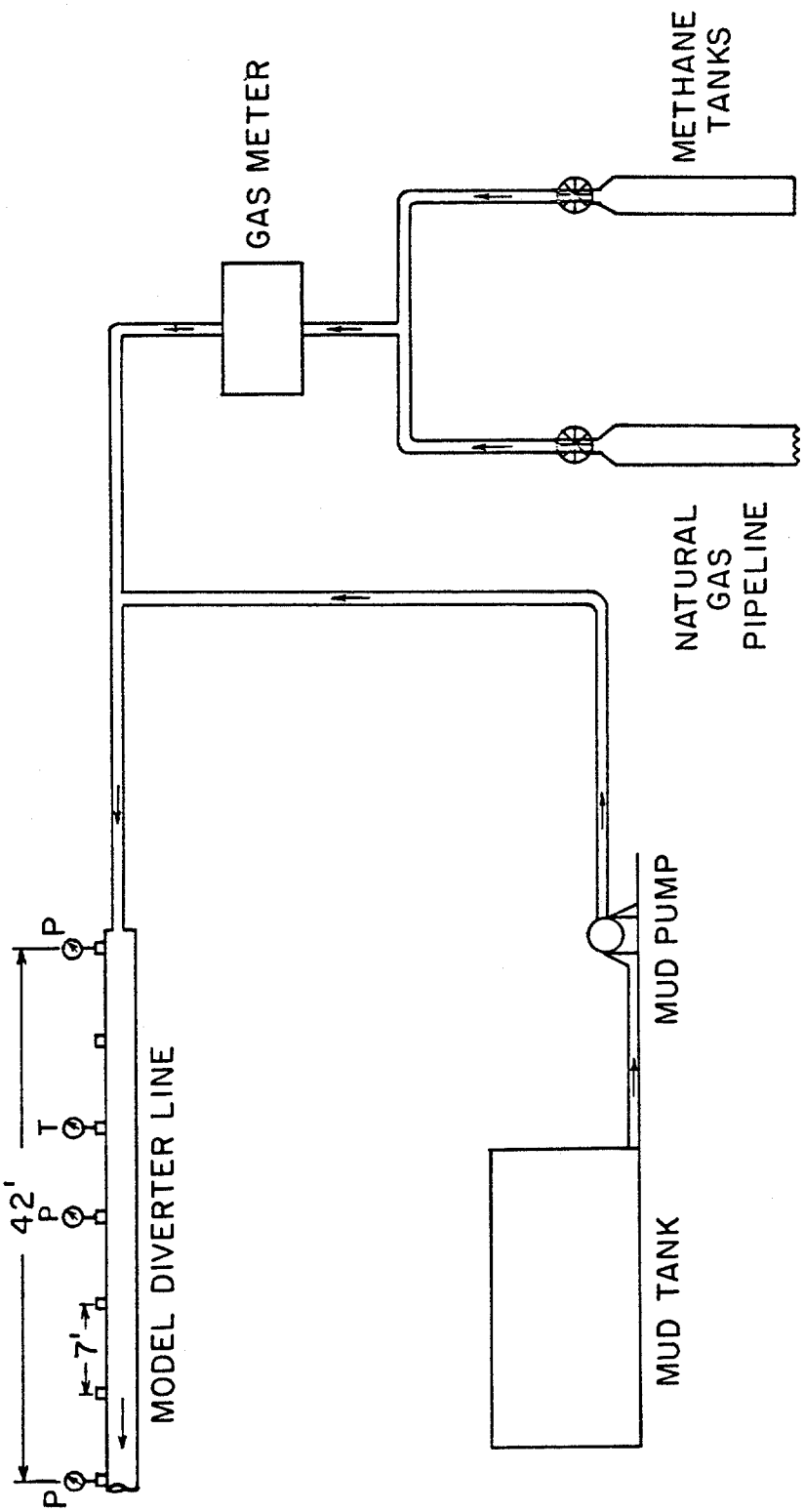

Figure 2.1 Schematic of the Experimental Apparatus.

b) Temperature

Rosemount temperature gauges were also mounted on the models to measure flowing temperature. The response times of the temperature gauges were measured and found to be adequate to provide accurate flowing temperatures. The locations of the pressure and temperature taps are presented in figures 2.2 and 2.3 for the 2-in. and 1-in. models, respectively.

c) Gas metering

Gas rates were measured by a standard orifice meter accurate to approximately 5 percent of total flow rate. A Daniel flow calculator was used to meter gas rates.

d) Water metering

Water rates were measured directly by use of a metering tank. The volume pumped at steady-state conditions over the time interval of a specific run provided the water flow rate for that run.

e) Recording devices

Flow rates and flowing temperatures were continuously recorded on a 4-20 ma chart recorder. Pressures were recorded on a Sperry-Sun MR-Six recorder, which has a built-in clock. Corresponding rates, pressures, and temperatures were correlated by time.

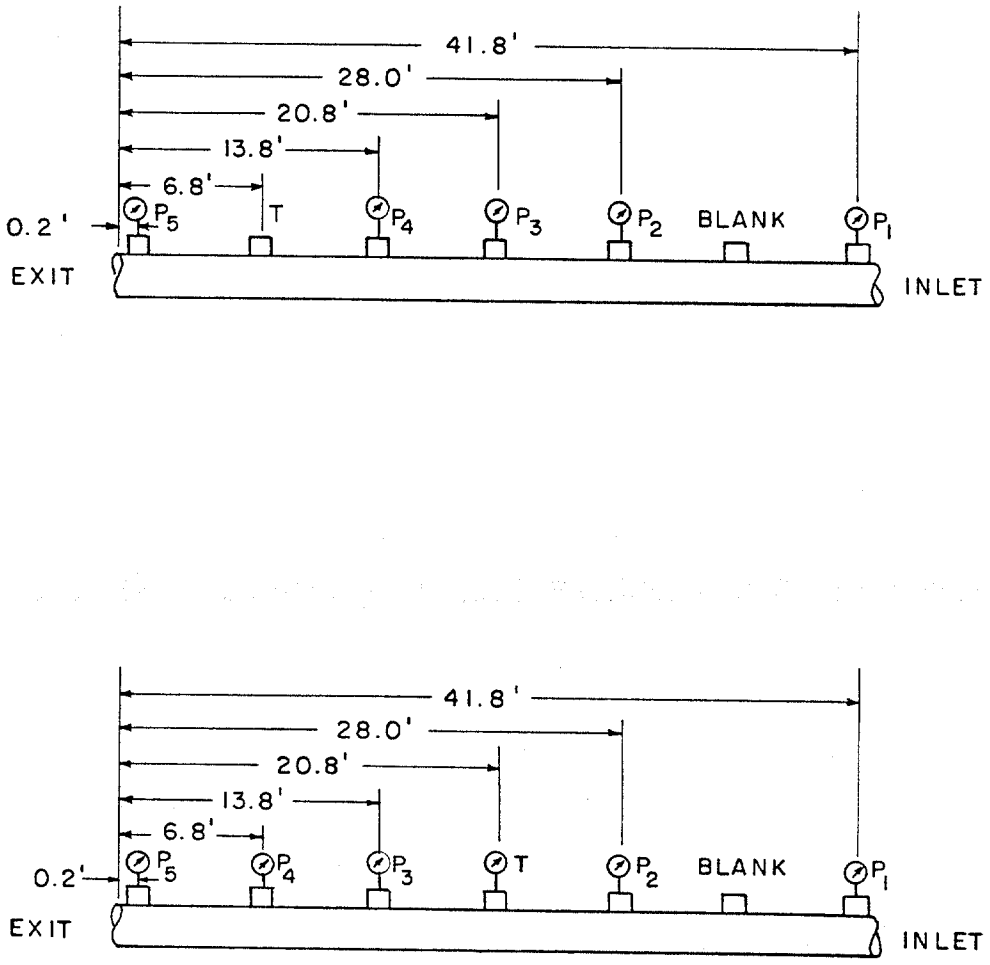

Figure 2.2 Schematic of the 2 in. Model Diverter Showing Temperature and Pressure Sensor Locations

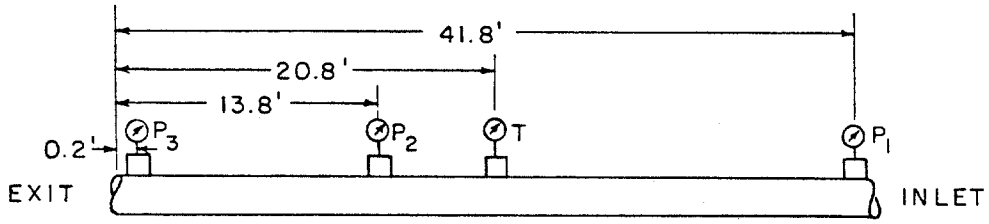

Figure 2.3. Schematic of the 1 in. Model Diverter Showing Temperature and Pressure Sensor Locations

2.3. Experimental Procedure

Experiments were conducted in both the 1-in. and 2-in. models for dry gas and gas-water mixtures. Flowing pressures were measured and recorded in the model diverter as the gas or gas-water mixture accelerated to critical velocity. By allowing the gas to expand to atmospheric pressure, an equilibrium flow rate is established during each test such that critical velocity is reached in the model at the outlet. Since pressure is being measured at the exit (outlet), critical velocities can be obtained from the measured flow rates. Critical flow was insured by increasing rates until pressure at the diverter exit exceeded atmospheric pressure. Traverses were recorded for steady-state flow only. Flow was deemed steady when the traverse remained constant with time for a constant flow rate. Gas flow rates were manually controlled by valves in the flow line and water rates by adjusting pump speed. Traverses were recorded over as wide a range of gas flow rates, water flow rates, and flowing pressures as allowed by the pressure restraints of the gas and/or water source.

Water only flow tests were run to estimate the roughness of the line pipe used in the models. Water was pumped through the model at high flow rates and the pressure traverse in the line recorded. By assuming incompressible flow, the pipe roughness, ε, can be extracted from the frictional pressure losses measured in the traverses.

2.4. Experimental Results

The experiments resulted in the collection of data for 35 dry gas traverses and 56 gas-water traverses. Flow rates ranged up to 21 MMSCFD gas and 4000 BBL/MMSCF water. Data is presented in Tables 2.1

TABLE 2.1

DRY GAS DATA FOR 1-IN. MODEL DIVERTER LINE (I.D. 0.918 IN.)

Run #	DISTANCE (FT) FROM EXIT	PRESSURE (PSIA)			GAS FLOW RATE (MMCFPD)
		0.2	13.8	41.8	
1		24	53	82	0.72
2		44	104	157	1.44
3		21	53	77	0.72
4		39	93	138	1.34
5		54	128	193	1.87
6		69	161	241	2.35
7		56	133	200	1.92
8		97	221	340	3.02
9		115	258	395	3.70
10		139	311	474	4.61
11		15	46	69	0.48
12		50	130	202	1.73
13		72	158	247	2.38
14		45	98	149	1.42
15		189	397	598	6.37
16		135	343	538	4.79
17		167	359	536	5.65
18		89	195	304	2.92

TABLE 2.2

DRY GAS DATA FOR 2-IN. MODEL DIVERTER LINE (I.D. 1.937 IN.)

Run #	DISTANCE (FT) FROM EXIT	PRESSURE (PSIA)						GAS FLOW RATE (MMCFPD)
		0.2	6.8	13.8	20.8	28.0	41.8	
1		128	220	272	---	335	379	20.9
2		97	---	215	243	268	301	17.28
3		96	172	215	---	265	297	16.2
4		67	---	149	168	183	203	11.04
5		44	76	96	---	118	130	7.63
6		28	---	65	75	83	91	4.92
7		27	---	59	66	73	79	4.56
8		26	48	57	---	72	79	4.51
9		24	---	51	---	60	68	4.03
10		22	39	49	---	58	68	3.72
11		22	---	44	---	53	60	3.6
12		18	---	40	---	47	53	3.19
13		17	---	35	---	42	47	2.88
14		16	---	35	---	42	46	2.86
15		15	22	29	---	34	37	2.06
16		15	---	22	---	25	28	1.44
17		15	16	17	---	18	19	0.08

and 2.2 for the dry gas flow tests and Tables 2.3 and 2.4 for the gas-water flow tests.

Exit pressures above atmospheric indicate critical flow in almost all of the runs. Flow was intentionally kept subcritical in several runs to provide data useful in calibrating the calculation procedures applied in Chapter III.

The data collected during the water flow tests is presented in Table 2.5.

2.5. Conclusions

Friction factors were calculated from the water flow tests and from the dry gas flow tests. From the friction factors, pipe roughness was calculated to be 0.0003 in. in the 1-in. line and 0.0006 in. in the 2-in. line. These values are well within the expected values for the line pipe used, therefore validating the apparatus and procedures used. The methods used to calculate friction factors and pipe roughness are presented in Appendix A.

The recorded exit pressures (Tables 2.1-2.4, col. 2) indicate that critical flow can cause a significant increase in the exit pressure of model diverters. Exit pressures well above atmospheric pressure were attained in both the 1-in. and 2-in. models for gas and gas/water flow. Exit pressures are considerably higher in two-phase flow, and approach 200 psia in the 1-in. experiments. These exit pressures would be neglected by the design procedures currently used by the drilling industry. Methods were developed to predict the increase in exit pressure as well as the pressure losses in the model

TABLE 2.3

TWO-PHASE DATA FOR 1-IN. MODEL DIVERTER LINE (I.D. 0.918 IN.)

Run #	DISTANCE (FT) FROM EXIT	PRESSURE (PSIA)			GAS FLOW RATE (MMCFPD)	WATER FLOW RATE (BBL/MMSCF)
		0.198	13.79	41.82		
1		129	279	428	2.95	392.6
2		177	370	590	3.84	325
3		172	472	586	2.98	554
4		134	355	603	1.73	1496
5		119	250	412	2.56	348.8
6		123	302	512	1.73	1134.9
7		85	206	340	1.39	900.4
8		182	396	595	3.95	278.9
9		153	383	619	1.84	1383.8
10		147	378	583	2.27	825.4
11		133	358	605	1.58	1744.6
12		145	359	605	2.30	890
13		173	374	574	3.56	362.7

TABLE 2.4

TWO-PHASE DATA FOR 2-IN. MODEL DIVERTER LINE (I.D. 1.937 IN.)

Run #	DISTANCE (FT) FROM EXIT	PRESSURE (PSIA)					GAS FLOW RATE (MMCFPD)	WATER FLOW (BBL/ MMSCF)
		0.198	6.79	13.79	28.02	41.82		
1		35	62	78	---	124	3.36	689.8
2		44	---	126	174	196	1.92	4457.1
3		21	41	58	72	89	2.64	793.5
4		56	102	131	165	197	4.8	900.7
5		49	83	133	165	201	2.04	4151.3
6		54	91	111	135	160	7.08	138.5
7		58	95	115	143	172	6.79	282.3
8		59	96	118	149	183	6.58	379.3
9		62	103	125	162	197	6.43	512.9
10		132	219	265	328	369	18.96	79.9
11		134	214	259	313	356	17.16	137.7
12		135	214	254	311	357	15.6	228.6
13		132	207	250	307	359	14.4	294
14		70	---	138	170	200	8.64	221.8
15		67	---	134	165	200	7.97	299.2
16		65	---	127	159	191	7.44	320.5
17		67	---	135	173	207	6.89	498.1
18		65	---	142	186	220	5.9	732.8
19		89	---	173	212	242	11.64	103.4
20		76	---	156	195	221	10.8	92.9
21		74	---	149	185	206	10.1	99.5
22		62	---	131	164	185	9.5	46.9
23		59	---	124	156	178	9.07	49.1
24		92	155	191	234	262	13.44	71.3
25		59	99	120	146	169	7.8	137.1
26		51	87	108	134	151	7.61	58.6
27		60	98	118	145	170	7.68	191.5

TABLE 2.4 (CONTINUED)

Run #	DISTANCE (FT) FROM EXIT	PRESSURE (PSIA)					GAS FLOW RATE (MMCFPD)	WATER FLOW (BBL/ MMSCF)
		0.198	6.79	13.79	28.02	41.82		
28		60	97	118	145	174	7.08	255
29		48	83	100	124	140	6.98	73.4
30		69	122	147	192	228	6.24	685.7
31		84	152	189	239	289	6.24	1028.6
32		96	175	214	271	323	6.00	1366.8
33		38	62	76	102	126	3.96	467.1
34		46	88	110	143	172	3.72	1114.3
35		54	105	139	178	215	3.55	1858.2
36		64	127	159	206	247	3.36	2520.4
37		28	---	60	73	86	3.72	131.8
38		31	---	65	83	101	3.41	366
39		32	---	68	90	111	3.17	534.3
40		25	---	51	64	77	3.12	178.6
41		26	---	54	70	85	3.00	364
42		23	---	47	59	71	2.88	193.4
43		33	---	76	98	121	2.98	777.8

TABLE 2.5

WATER FLOW TEST DATA FOR 2-IN. MODEL DIVERTER

Run #	DISTANCE (FT) FROM EXIT	PRESSURE (PSIA)				WATER FLOW RATE (GPM)
		.2	13.8	28.0	41.8	
1		15	21	27	32	247
2		15	21	30	36	283
3		15	18	23	26	209

diverter lines. These methods were then used to predict the behavior of full-sized diverter lines.

The experimental traverses can be used as a basis in theoretically modeling critical flow. Chapter III concentrates on developing calculation procedures to be used to model the pressure profile in a diverter line under conditions of critical flow.

CHAPTER III

ANALYSIS OF CRITICAL FLOW IN DIVERTER LINES

3.1 Introduction

As stated in the introductory chapter, methods used to estimate the backpressure placed on a well by a diverter system are based upon the assumptions that flow in the diverter line is subcritical and that fluid acceleration effects can be neglected when making pressure loss calculations. Chapter II presented experimental evidence showing that critical flow definitely occurs in model diverter lines at only moderately high flow rates, subsequently causing a significant increase in the pressure recorded in the models. This chapter will present theory that will predict the magnitude of this increase in pressure, and determine the significance of critical flow in full-sized diverters.

Computational methods are presented that can be used to calculate pressure losses in diverter lines in which flow is critical. The effects of neglecting fluid acceleration losses when making these calculations are demonstrated. The experimental pressure traverses presented in Chapter II are used to show the accuracy of these methods.

The theory presented in this chapter will be applied to make improved backpressure calculations, and an analysis of the design assumptions currently in use will be presented.

3.2 Prediction of Exit Pressures

The velocity of fluid flowing in a pipe is limited by the critical (acoustic, sonic) velocity of the fluid. Once critical velocity is attained, pressure transients, which propagate at sonic velocity, can no longer travel upstream, and downstream pressure decreases can not be sensed. Thus, when a decrease in downstream pressure does not change the flow rate, flow is critical.

In pipe flow open to the atmosphere, the fundamental laws of fluid mechanics, as expressed by the general energy equation, demand that atmospheric pressure be maintained at the pipe exit in subcritical flow, and that an equilibrium flow rate be established in critical flow such that critical velocity is attained only at the exit (Smith and van Ness, p. 461). Minimum critical mass flow rate is one at which critical velocity is attained at the exit, with pressure at the exit atmospheric. Once minimum critical flow rate is reached, an increase in mass flow rate will neccessitate an increase in density and pressure. Increases in mass flow rate will therefore cause pressure to increase above atmospheric at the exit. Pressures above atmospheric at the exit provide a suitable indication of critical flow in pipes of constant cross-sectional area. The one parameter that governs equilibrium rates and pressures of critical flow is the critical velocity of the fluid. By combining equations for flow rate and critical velocity, the increase in pressure at the exit can be quantified.

3.2.1. Dry Gas Critical Velocity

The acoustic velocity of a gas is given as

$$V_g^* = 41.4 \sqrt{\frac{kZT}{\gamma_g}} \tag{3.1}$$

The polytropic expansion coefficient of the gas, k, can be determined by the following equation

$$k = \frac{C_v}{C_p} \tag{3.2}$$

Appendix B presents a method by which k is estimated from gas properties.

Critical velocity is strongly dependent on the temperature of the gas, and indirectly dependent on pressure through the gas compressibility factor, Z. Gas properties have only a slight effect on the critical velocity of a natural gas.

If it is assumed the critical velocity of the fluid is represented by an average velocity, a critical mass flow rate can be determined by combining the definition of flow rate,

$$q_g = V_g A, \tag{3.3}$$

with the real gas equation of state,

$$Pv = znRT, \tag{3.4}$$

and the critical velocity of gas, V_g^*. The resulting equation

$$Q_g^* = \frac{V_g^* D^2 P_e T_{STD}}{2122 z T_e P_{STD}} \tag{3.5}$$

relates critical mass flow rate to pipe diameter, exit pressure, exit temperature, and critical velocity. The mass flow rate is a strong function of the pressure at the diverter exit and of the critical velocity of the gas.

These equations (3.1, 3.5) can be used to calculate critical velocities and flow rates of dry gas for given pipe dimensions, temperatures, and pressures. The experimental data presented in

Chapter II provided information on critical velocities, flow rates, and the pressures and temperatures at which they occur. Using the temperatures and pressures measured at the model diverter exit to calculate expected critical velocities and flow rates, the experimental data can be compared to theoretical estimates of critical velocity and flow rate. Table 3.1 presents the critical velocities and flow rates measured by the experiments against those calculated by the theory presented. Equations 3.1 and 3.5 predict the experimental data with less than 5 percent error. Figure 3.1 shows predicted critical flow rates plotted against measured critical flow rates. The results plot along a 45 degree line, indicating the accuracy of the theory.

Equation 3.5 relates critical flow rate to the pressure at the diverter exit. A given flow rate, if it is critical, will be associated with a unique exit pressure. A functional relationship between flow rate and exit pressure can be established for a given pipe geometry. Figure 3.2 shows an example of this relationship. Thus, if a flow rate expected during diverter operations can be predicted, the corresponding exit pressure can be determined.

3.2.2. Critical Velocities of Gas-Liquid Mixtures

The critical velocity of a gas-liquid mixture is not a well understood phenomenon (Beggs and Brill, Wallis). Two-phase flow in general is very difficult to describe theoretically, so many investigators have resorted to empirical work to describe the phenomena associated with two-phase flow. Various flow regimes, or types of flow, have been defined by many investigators, and

TABLE 3.1

COMPARISON OF MEASURED AND CALCULATED FLOW RATES AND VELOCITIES FOR 1-IN. AND 2-IN. MODEL DIVERTER DATA

GAS FLOW RATE MMSCFPD (MEASURED)	GAS FLOW RATE MMSCFPD (CALCULATED)	EXIT PRESSURE PSIA (MEASURED)	VELOCITY FT/SEC (CALCULATED)	VELOCITY FT/SEC (MEASURED)
0.7	0.8	24	1309	1191
1.4	1.4	44	1309	1295
0.7	0.7	21	1309	1362
1.3	1.3	39	1309	1365
1.9	1.8	54	1307	1364
2.3	2.3	69	1307	1338
1.9	1.9	56	1305	1344
3.0	3.3	97	1305	1213
3.7	3.9	115	1304	1244
4.6	4.7	139	1304	1278
0.5	0.5	15	1309	1272
1.7	1.7	50	1282	1303
2.9	3.0	89	1285	1231
2.4	2.4	72	1292	1261
1.4	1.5	45	1285	1197
6.4	6.5	189	1294	1265
4.8	4.6	135	1292	1339
5.7	5.8	167	1287	1257
4.9	4.8	28	1466	1509
11.0	11.5	67	1466	1404
17.3	16.8	97	1466	1509
4.6	4.6	27	1466	1451
2.1	2.6	15	1466	1182*
3.7	3.8	22	1466	1454
0.1	2.6	15	1466	45*
16.2	16.6	96	1466	1430
4.5	4.4	26	1466	1490
7.6	7.5	44	1466	1485
20.9	22.3	128	1466	1375
1.4	2.6	15	1466	826*
2.9	2.9	17	1466	1458
4.0	4.1	24	1466	1443
3.6	3.7	22	1466	1407
3.2	3.1	18	1466	1525
2.8	2.7	16	1466	1538

* subcritical flow

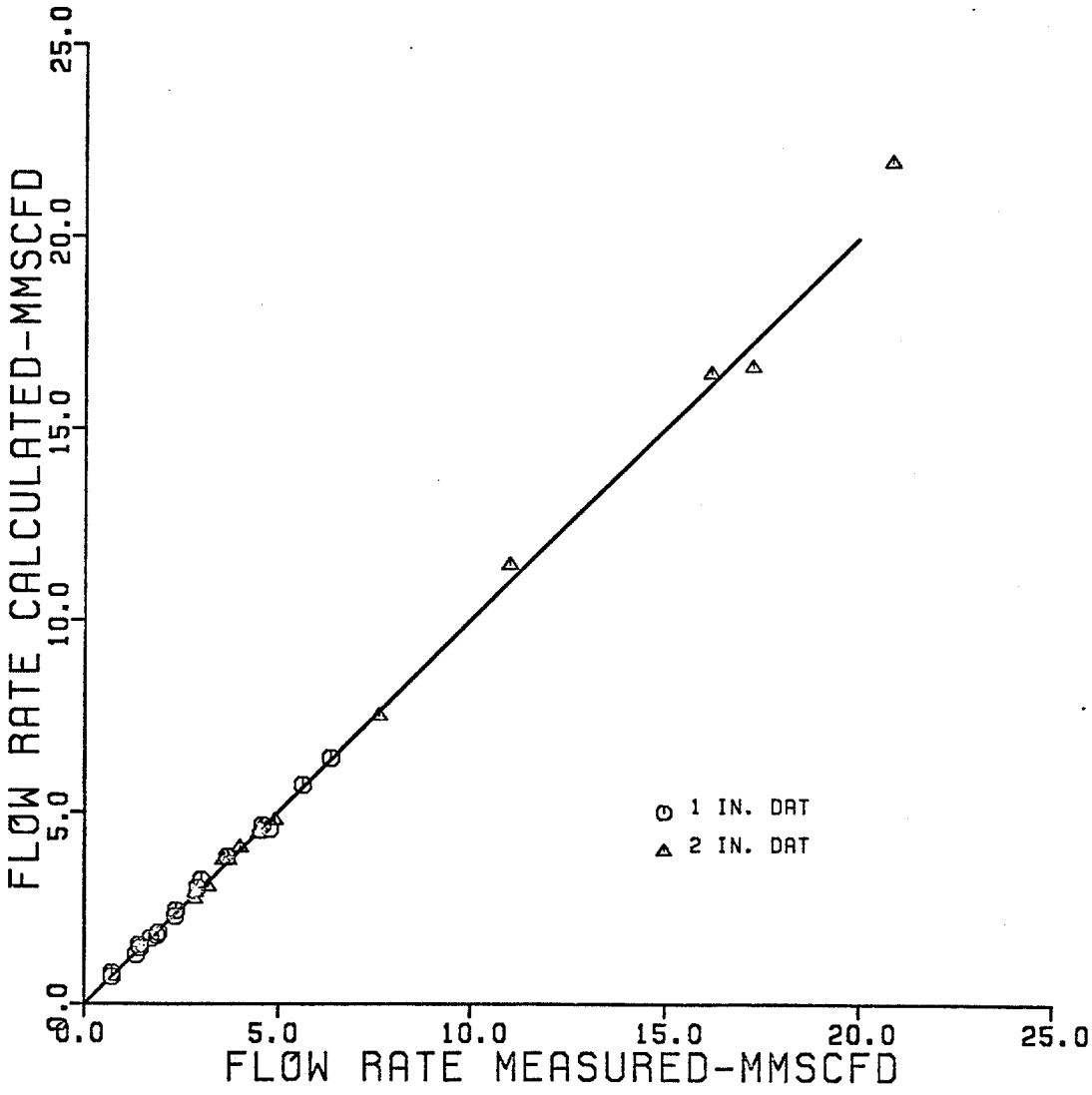

Figure 3.1. Comparison of Measured Critical Flow Rates to Predicted Critical Flow Rates for Dry Gas Flow

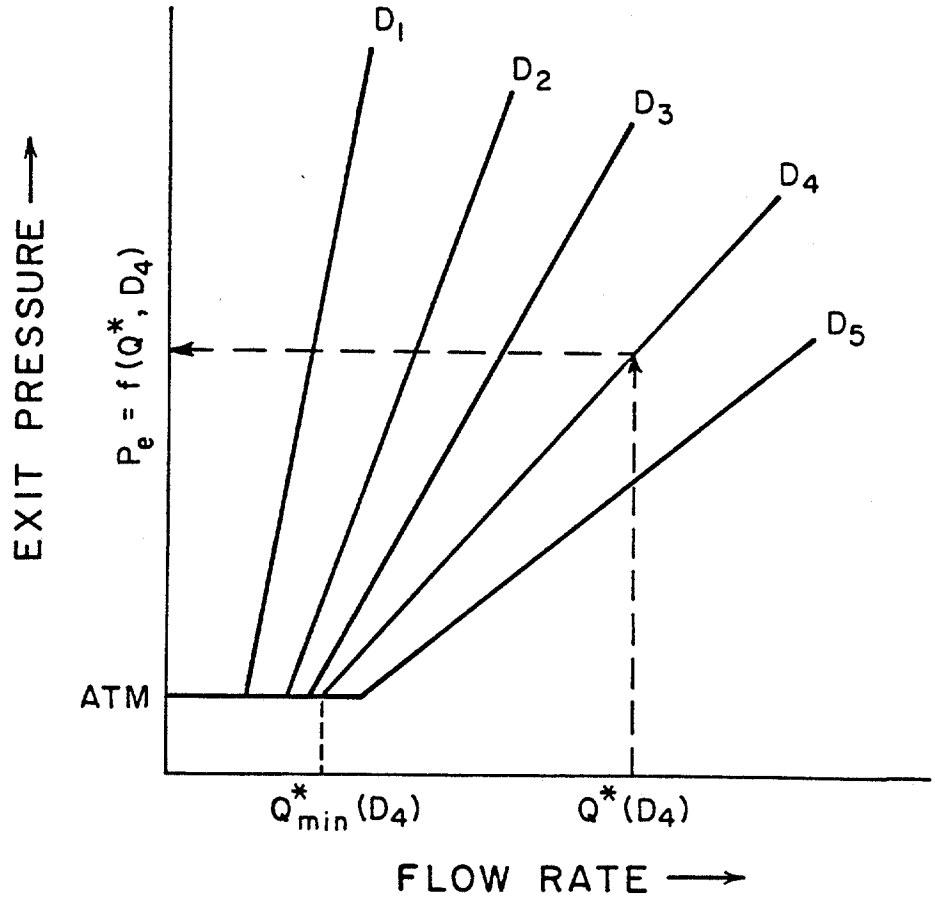

Figure 3.2. An Example of Exit Pressure as a Function of Flow Rate

includes bubble, slug, transition, and mist flow regimes. The flow regime most likely associated with flow in a diverter line is the mist flow regime. During mist flow, liquid droplets are carried along by a continuous gas phase. The exact distribution of the liquid droplets will affect the critical velocity of the mixture, but is impossible to predict. In other flow regimes similar difficulties arise, making it very difficult to predict with accuracy the critical velocities of two-phase mixtures. Other problems are encountered related to slippage between the gas and liquid phase, which results in the phases traveling at different velocities. Two-phase critical velocity should be expressed in terms of the velocity of the mixture, not of the individual components. Mixture velocity is defined by the total volumetric flow rate of the mixture.

$$V = \frac{q_g + q_w}{A} \tag{3.6}$$

The critical velocity of any fluid is given by:

$$V^* = 68.1 \sqrt{\frac{1}{\rho c}} \tag{3.7}$$

If appropriate values of density and compressibility can be determined, this equation should be useful in calculating critical velocities of two-phase mixtures. Difficulties arise in defining two-phase compressibilities and densities.

Equation 3.1 was derived from equation 3.7 for dry gas. Fortunati (1972) modified equation 3.1 to define two-phase critical velocities. His equation for two-phase critical velocity is given as:

$$V^* = 68.1 \sqrt{\frac{m P_e}{\lambda_g \rho_{tp}}} \tag{3.8}$$

The "m" term, somewhat tenuous, is called a two-phase expansion coefficient and is defined as:

$$m = \frac{(1-x)(Cv_\ell) + xCp_g}{(1-x)(Cv_\ell) + Cv_g} \tag{3.9}$$

where

$$x = \frac{\text{gas mass rate}}{\text{total mass rate}} \tag{3.10}$$

Wallis (1969) derived an expression for two-phase critical velocity as:

$$V^* \left[(\lambda_g \rho_g + \lambda_w \rho_w)\left(\frac{\lambda_g}{\rho_g V^{*2}_g} + \frac{\lambda_w}{\rho_w V^{*2}_w}\right)\right]^{-\frac{1}{2}} \tag{3.11}$$

The velcoity of the liquid phase is determined from equation 3.7, and the gas phase by equation 3.1. The Wallis equation has straight forward applicability.

Equations 3.8 and 3.11 can be used to calculate two-phase critical velocities. A typical two-phase critical velocity function (eqn. 3.8) is presented in Figure 3.3. Theory predicts a rapid decrease in critical velocity upon the addition of a second phase, as seen in the figure. The decrease in critical velocity approaches an order of magnitude. Minimum values of critical velocity are predicted by both equations at a liquid holdup of 0.5. This behavior was observed in the experimental data.

Critical velocities were calculated by equations 3.8 and 3.11 at the conditions of pressure and temperature measured in the experiments. Table 3.2 presents critical velocities and flow rates calculated by both equations, and compares them with the experimental two-phase flow data. Equation 3.8 predicts the

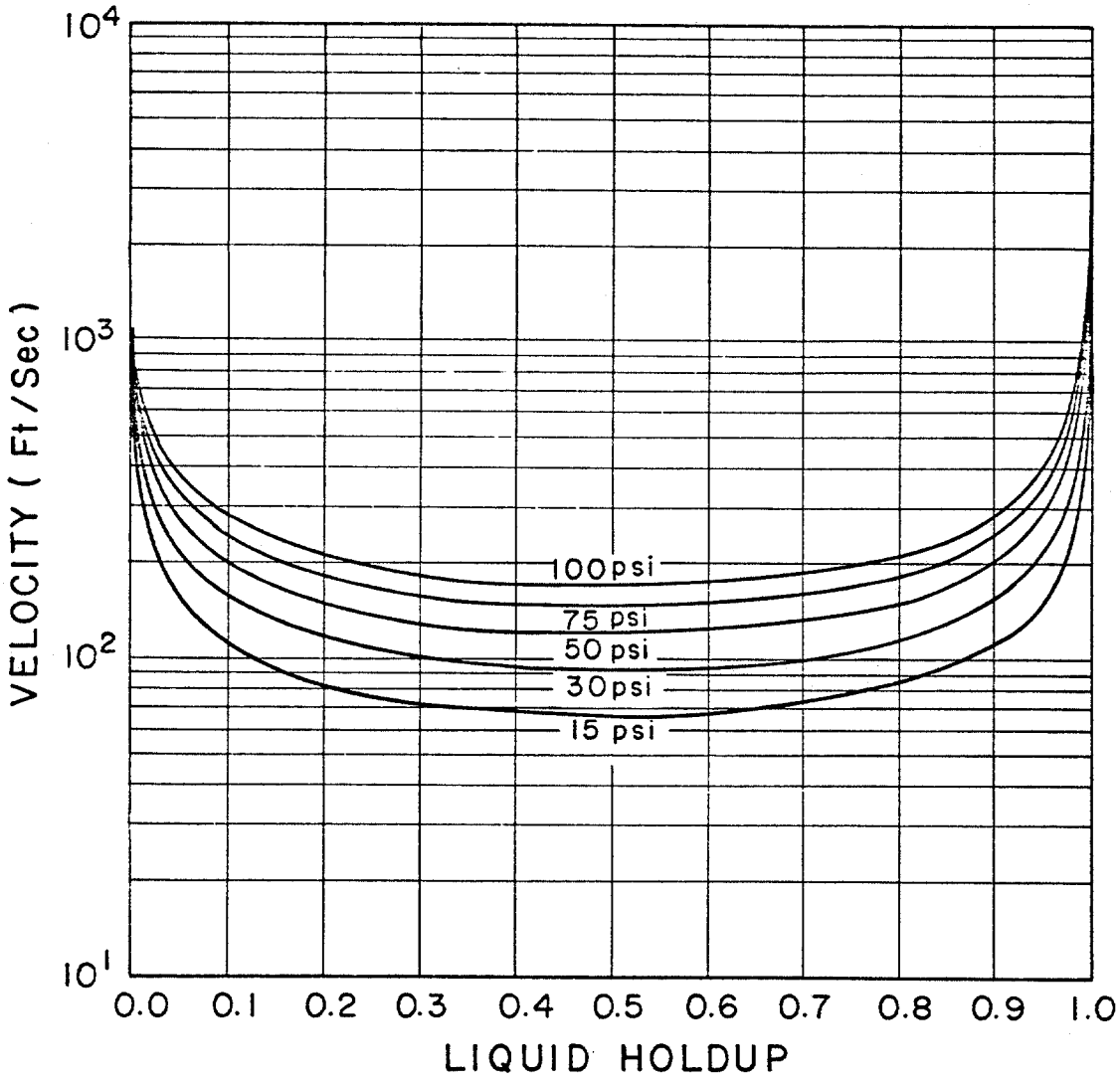

Figure 3.3. A Typical Two-Phase Critical Velocity Function

TABLE 3.2

COMPARISON OF MEASURED AND CALCULATED CRITICAL VELOCITIES AND FLOW RATES FOR TWO-PHASE FLOW

FLOW RATES (MMSCFD)			VELOCITIES (FT/SEC)			AVERAGE ERROR	AVERAGE ERROR
MEASURED	WALLIS	FORTUNATI	MEASURED	WALLIS	FORTUNATI	WALLIS	FORTUNATI
2.9	2.3	2.3	884	700	681	0.21	0.23
3.8	3.4	3.4	833	746	728	0.10	0.13
3.0	2.7	2.6	674	623	601	0.08	0.11
1.7	1.4	1.3	527	426	399	0.20	0.25
2.6	2.2	2.2	852	788	721	0.13	0.15
1.7	1.4	1.4	563	472	446	0.16	0.21
1.4	1.1	1.0	644	512	487	0.20	0.24
4.0	3.7	3.6	840	782	766	0.07	0.09
1.8	1.6	1.5	489	442	414	0.10	0.16
2.3	2.0	1.9	612	537	512	0.12	0.16
1.6	1.3	1.2	491	401	374	0.19	0.25
2.3	1.9	1.8	630	521	495	0.18	0.21
3.6	3.2	3.1	807	727	709	0.10	0.12
7.1	6.2	6.1	1152	1008	995	0.12	0.14
6.8	5.3	5.2	1031	813	794	0.21	0.23
6.6	4.9	4.7	985	732	710	0.26	0.28
6.4	4.6	4.4	918	653	628	0.29	0.32
6.2	4.5	4.3	805	582	556	0.28	0.31
6.2	4.6	4.3	669	495	466	0.26	0.30
6.0	4.6	4.3	571	442	412	0.23	0.28
7.8	6.8	6.7	1161	1011	998	0.13	0.14
7.6	7.0	7.0	1310	1207	1199	0.08	0.08
7.7	6.3	6.2	1125	921	905	0.18	0.20
7.1	5.7	5.6	1039	842	823	0.19	0.21
7.0	6.3	6.3	1277	1161	1152	0.09	0.10
19.0	17.3	17.1	1251	1139	1130	0.09	0.10
17.2	15.5	15.3	1118	1009	995	0.10	0.11
15.6	13.4	13.2	1013	873	855	0.14	0.16
14.4	12.0	11.7	960	802	782	0.16	0.19
13.4	12.3	12.2	1277	1165	1157	0.09	0.09
11.6	11.0	10.9	1145	1081	1070	0.06	0.06
10.8	9.6	9.5	1245	1107	1097	0.11	0.12
10.1	9.2	9.1	1194	1091	1080	0.09	0.09
9.5	8.7	8.7	1343	1235	1229	0.08	0.08
9.1	8.3	8.3	1346	1238	1232	0.08	0.08
8.6	7.0	6.9	1085	881	863	0.19	0.20
8.0	6.1	5.9	1048	798	777	0.24	0.26
7.4	5.7	5.6	1009	779	758	0.23	0.25
6.9	5.0	4.8	911	661	637	0.27	0.30
5.9	4.1	3.9	808	566	539	0.30	0.33
4.0	2.9	2.8	921	676	652	0.27	0.29
3.7	2.4	2.3	723	472	444	0.35	0.39

TABLE 3.2 (CONTINUED)

FLOW RATES (MMSCFD)			VELOCITIES (FT/SEC)			AVERAGE ERROR	AVERAGE ERROR
MEASURED	WALLIS	FORTUNATI	MEASURED	WALLIS	FORTUNATI	WALLIS	FORTUNATI
3.5	2.3	2.1	597	380	351	0.36	0.41
3.4	2.3	2.1	486	336	307	0.31	0.37
3.7	3.2	3.2	1170	1022	1009	0.13	0.14
3.4	2.6	2.5	971	741	719	0.24	0.26
3.2	2.3	2.2	876	640	615	0.27	0.30
3.0	2.0	1.9	801	549	522	0.31	0.35
3.1	2.7	2.6	1100	940	924	0.14	0.16
3.0	2.2	2.1	1018	742	720	0.27	0.29
2.9	2.4	2.3	1103	918	902	0.17	0.18
2.6	1.3	1.2	1113	543	516	0.51	0.54
4.8	3.3	3.1	765	519	491	0.32	0.36
2.0	1.4	1.2	392	268	242	0.32	0.39
1.9	1.2	1.1	410	258	233	0.37	0.43
3.4	2.3	2.2	851	577	551	0.32	0.35

experimental values of critical velocity with an average error of 22 percent, and equation 3.11 with an average error of 20 percent. Both equations predict the data with a standard deviation of 10 percent. These errors are of the magnitude typically associated with two-phase flow. However, the error in predicting critical velocity increases with increasing liquid holdup, indicating a fundamental error the theory. Figure 3.3 shows that critical velocities change very little between liquid holdup values of 0.2 to 0.8, and the liquid holdup data of the experiments reached only 0.10. If the experiments had recorded higher liquid holdup values, the average error between the theory and the experiments would probably be slightly higher.

Critical flow rates can be calculated from two-phase critical velocities by the following equation:

$$Q_g^* = \frac{V^* D^2}{\frac{2122.1\ z\ TP_{STD}}{P\ T_{STD}} + \frac{Y_w}{83.9}} \qquad (3.12)$$

The derivation of this equation is presented in Appendix C. It is assumed in the derivation that no gas slippage occurs at the exit. This assumption is supported by other authors (Fortunati, Beggs and Brill).

Figures 3.4 and 3.5 present measured critical flow rates plotted against critical flow rates calculated by equation 3.12. Figure 3.4 plots flow rates based on the Wallis equation, and Figure 3.5 rates based on the Fortunati equation. In both figures, predicted flow rates are consistently less than the measured flow rates due to the fact that equations 3.8 and 3.11

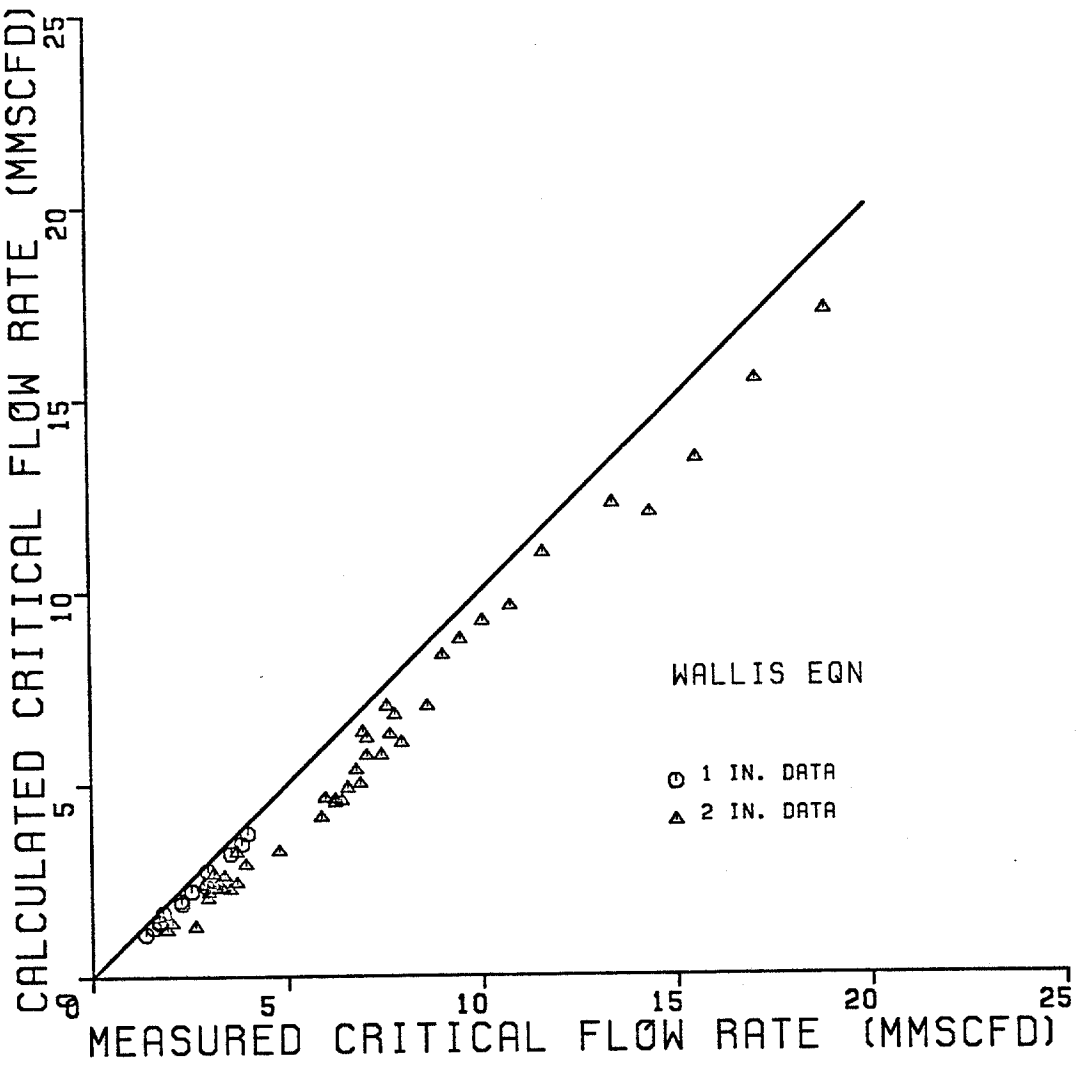

Figure 3.4. Comparison of Measured Critical Flow Rates and Flow Rates Predicted Using the Wallis Equation for Critical Velocity

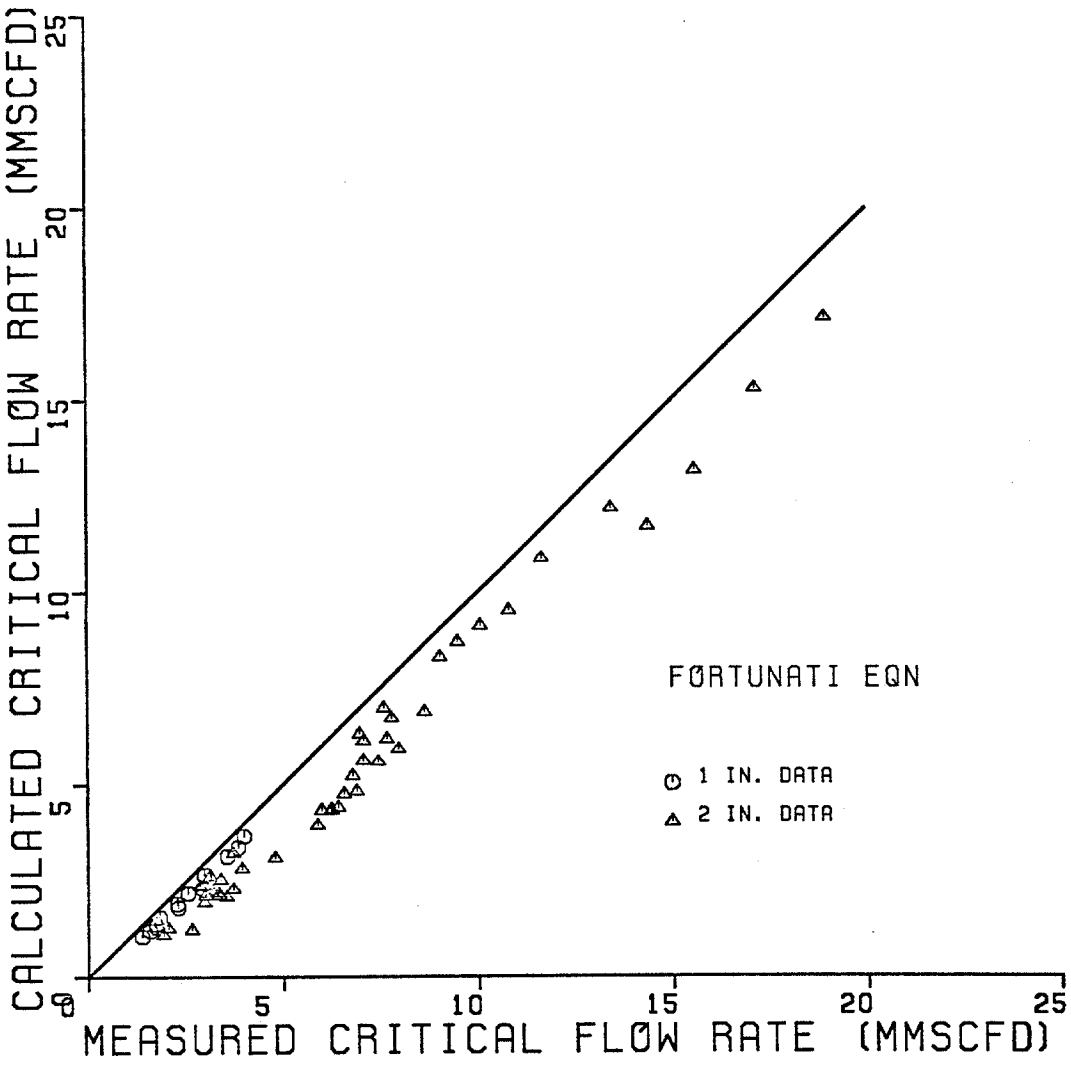

Figure 3.5. Comparison of Measured Critical Flow Rates and Flow Rates Predicted Using the Fortunati Equation for Critical Velocity.

both underpredict critical velocities. The largest deviations from the 45 degree line are associated with higher liquid flow rates, thus higher liquid holdup. It would appear from this plot, and from the statistics, that the Wallis equation provides the best estimate of two-phase critical velocity.

Although there is some error involved, equations 3.8 and 3.11 can be used in equation 3.12 to predict the relationship between critical flow rate and exit pressure with reasonable engineering accuracy. When using these equations for design work, it should be noted that the amount of water, or liquid holdup, in the system will greatly influence the pressures and flow rates calculated. Two-phase flow with a liquid holdup of 0.5 will result in the lowest flow rate and highest exit pressure and should be the worst case encountered in diverter operations. Two-phase critical flow also results in higher exit pressures than does dry gas critical flow.

3.3. Pressure Loss Calculations

Just as the exit pressure caused by critical flow will apply backpressure to a well, pressure losses in the diverter line also represent backpressure on the well, and should be investigated. Special consideration is given to critical flow in that certain assumptions made in calculating pressure losses that may be valid for most instances of flow in a well may not be valid for critical flow. One such assumption is that pressure losses due to acceleration are negligible. Critical flow in diverter lines involves accelerating a relatively high density gas to very high velocities. To attain high

velocities, density decreases as velocity increases, and the kinetic energy of the gas changes, which results in a pressure loss. It would therefore be expected that acceleration losses could be significant in critical flow. A method of calculating these losses is needed. Another questionable assumption is that the empirical correlations used to calculate frictional pressure losses are applicable to critical flow. These correlations need to be tested against known pressure traverses to determine their applicability.

The general energy equation governs fluid flow in pipes, and has been derived by several authors (Beggs and Brill, Smith and van Ness). It can take may different forms, but is usually presented as a conservation of kinetic, potential, and internal energies, as well as any irreversibilities (friction) or work done by the fluid. The following is a general form of the general energy equation.

$$dU + d\left(\frac{P}{\rho}\right) + \frac{VdV}{g_c} + \frac{g}{g_c}dz + dq + dW = 0 \qquad (3.13)$$

This equation can be manipulated and expressed in terms of pressure gradients. From the general energy equation, the total flowing pressure gradient of fluid flowing in a pipe consists of three basic components. These components are the friction loss component, the hydrostatic component, and the acceleration component. The total pressure gradient is the sum of these components, and is presented as the pressure gradient equation:

$$\left(\frac{\Delta P}{\Delta L}\right)_{Total} = \left(\frac{\Delta P}{\Delta L}\right)_{friction} + \left(\frac{\Delta D}{\Delta L}\right)_{elev.} + \left(\frac{\Delta P}{\Delta L}\right)_{accel.} \qquad (3.14)$$

The pressure gradient equation is simply another form of the general energy equation. In horizontal flow, as occurs in diverter lines,

there is no hydrostatic component of the pressure gradient, so that the pressure gradient equation becomes

$$\left(\frac{\Delta P}{\Delta L}\right)_{Total} = \left(\frac{\Delta P}{\Delta L}\right)_{friction} + \left(\frac{\Delta P}{\Delta L}\right)_{accel.} \qquad (3.15)$$

Pressure losses can be calculated from this equation for either dry gas or two-phase flow. Differences arise in the methods used to calculate each component.

3.3.1. Pressure Losses in Dry Gas Flow

The compressible flow of dry gas (i.e. no liquid phase) has been extensively studied, and methods of calculating frictional pressure losses for dry gas are well established and accepted.

As in incompressible flow, the friction factor concept is used to calculate frictional pressure gradients in dry gas flow. The Darcy-Weisbach equation

$$\left(\frac{\Delta P}{\Delta L}\right)_{friction} = \frac{f\rho V^2}{2g_c\, d} \qquad (3.16)$$

relates the frictional pressure gradient to a friction factor. The friction factor used is the Moody friction factor and is defined by the Colebrook equation:

$$\frac{1}{\sqrt{f}} = 1.74 - 2\log_{10}\left(\frac{2\varepsilon}{d} + \frac{18.7}{N_r\sqrt{f}}\right) \qquad (3.17)$$

The Reynold's number is used as a correlating parameter in the Colebrook equation, and is defined as:

$$N_r = \frac{\rho V d}{\mu} \qquad (3.18)$$

Pressure gradients due to fluid acceleration can be calculated by calculating the change in kinetic energy of the

gas. In terms of a pressure gradient, acceleration losses can be expressed as:

$$\left(\frac{\Delta P}{\Delta L}\right)_{accel.} = \frac{\Delta(\rho V^2)}{2g_c \Delta L} \tag{3.19}$$

The derivation of this equation is presented in Appendix D.

Frictional and acceleration gradients are used to calculate a pressure traverse. Beggs and Brill (1978, p. A-18) present an iterative finite element method of calculating a theoretical pressure traverse in a pipe. This method allows pressure to be calculated throughout the pipe from a pressure known at one point in the pipe. If downstream pressure is known, upstream pressure can be calculated, and vice versa. This technique is employed to calculate pressure losses for compressible flow, such as gas or two-phase flow. Using equations 3.14, 3.16, and 3.17 in this technique, theoretical pressure traverses can be calculated and compared to the experimental traverses presented in Chapter II. Inlet pressures were calculated based on the experimental values of exit pressure and flow rate. Tables 3.3 and 3.4 compare the results of these calculations to the measured pressures. Calculated inlet pressures, along with percent error, are shown with the original data. The experimental data from the 1-in. experiments are predicted with 4 percent average error and the data from the 2-in. experiments with 8.5 percent average error, which is excellent. Figure 3.6a presents a graphical comparison between an experimental traverse and a computed traverse. As can be seen from this figure, the theoretical traverse closely matches the experimental traverse. Figure 3.6b shows the same

TABLE 3.3

MEASURED AND PREDICTED INLET PRESSURES FOR THE 1-IN. DRY GAS DATA

RUN #	INLET PRESSURES		% ERROR	GAS RATE
	MEASURED (PSIA)	PREDICTED (PSIA)		(MMSCFPD)
1	82	80	0.03	0.7
2	157	151	0.04	1.4
3	77	75	0.03	0.7
4	138	135	0.02	1.3
5	193	187	0.03	1.9
6	241	233	0.03	2.3
7	200	193	0.03	1.9
8	340	327	0.04	3.0
9	395	380	0.04	3.7
10	474	456	0.04	4.6
11	69	64	0.07	0.5
12	202	189	0.06	1.7
13	247	237	0.04	2.4
14	149	142	0.05	1.4
15	598	576	0.04	6.4
16	538	509	0.05	4.8
17	536	513	0.04	5.6
18	304	291	0.04	2.9

TABLE 3.4

MEASURED AND PREDICTED INLET PRESSURES FOR THE 2-IN. DRY GAS DATA

	INLET PRESSURES			
RUN #	MEASURED (PSIA)	PREDICTED (PSIA)	% ERROR	GAS RATE (MMSCFPD)
1	379	332	0.12	20.9
2	301	275	0.09	17.3
3	297	258	0.13	16.2
4	203	177	0.13	11.0
5	130	122	0.06	7.6
6	91	79	0.13	4.9
7	79	73	0.08	4.6
8	79	73	0.08	4.5
9	68	65	0.04	4.0
10	68	60	0.12	3.7
11	60	58	0.03	3.6
12	53	51	0.04	3.2
13	47	47	0.00	2.9
14	46	46	0.00	2.9
15	37	34	0.08	2.1
16	28	26	0.07	1.4
17	19	15	0.21	0.1

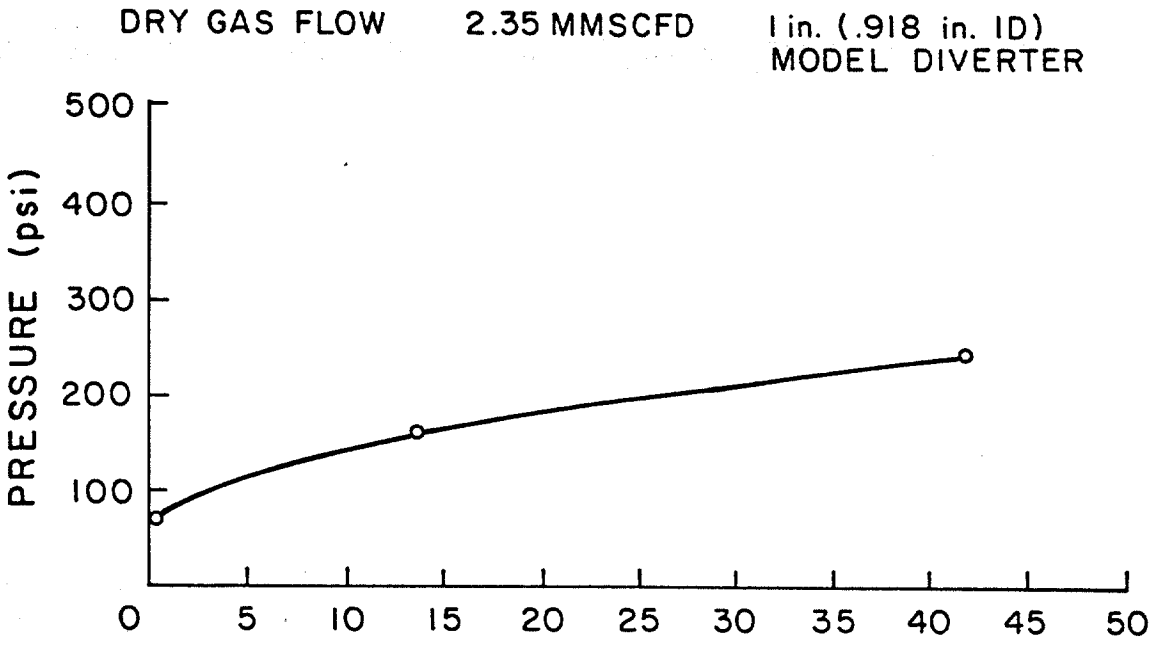

Figure 3.6.a. Theoretical Pressure Traverse (Calculated Including Acceleration Losses) Versus the Experimentally Measured Traverse, 1 in. Dry Gas Model Diverter Data

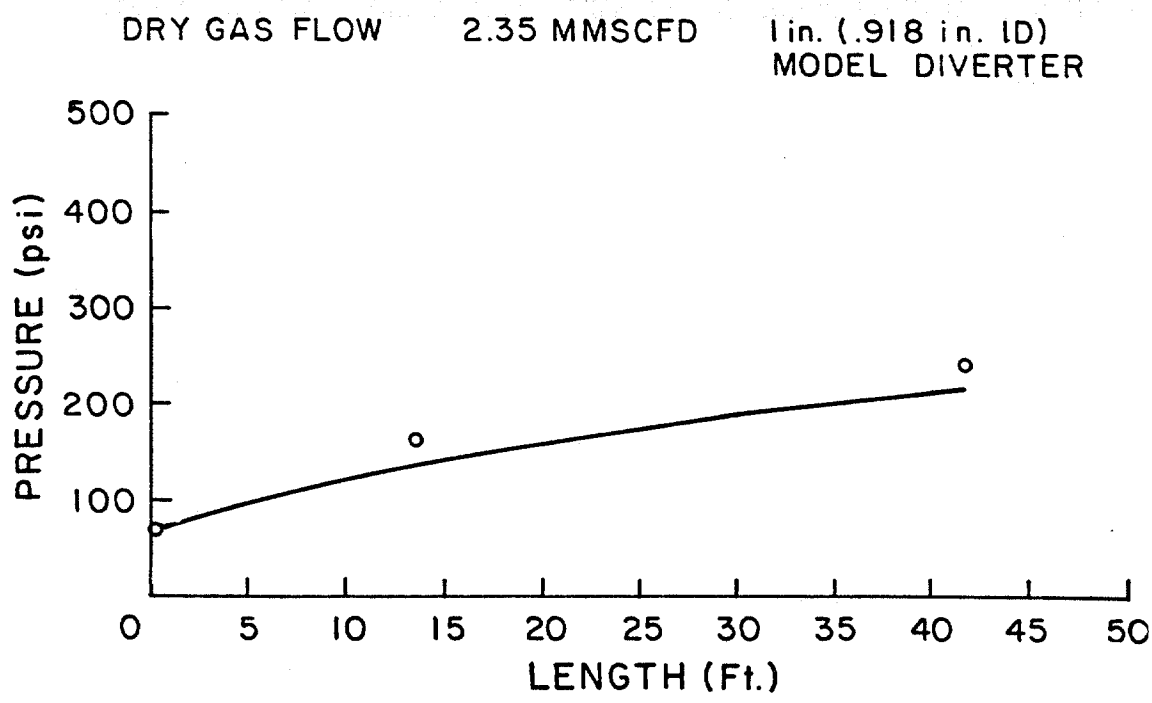

Figure 3.6.b. Theoretical Pressure Traverse (Calculated Neglecting Acceleration Losses) Versus the Experimental Traverse, 1 in. Dry Gas Model Diverter Data

traverse, but with the acceleration gradient neglected. Neglecting acceleration results in considerable underestimation of the pressure losses measured in the model diverters. The effect of neglecting acceleration in full-sized diverters will be shown shortly.

Figure 3.7 shows the relative magnitude of the acceleration component in the total pressure gradient, as predicted by equation 3.17. The friction component is dominant at the upstream end of the pipe, but as the flow accelerates to the exit, the acceleration component increases drastically. Acceleration can account for as much as 60 percent of the total pressure gradient at the diverter exit. Since the total gradient can be very large at the exit, acceleration effects can represent a significant pressure loss.

Comparisons to the experimentally measured traverses show that equations 3.14 through 3.17 can be used to model the pressure losses of dry gas critical flow in the model diverter lines.

3.3.2. Pressure Losses in Gas-Water Mixtures

Pressure loss calculations for two-phase flow are generally based on empirical correlations, and these correlations should be applied to critical flow with caution. Numerous investigators have developed empirical two-phase flow correlations, but any correlation is basically limited by the experimental data used to develop that correlation. Most researchers have chosen to use dimensionless correlating parameters or numbers (such as the

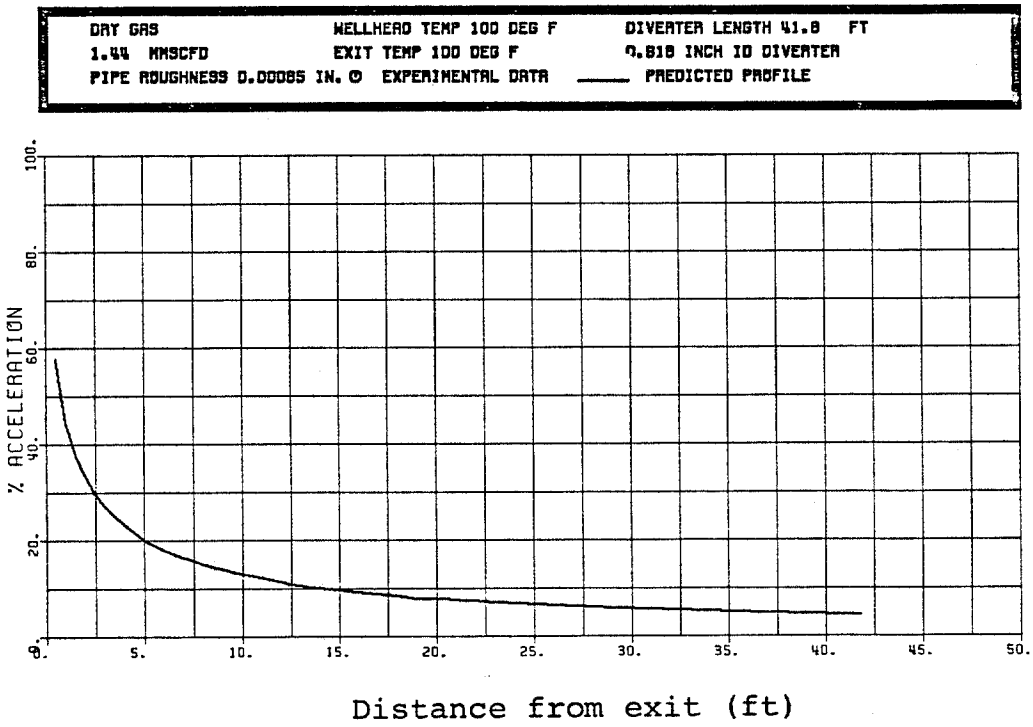

Figure 3.7. Relative Magnitude of Acceleration Losses in a Theoretical Dry Gas Pressure Traverse

Reynold's number) to develop a correlation so that the correlation can be extrapolated to conditions not actually measured in the experiments used as a basis for the correlation. Experience has shown that extrapolation of any correlation too far past the conditions of the original data can result in large errors.

Advanced two-phase flow correlations concentrate on two parameters. Liquid holdup, or the fraction of liquid in the flow, depends on the amount of slippage of the gas phase past the liquid phase, as well as the volumetric flow rates of each phase, and must be determined by the correlation. A two-phase friction factor, for use in the Darcy-Weisbach equation (Eqn. 3.16), is also determined by the correlation. Determination of these two parameters forms the basis of most two-phase flow correlations.

Beggs and Brill have compiled many of the two-phase flow correlations into FORTRAN subroutines that can easily be incorporated into the pressure traverse technique discussed earlier. The subroutines always calculate frictional pressure gradients, but may or may not include acceleration gradients. The subroutines may also terminate execution when flow approaches critical conditions. An argument can be made to the applicability of these correlations to critical flow in that flow is critical only at the diverter exit, and thus subcritical in the remainder of the line, and the correlations should apply to subcritical flow. However, because two-phase flow correlations are empirical, they may or may not be applicable to specific pipe diameter or gas-liquid ratios.

The experimentally measured pressure traverses were used to test the Dukler correlation for applicability to critical flow calculations. The Dukler correlation applies to horizontal flow and is widely used in the petroleum and natural gas industries to calculate pressure losses. The friction factor and liquid holdup correlations used in the Beggs and Brill subroutine are inherent to the Dukler correlation and were retained for use in the modeling. The acceleration component used in the subroutine from Beggs and Brill prevented use at critical flow conditions, and was replaced by an alternate method of calculation. Equation 3.17, the acceleration gradient equation used for dry gas, was adapted to two-phase flow by replacing the density term by a two-phase density defined by:

$$\rho_{tp} = \lambda_g \rho_g + \lambda_w \rho_w \tag{3.20}$$

The velocity term used is the mixture velocity, which is the sum of the superficial velocities of the gas and water:

$$V = \frac{q_g + q_w}{A} \tag{3.21}$$

Just as for dry gas flow, theoretical traverses were calculated and compared to the experimental traverses. Tables 3.5 and 3.6 compare the measured inlet pressures to those calculated. Using measured exit pressures and flow rates, upstream pressures were calculated by the Dukler correlation, with the modified acceleration term, with 5 percent average error in the 1-in. line and 9 percent average error in the 2-in. line. Figure 3.8a shows good agreement between a theoretical and experimental traverse from the 1-in. experimental data. Figure

TABLE 3.5

MEASURED AND PREDICTED INLET PRESSURES FOR THE 1-IN. GAS/WATER DATA

RUN #	INLET PRESSURES		% ERROR	GAS RATE (MMSCFPD)	WATER RATE (BBL/MMSCF)
	MEASURED (PSIA)	PREDICTED (PSIA)			
1	428	521	0.22	2.9	393
2	590	624	0.06	3.8	325
3	586	612	0.04	3.0	554
4	603	599	0.01	1.7	1496
5	412	433	0.05	2.6	349
6	512	519	0.01	1.7	1135
7	340	361	0.06	1.4	900
8	595	613	0.03	3.9	279
9	619	610	0.01	1.8	1384
10	583	567	0.03	2.3	825
11	605	601	0.01	1.6	1745
12	605	599	0.01	2.3	890
13	574	607	0.06	3.6	363

TABLE 3.6

MEASURED AND PREDICTED INLET PRESSURES FOR THE 2-IN. GAS/WATER DATA

RUN #	INLET PRESSURES MEASURED (PSIA)	INLET PRESSURES PREDICTED (PSIA)	% ERROR	GAS RATE (MMSCFPD)	WATER RATE (BBL/MMSCF)
1	124	118	0.05	3.4	690
2	196	182	0.07	1.9	4457
3	89	103	0.16	2.6	793
4	197	193	0.02	4.8	901
5	201	185	0.08	2.0	4151
6	160	134	0.16	7.1	138
7	172	166	0.03	6.8	282
8	183	180	0.02	6.6	379
9	197	200	0.01	6.4	513
10	369	318	0.14	19.0	80
11	356	330	0.07	17.2	138
12	357	352	0.01	15.6	229
13	359	356	0.01	14.4	294
14	200	194	0.03	8.6	222
15	200	199	0.00	8.0	299
16	191	191	0.00	7.4	320
17	207	211	0.02	6.9	498
18	220	216	0.02	5.9	733
19	242	208	0.14	11.6	103
20	221	185	0.16	10.8	93
21	206	177	0.14	10.1	99
22	185	140	0.24	9.5	47
23	178	134	0.25	9.1	49
24	262	217	0.17	13.4	71
25	169	148	0.12	7.8	137
26	151	115	0.24	7.6	59
27	170	164	0.03	7.7	191
28	174	167	0.04	7.1	255
29	140	120	0.14	7.0	73
30	228	221	0.03	6.2	686
31	289	270	0.07	6.2	1029
32	323	301	0.07	6.0	1367
33	126	118	0.06	4.0	467
34	172	167	0.03	3.7	1114
35	215	208	0.03	3.5	1858
36	247	233	0.06	3.4	2520
37	86	65	0.24	3.7	132
38	101	91	0.10	3.4	366
39	111	100	0.10	3.2	534
40	77	60	0.22	3.1	179
41	85	79	0.10	3.0	364
42	71	56	0.21	2.9	193
43	121	111	0.08	3.0	778

TABLE 3.7

COMPARISON OF BACKPRESSURES CALCULATED BY VARIOUS ASSUMPTIONS

150' length, Dry Gas

DIAMETER (IN.)	FLOW RATE MMSCFD	BACKPRESSURE @ WELLHEAD 1 CRITICAL FLOW W/ACCELERATION	2 CRITICAL FLOW W/O ACCELERATION	3 SUBCRITICAL FLOW W/O ACCELERATION	1 VS. 2 ERROR	1 VS. 3 ERROR
6"	20	53	47	46	.10	.12
	40	104	93	87	.10	.17
	60	154	140	129	.09	.16
	80	204	185	171	.09	.16
	100	254	231	213	.09	.16
	150	379	343	318	.09	.16
8"	40	49	42	40	.14	.18
	80	96	84	76	.13	.21
	120	141	125	112	.11	.20
	160	186	166	149	.11	.20
	200	233	207	185	.11	.21
10"	80	55	46	43	.16	.22
	120	82	69	62	.16	.24
	160	105	92	81	.13	.23
	200	131	115	100	.12	.24
12"	75	33	27	27	.18	.18
	100	44	36	34	.18	.23
	150	65	54	47	.17	.28
	200	87	71	62	.18	.29

TABLE 3.7 (CONTINUED)

150' length, 1000 bbl/MMSCF

DIAMETER (IN.)	FLOW RATE MMSCFD	BACKPRESSURE @ WELLHEAD 1 CRITICAL FLOW W/ACCELERATION	2 CRITICAL FLOW W/O ACCELERATION	3 SUBCRITICAL FLOW W/O ACCELERATION	1 VS. 2 ERROR	1 VS. 3 ERROR
6"						
	10	76	63	62	.17	.18
	20	144	126	118	.13	.18
	40	286	253	231	.12	.19
	60	429	380	346	.11	.19
8"						
	20	73	57	53	.21	.27
	40	135	114	102	.16	.24
	60	200	170	151	.15	.25
	80	266	227	200	.15	.25
	100	333	284	250	.15	.25
10"						
	40	81	63	56	.22	.31
	80	153	126	108	.18	.29
	120	227	188	160	.17	.30
	160	302	252	213	.17	.30
12"						
	40	58	40	36	.31	.38
	80	100	79	67	.21	.33
	120	147	118	98	.20	.33
	160	194	157	130	.19	.33
	200	242	196	162	.19	.33

TABLE 3.8

EXIT PRESSURES AND EQUIVALENT DENSITIES OF VARIOUS DIVERTER DIAMETERS

DIVERTER DIAMETER	GAS FLOW RATE MMSCFD	0 BBL/MMSCF		250 BBL/MMSCF		500 BBL/MMSCF		1000 BBL/MMSCF	
		P_e	ECD	P_e	ECD	P_e	ECD	P_e	ECD
6"	40	41	1.7	67	3.3	85	4.5	113	6.3
	80	92	4.9	123	6.9	170	9.9	226	13.5
	120	123	6.9	199	11.8	-	-	-	-
	160	163	9.5	264	16.0	-	-	-	-
	200	203	12.1	-	-	-	-	-	-
		P_e	ECD	P_e	ECD	P_e	ECD	P_e	ECD
8"	40	22	0.4	35	1.3	45	1.9	60	2.9
	80	43	1.8	70	3.5	89	4.7	119	6.7
	120	65	3.2	105	5.8	133	7.6	178	10.5
	160	86	4.6	140	8.0	178	10.5	-	-
	200	107	5.9	175	10.3	221	13.2	-	-
		P_e	ECD	P_e	ECD	P_e	ECD	P_e	ECD
10"	40	15	0.0	22	0.5	28	0.8	37	1.4
	80	27	0.8	43	1.8	55	2.6	73	3.7
	120	40	1.6	65	3.2	82	4.3	110	6.1
	160	53	2.4	86	4.6	110	6.1	145	8.3
	200	66	3.3	107	5.9	137	7.8	182	10.7
		P_e	ECD	P_e	ECD	P_e	ECD	P_e	ECD
12"	40	15	0.0	15	0.0	19	0.2	25	0.6
	80	18	0.2	29	0.9	37	1.4	50	2.2
	120	27	0.8	44	1.9	56	2.6	74	3.8
	160	36	1.4	58	2.8	75	3.9	99	5.4
	200	45	1.9	73	3.7	93	5.0	123	6.9

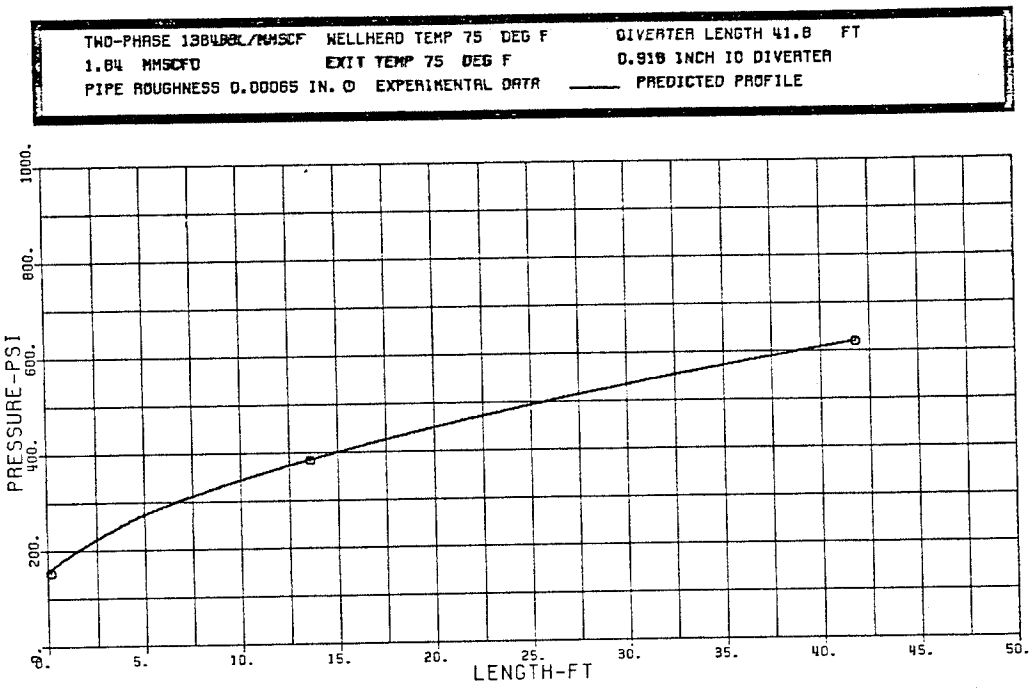

Figure 3.8.a. Theoretical Pressure Traverse (Calculated Including Acceleration Losses) Versus the Experimentally Measured Traverse, 1 in. Gas/Water Model Diverter Data

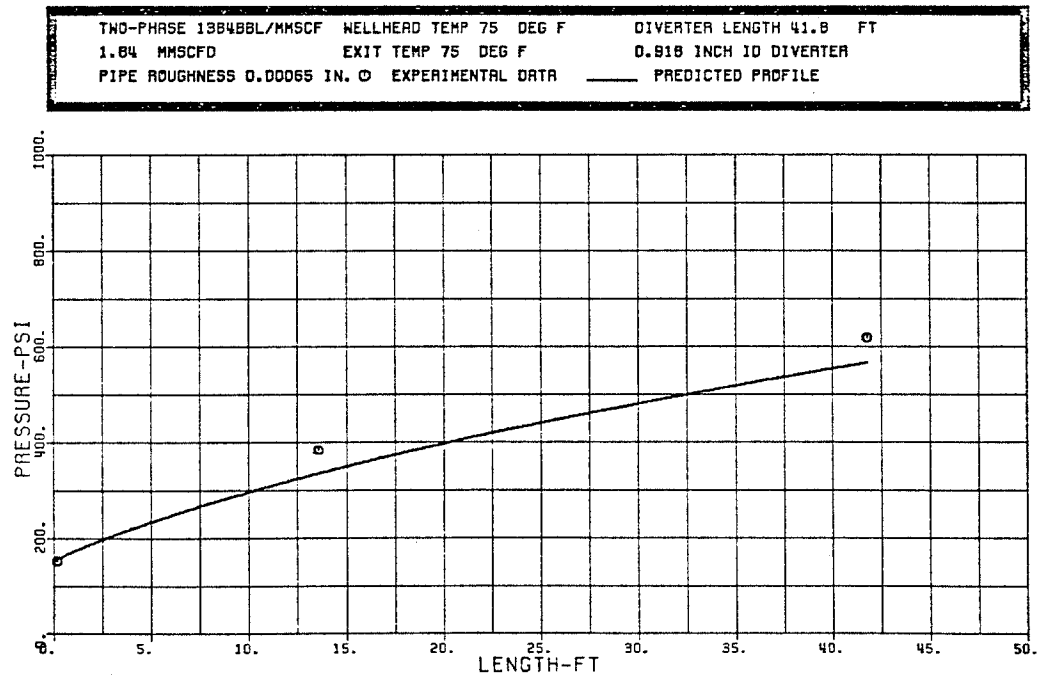

Figure 3.8.b. Theoretical Pressure Traverse (Calculated Neglecting Acceleration Losses) Versus the Experimentally Measured Traverse, 1 in. Gas/Water Model Diverter Data

3.8b shows that neglecting acceleration in two-phase flow will lead to an underestimation of the flowing pressures in the model diverter line. Figure 3.9 shows the relative magnitude of the acceleration gradient, in terms of a percent of total, in a traverse. As was observed for dry gas flow, the acceleration term increases in magnitude near the exit to the point that it becomes the dominant form of pressure loss in the line at the exit.

The Dukler correlation, when modified to account for acceleration losses, provides an adequate means of calculating pressure losses in horizontal two-phase critical flow. It appears that no modification to the frictional pressure loss calculations is necessary, and that the correlation extends to critical flow.

3.4 Acceleration Losses in Full-sized Diverter Lines

To analyse the assumption that acceleration losses are negligible in diverter line flow, total pressure losses were calculated and compared to frictional pressure losses in full-sized diverter lines of various diameters for both gas and gas/water flow. Table 3.7 presents the results of this comparison. The minimum error due to neglecting acceleration is about 9 percent, and occurs in the smaller diameter diverter line (6-in.) for dry gas flow. The maximum error occurs in two-phase flow (1000 bbl/mmscf) in the larger diameter line (12-in.), and is over 30 percent. These results indicate that neglecting losses due to acceleration, as is currently practiced, can lead to significant error in the calculation of pressure losses.

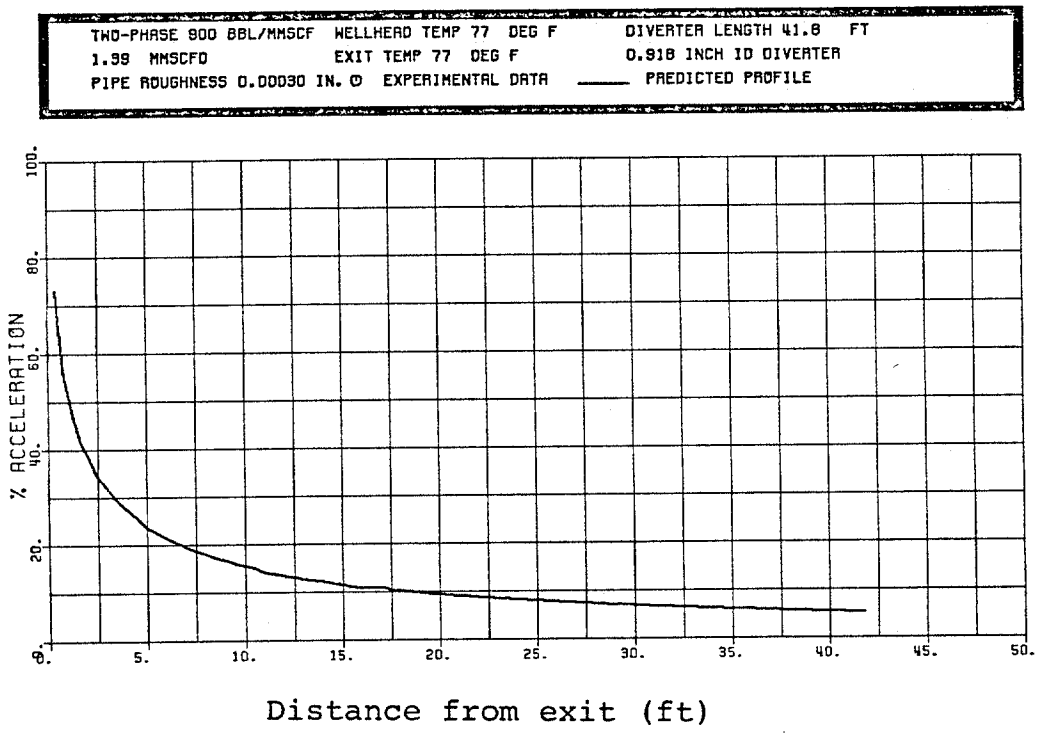

Figure 3.9. Relative Magnitude of Acceleration Losses in a Theoretical Two-Phase Pressure Traverse

The computer program used to model the experimental pressure traverses and to predict the effects of acceleration in full-sized diverter lines is presented in Appendix E.

3.5 Exit Pressures in Full-Sized Diverter Lines

Critical flow caused large increases in the exit pressures recorded in the experiments discussed in Chapter II. The critical velocity and flow rate theory presented earlier in this chapter can be used to determine whether similar increases in exit pressure can be expected in full-sized diverters. Exit pressures expected at various flow rates were calculated for a variety of diverter diameters and liquid rates. The results of this study are presented in Table 3.8. As expected, the exit pressures decrease as diameter increases, and increase with increasing liquid flow rate. In the smaller diameter lines (6-, 8-in.), exit pressures become extremely high at relatively low flow rates. It is generally assumed in design work that exit pressure in the larger diameter lines becomes negligible, but this is not the case. Exit pressures in the 12-in. line become very large at the higher gas and liquid flow rates. The magnitude of the exit pressure is even more alarming when presented in terms of an additional fracture pressure placed on the conductor shoe. For a conductor shoe at 750 ft. (350 ft. water depth, 400 ft. BML) an additional fracture pressure of 5.7 ppg would result from the exit pressure of an 8 in. diverter line flowing 200 mmscfd with 500 bbl/mmscf (which are very reasonable rates). The assumption that flow is subcritical results in this fracture pressure being neglected, and is in obvious error.

3.6 Design Applications

As stated in the introductory section, methods currently being used to design diverter systems are based on calculating the backpressure placed on the well by the diverter system by assuming subcritical flow and by neglecting acceleration losses. Methods presented in this chapter show that critical flow effects can significantly increase the backpressure on the well, and acceleration effects can cause considerable pressure loss. Methods of calculating backpressure which account for critical flow, frictional losses, and acceleration losses have been presented. Current design practices can therefore be improved by the application of the theory so far presented.

Curves relating backpressure at the wellhead to flow rate for various diameter diverters and various liquid rates were calculated for use in basic design work, and are presented in Figures 3.10-3.13. These curves assume critical flow at the diverter exit and use the pressure loss calculation procedures presented. Backpressures were also calculated assuming subcritical flow and neglecting acceleration losses, as is currently practiced. It should be pointed out that the subcritical flow assumption (i.e. atmospheric exit pressure) actually forces fluid velocities greater than critical velocity, which is physically impossible in pipe flow. The extremely high velocities generated by the subcritical flow cause very high frictional pressure losses to be calculated which tend to decrease the error observed between the two methods. Table 3.7 compares backpressures calculated by both means for dry gas and two-phase flow. The difference between the two methods ranges between about 12 percent in the smaller

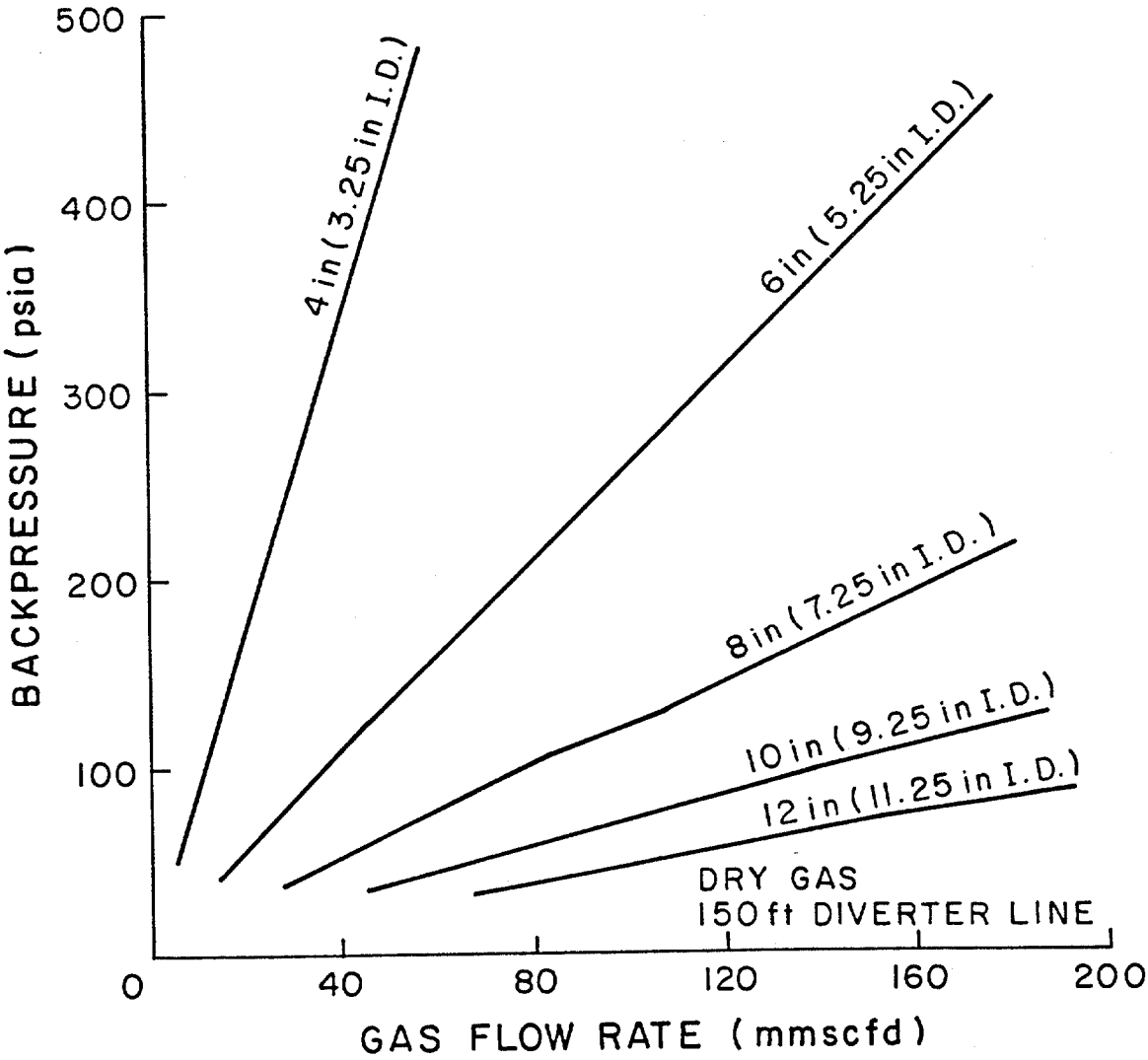

Figure 3.10. Backpressure as a Function of Flow Rate for Various Diverter Diameters (Dry Gas)

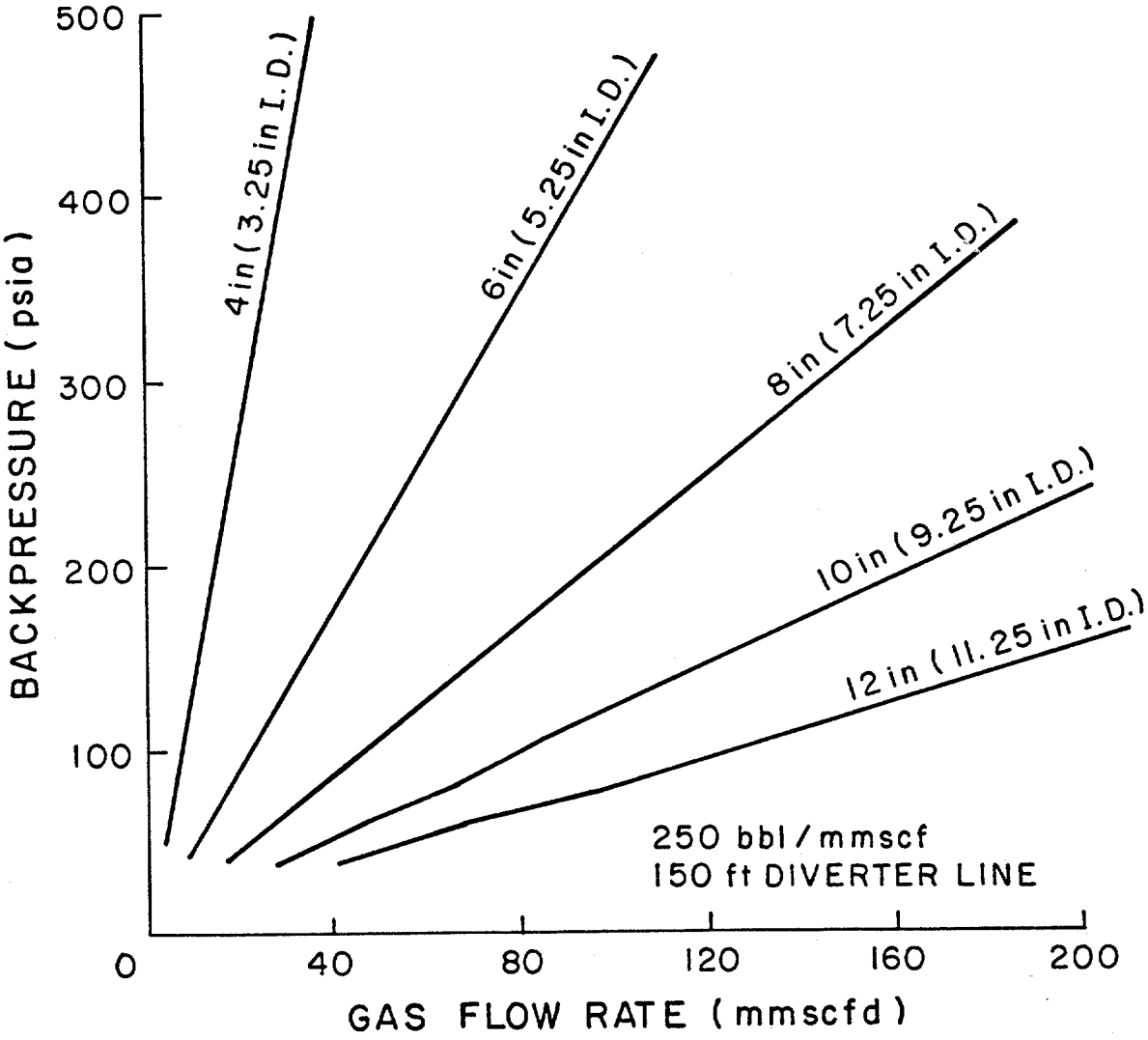

Figure 3.11. Backpressure as a Function of Flow Rate for Various Diverter Diameters (250 bbl/MMSCF)

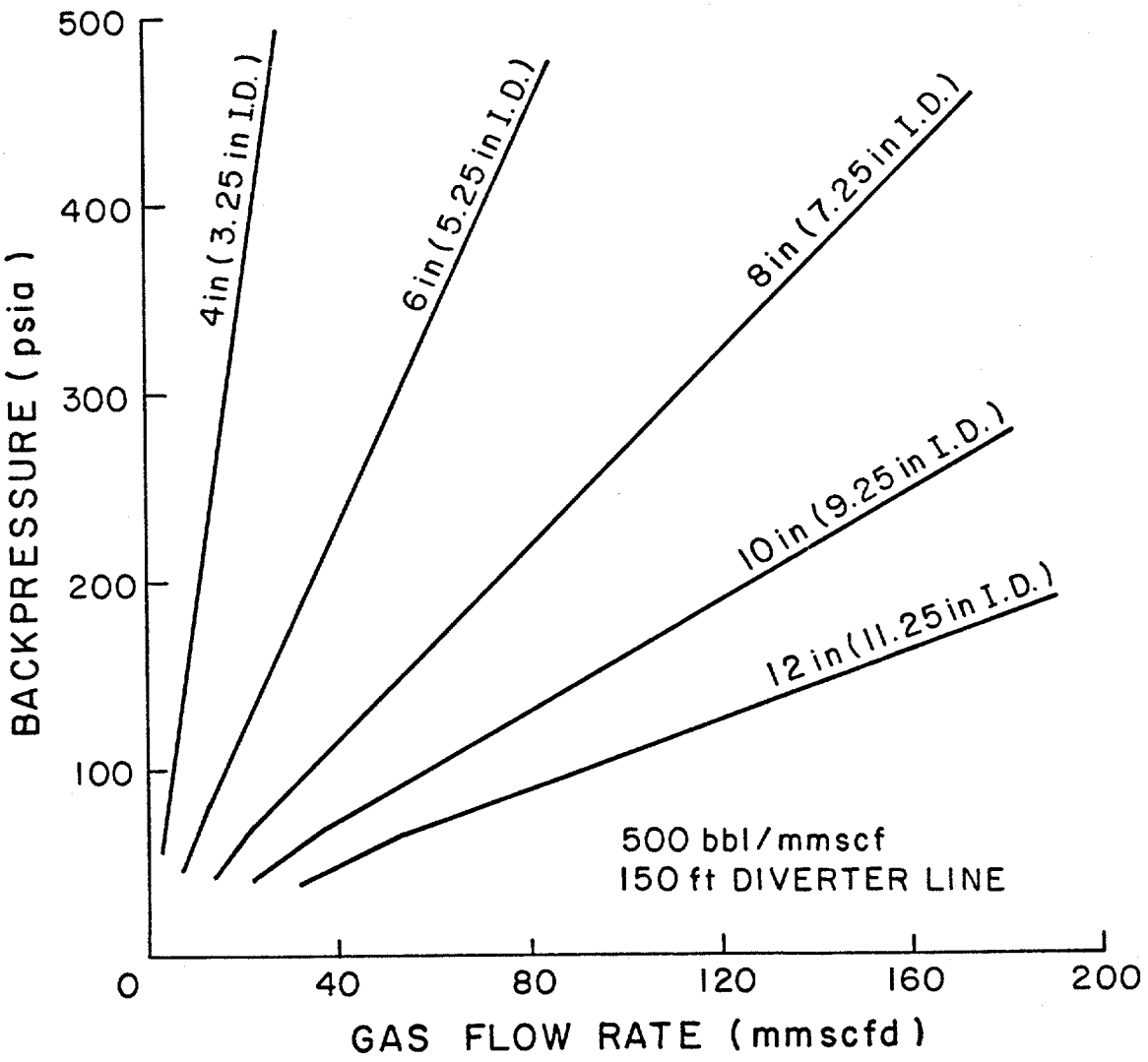

Figure 3.12. Backpressure as a Function of Flow Rate for Various Diverter Diameters (500 bbl/MMSCF)

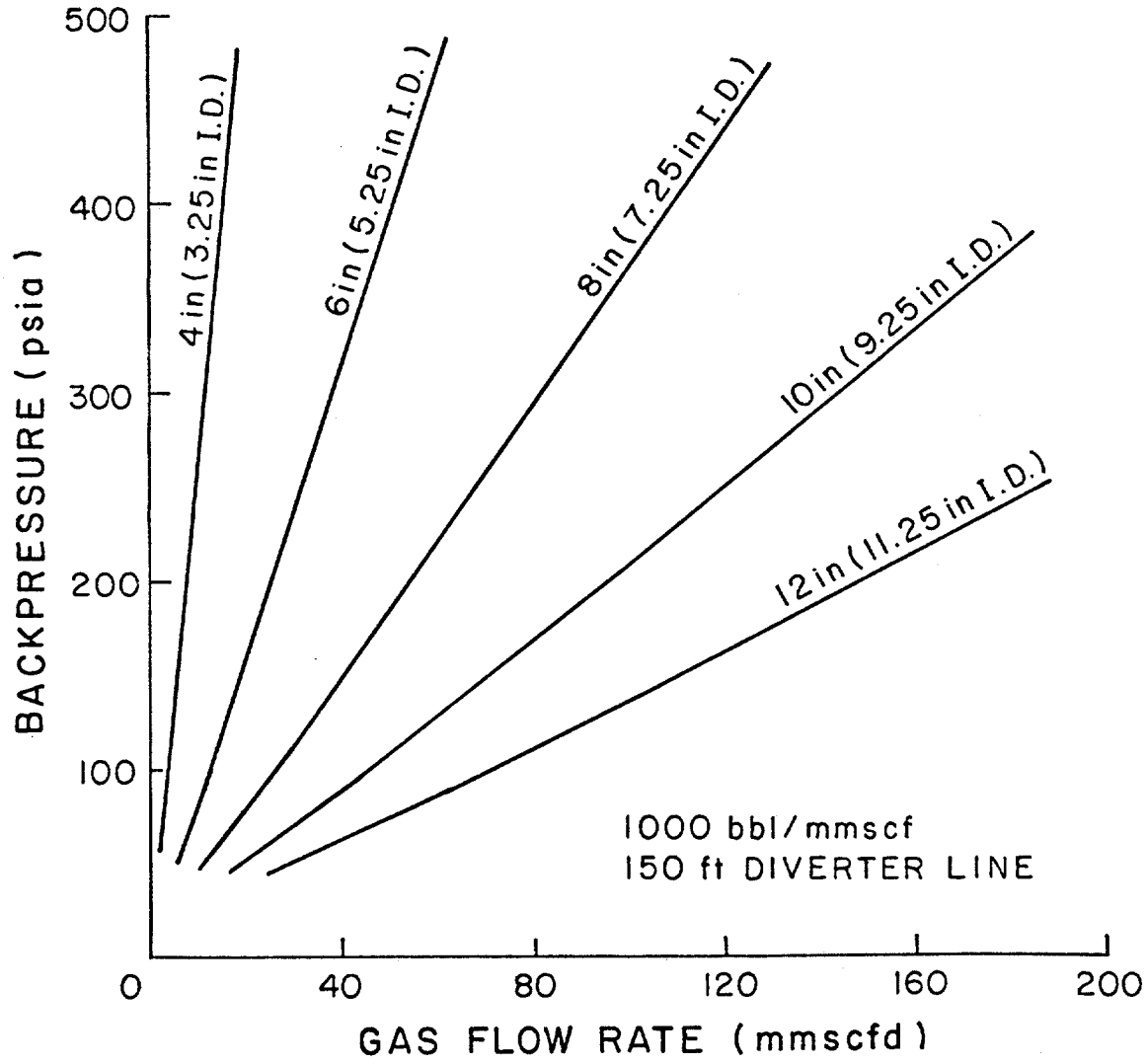

Figure 3.13. Backpressure as a Function of Flow Rate for Various Diverter Diameters (1000 bbl/MMSCF)

diameter lines to almost 40 percent in the larger diameter lines. The difference between the two methods is more pronounced in two-phase flow.

It is concluded that critical flow effects should be accounted for in diverter backpressure calculations and that acceleration effects should not be neglected in these calculations. Calculation procedures presented in this chapter can be used to calculate the backpressure placed on a well by a diverter system with more accuracy than was previously available. However, there remains the problem of estimating the flow rate at which to design the diverter system. Chapter IV will present a method by which the flow rate expected during diverter operations can be estimated and applied to the deisgn of the diverter system.

CHAPTER IV

SYSTEMS ANALYSIS OF DIVERTER OPERATIONS

4.1 Introduction

Methods presented in Chapter III concentrated on the accurate calculation of the backpressure placed on a well by a diverter system. Backpressure can be calculated at any flow rate of interest, but the question remains as to what that flow rate is. Flow rates that can be expected during diverter operations are dependent upon the diverter vent line geometry, the geometry of the wellbore, and the characteristics of the reservoir from which the well has blown out. The diverter system will function under flow rates dictated by the reservoir and the well itself, and should be designed as such.

A successful diverter design should insure flowing pressures in the well, from the reservoir to the diverter exit, that will not fracture exposed formations or exceed the working pressures of the surface equipment in the diverter system. This chapter will develop a design procedure, based on wellbore geometry and reservoir characteristics, resulting in the estimation of the pressures applied to the diverter system. The procedure will also provide a means of integrating the design of the diverter system into the design of the well, thus preventing or protecting against high wellbore pressures that could fracture formations.

4.2 Systems Analysis

4.2.1 Production Systems Analysis

Petroleum production engineers commonly face complex design problems when completing a well. Tubing diameters, perforation

densities, reservoir parameters, and surface operating pressures all interact to govern the performance of a given well. "Systems analysis" is used to optimally design some of these parameters, as well as to predict the effects of others. Brown and Beggs (1977), Crouch and Pack (1980), and others have presented the theory of systems analysis of a producing well. This method has received widespread acceptance in the oil industry, and applications of systems analysis are still being developed. One such application is to diverter operations. A diverted well is similar to a producing well, allowing the methods used in production systems analysis to be modified and applied to a well flowing through a diverter system.

4.2.2 Theory of Diverter Systems Analysis

During diverter operations, the diverter, wellbore, and reservoir act as a single hydraulic system (Clark and Perkins, 1980). Flowing pressures within the system are constrained by the formation pressure and the pressure at the diverter exit. Figure 4.1 is a schematic of the diverter/wellbore/reservoir system, and shows the pressures and pressure losses that occur while the well is flowing. Pressure at any point in the well can be determined by summing pressure losses from either the exit or formation to a point of interest, or node point. Two equations can be written to calculate pressure at a node point. For example, if the node is the wellhead, flowing wellhead pressure, FWHP, as a function of flow rate, Q, can be written as the sum of

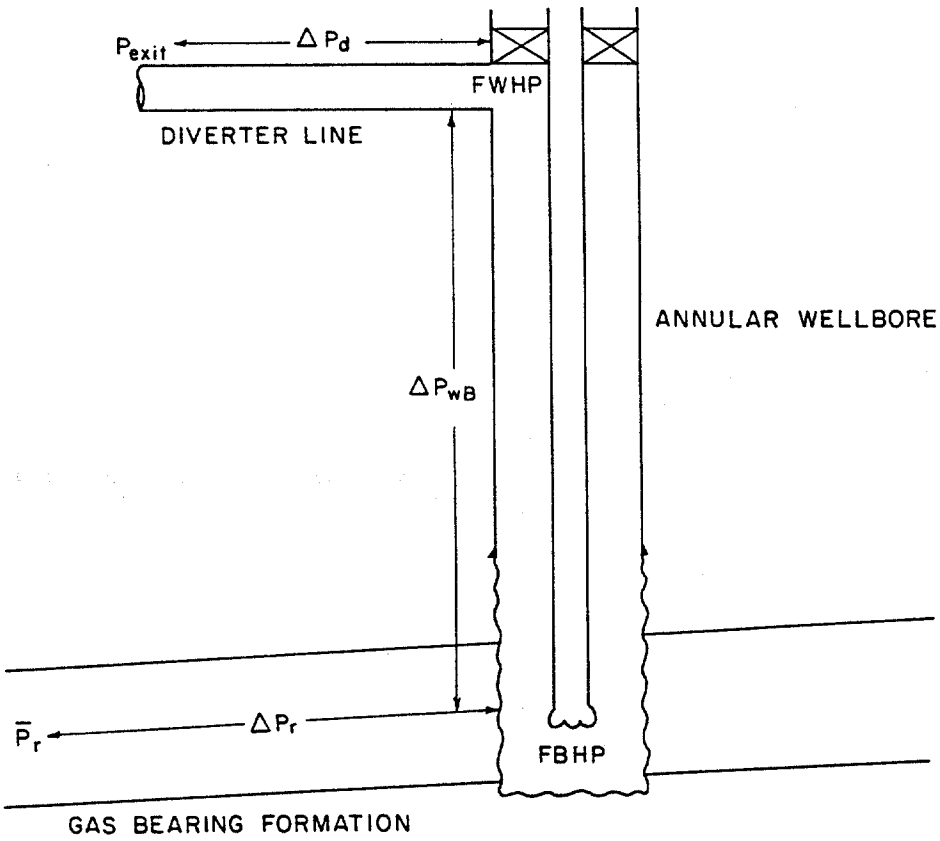

Figure 4.1 Schematic of Diverter/Wellbore/Reservoir System

the pressure losses downstream of the node plus the pressure at the diverter exit

$$FWHP\ (Q) = P_e(Q) + \Delta P_d(Q) \tag{4.1}$$

or as the sum of the pressure losses upstream of the node subtracted from the formation pressure

$$FWHP\ (Q) = P_r - \Delta P_r(Q) - \Delta P_{wb}(Q) \tag{4.2}$$

Only the formation pressure, Pr, is independent of flow rate, Q. The simultaneous solution of these equations results in the determination of a unique flowing wellhead pressure, FWHP, at a unique flow rate, Q. These values of flow rate and flowing wellhead pressure are those expected if the well is allowed to reach equilibrium conditions. The pressure profile of the well can be calculated, assuming a pressure traverse, from these values of flow rate and flowing wellhead pressure.

The node point can be chosen at any point in the well. If the node is placed at the bottom of the well, two equations, in terms of flowing bottom hole pressure, FBHP, can be written.

$$FBHP\ (Q) = P_e(Q) + \Delta P_d(Q) + \Delta P_{wb}(Q) \tag{4.3}$$

$$FBHP\ (Q) = P_r - \Delta P_r(Q) \tag{4.4}$$

The simultaneous solution of these equations will yield the same unique equilibrium flow rate as before, but flowing bottom hole pressure, rather than flowing wellhead pressure, will be determined.

The simultaneous solution of the two equations relating pressure drops about the node forms the basis of systems analysis, and can be obtained graphically. Each equation defines a "performance" curve, which relates flowing pressure at a node

point to flow rate. Figure 4.2 is an example of the graphical solution to equations 4.1 and 4.2. Flowing wellhead pressure is calculated by each equation at various flow rates. The two curves intersect at the flow rate and flowing wellhead pressure that would be observed if the well were allowed to attain equilibrium. This solution to the systems analysis is different from production systems analysis in that the well is allowed to flow to the atmosphere rather than to a set surface flowing pressure. The exit pressure, P_e, must be determined in diverter systems analysis, were as it is simply an assumed value in production systems analysis.

To perform the systems analysis, pressure traverses are used to calculate the pressure losses in the diverter and wellbore, while well known reservoir engineering techniques are applied to calculate pressure losses in the reservoir. Pressure losses must be calculated for horizontal and vertical flow of gas or gas/water mixtures, and the methods used must be applicable to the high flow rates that are generally expected during diverter operations. The possibility of critical flow exists, as discussed in Chapter III, and must be considered.

4.2.3 Dry Gas versus Gas-Water Flow

Either dry gas or gas/water flow may occur during a blowout from a shallow gas sand. The type of flow that occurs is dependent upon the presence of water bearing zones above the gas zone, or of an aquifer in the gas zone.

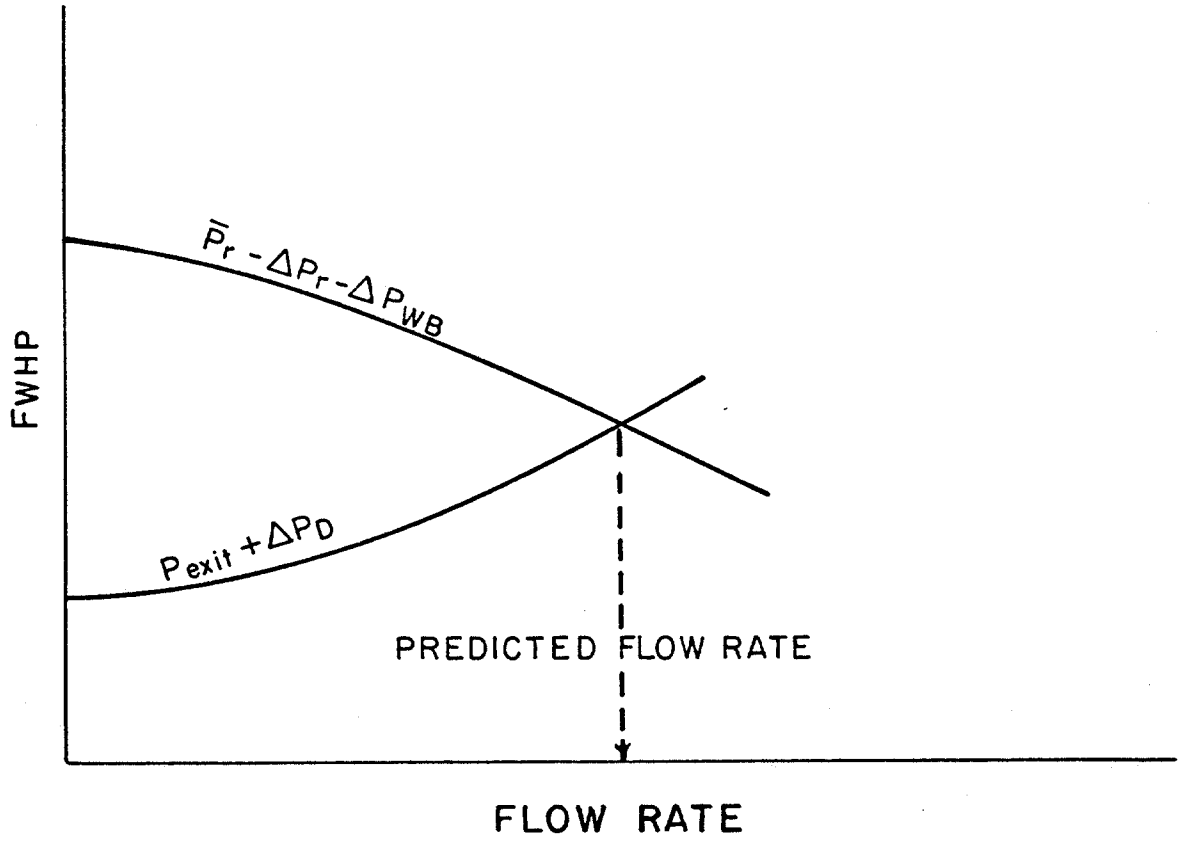

Figure 4.2 Graphical Solution of Systems Analysis

4.2.4 Critical Flow

Critical flow will result in an increase in pressure at the diverter exit. Chapter III presented methods of calculating the increase in pressure associated with critical flow, and these methods will be applied to calculate the pressure at the diverter exit, P_e (Q).

Dry Gas

Equation 3.3 related exit pressure to flow rate and critical velocity as

$$Q_g^* = \frac{V_g^* D^2 P_e T_{STD}}{2122 Z T_e P_{STD}} \qquad (3.3, 4.5)$$

This equation is most easily evaluated by assuming an exit pressure, calculating the critical velocity of the gas at that pressure, and then calculating the flow rate at that pressure. The calculated flow rate can then be used in a pressure traverse to calculate the other terms in the performance equation (as in eqns. 4.1 or 4.3), with the assumed exit pressure the starting point for the traverse. A single point on the performance curve will be calculated from the assumed exit pressure. By assuming other exit pressures, the complete performance curve will be generated. Calculating the performance curve in this manner is based on the assumption that flow will be critical at the diverter exit during diverter operations.

Gas/Water

Equation 3.10, presented in Chapter III, relates gas flow rate to exit pressure at a constant value of gas-liquid ratio. This equation

$$Q_g^* = \frac{V^* D^2}{\frac{2122.1\ z\ T\ P_{STD}}{P\ T_{STD}} + \frac{Y_w}{83.9}} \qquad (3.10)(4.6)$$

is applied in exactly the same manner as equation 4.5 to generate a performance curve based on critical flow at the diverter vent line exit. Gas-liquid ratios suitable for design work will be presented in Chapter VI.

4.2.5 Horizontal Flow

Methods of calculating pressure losses for horizontal flow in diverter vent lines were presented in Chapter III for both gas and gas/water flow. These methods should be employed to calculate the $\Delta P_d(Q)$ term in the performance equations.

4.2.6 Vertical Flow

The complete pressure gradient equation, equation 3.14, applies to vertical flow, and is used to calculate pressure losses in the wellbore, $\Delta P_{wb}(Q)$. Vertical flow differs from horizontal flow only in that hydrostatic pressure losses must be considered, and that special two-phase flow correlations apply.

Dry Gas Vertical Flow

The hydrostatic component of the pressure gradient in dry gas flow is based on gas density.

$$\left(\frac{\Delta P}{\Delta L}\right)_{Hyd} = \frac{g}{g_c}\rho_g \qquad (4.7)$$

Gas density is calculated from the real gas equation of state as

$$\rho_g = \frac{2.7\ P\ \gamma_g}{z\ T} \qquad (4.8)$$

The hydrostatic pressure gradient, along with the friction and acceleration gradients presented in Chapter III, is used in Equation 3.12, and the pressure traverse technique applied to calculate pressure losses for vertical flow.

Gas/Water Flow

Many two-phase flow correlations exist for vertical flow, but most employ inadequate means of accounting for acceleration losses. The method of accounting for acceleration losses in horizontal two-phase flow (Chapter III) is also applicable to vertical two-phase flow, and should be applied to high flow rate calculations. Elfaghi, et al. (1983), Lawson and Brill (1973), Vohra, et al. (1973), and others have shown that the Hagedorn and Brown vertical two-phase flow correlation (Hagedorn and Brown, 1964) is statistically the most accurate of the two-phase flow correlations. Elfaghi, et al., also showed that the Hagedorn and Brown correlation is applicable to annular flow, making it the most attractive correlation for use in drilling operations.

No-Slip Calculations

It has been observed that many of the vertical two-phase flow correlations apparently underpredict pressure losses at the flow rates expected during diverter operations. This is probably due to the fact that the high flow rates result in dimensionless

parameters that exceed those used in defining friction factors and liquid holdups in a given correlation. One alternative to using a two-phase flow correlation is to assume that slippage between the gas and liquid phase is negligible, allowing the methods used for gas flow to be applied to gas/water flow. The only modifications that need to be made are to use two-phase fluid properties in place of gas properties. A summary of recommended two-phase properties are presented in Appendix F. A study by Browne (1974) showed that, under conditions of high flow rate, no-slip calculations approach the accuracy of the correlations that assume slippage. When working with the high flow rate, no-slip calculations approach the accuracy of the correlations that assume slippage. When working with the high flow rates associated with diverter operations, the author feels that the no-slip assumption is probably more valid than many of the correlations, and more closely represents the pressure losses in the vertical wellbore. The no-slip assumption should be used when no-slip calculations result in a higher pressure loss than do the correlation calculations.

4.2.7 Reservoir Flow

Pressure losses in the reservoir can be calculated by Darcy's law:

$$\Delta(P^2) = \frac{Q_g \, Tz}{703 \times 10^{-9} \, KH} \ln \left(\frac{r_e}{r_w} \right) \qquad (4.9)$$

However, extremely high flow rates can cause pressure losses near the wellbore that are not included in Darcy's law. Jones (1974) presented an equation that accounts for pressure losses due to

non-Darcy flow, and this equation is commonly used to predict the inflow performance of the reservoir, (the $P_r(Q)$ term in equations 4.2 and 4.4). Jones' equation is given as

$$\Delta(P^2) = AQ + DQ^2 \tag{4.10}$$

where

$$A = \frac{1.424\ \mu_g\ z\ T}{KH} \left[\ln \left(.472 \frac{r_e}{r_w}\right) + S \right] \tag{4.11}$$

$$D = \frac{3.16 \times 10^{-18} \beta \gamma_g\ z\ T}{H^2} \left(\frac{1}{r_w} - \frac{1}{r_e} \right) \tag{4.12}$$

This equation contains many variables, such as permeability and reservoir thickness, that are not known when design work is being performed. The worst case, or maximum expected values of these variables should be assumed when applying this equation.

4.2.8 Analysis of Complex Geometries

The procedures presented thus far allow critical flow to be accounted for only at the diverter exit. The possibility exists that critical flow will occur at some point in the wellbore, particularly at a change in wellbore geometry. Systems analysis can be used to predict the occurrence of critical flow downhole, thereby providing a design procedure applicable to a variety of situations that may be encountered while drilling the surface hole.

Basic systems analysis requires two performance curves to be calculated. To investigate the possibility of critical flow within the well a third equation is needed. Critical flow downhole is governed by the same equations governing critical

flow at the diverter exit, eqns. 4.5 or 4.6. If the conditions of pressure and flow rate result in velocity calculations in the wellbore greater than critical velocity, flow will be restricted at the point critical velocity is attained. The third equation used in systems analysis is thus eqn. 4.5 (or 4.6, depending on single or two-phase flow) evaluated at the flowing pressure of the node point rather than at the exit. The node is thus placed at the point where critical flow is suspected to occur. A system of three equations can be developed relating pressure losses about a node point and critical pressures. For a node point at any location in the well, flowing node pressure, FNP(Q), can be determined as

$$FNP(Q) = P_e(Q) + \Delta P_d(Q) + \Delta P_{wb_1}(Q) \tag{4.13}$$

or as

$$FNP(Q) = P_r - \Delta P_r(Q) - \Delta P_{wb_2}(Q) \tag{4.14}$$

where $\Delta P_{wb_1}(Q)$ is the pressure drop in the section of wellbore downstream of the node, and $\Delta P_{wb_2}(Q)$ is the pressure drop in the section upstream of the node. These relationships are seen in Figure 4.3.

A third equation can be written for critical pressure at the node

$$FNP(Q) = P^* \tag{4.15}$$

where P* is the pressure at which flow is critical at the node. P* must therefore meet the critical conditions imposed by equations 4.5 or 4.6 for dry gas or two-phase flow, respectively. These equations can be evaluated at nodal conditions and geometry

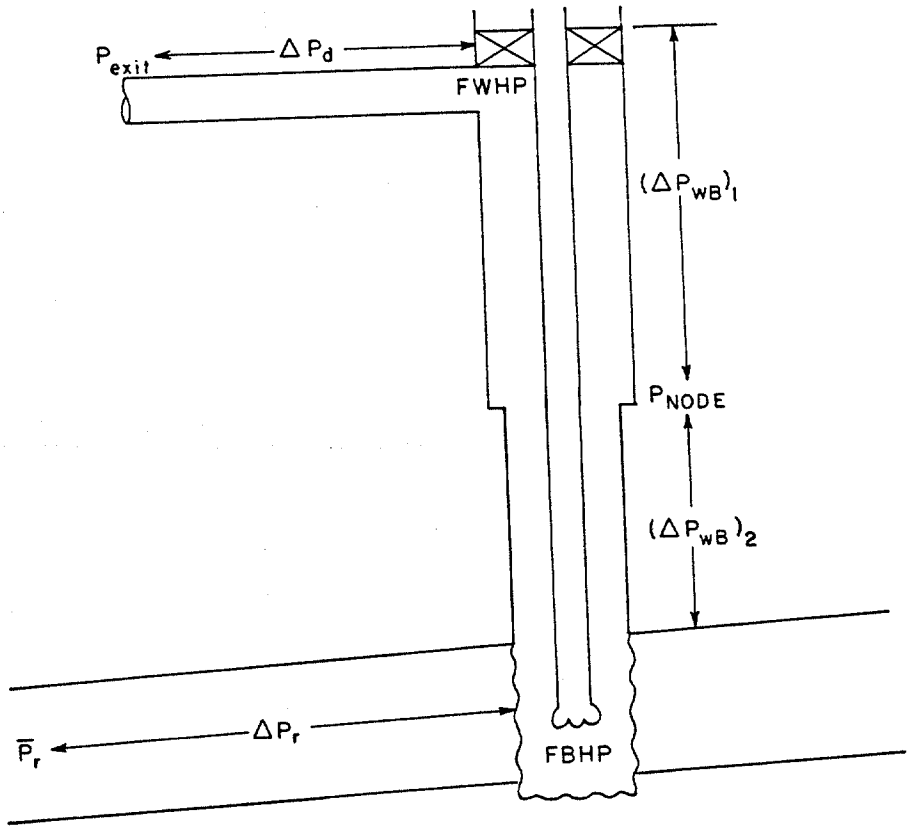

Figure 4.3 Schematic of Diverter/Wellbore/Reservoir System Showing Nodal Locations and Pressure Drops

to generate a performance curve of critical flow rate and critical pressure.

The flow rate of the well will be controlled by the first, or farthest upstream occurence of critical flow in the well. If critical velocity occurs in the wellbore, flow rate will be restricted at that point, and pressure at that point will be defined by equation 4.15. Therefore, if flow is critical at the chosen node, eqns. 4.14 and 4.15 are the equations applicable to the systems analysis, and their simultaneous solution results in the determination of flow rate and flowing pressure at the node. If flow is not critical at the node, Eqns. 4.13 and 4.14 provide the solution to the systems analysis, and the method is identical to that previously described. To investigate the possibility of critical flow, the node point must be placed at the point suspected of causing critical flow, and the systems analysis performed.

Figure 4.4 presents the graphical solution to the procedure just described. All three performance curves can be calculated, resulting in two points of intersection. The lowest flow rate resulting from the intersection of the curves will be the flow rate of equilibrium, and the presence of critical flow determined. If the intersection of Eqns. 4.14 and 4.16 result in the lowest flow rate, flow is critical at the node. A pressure drop will occur at the node, the magnitude of which is determined by the difference between the pressures on the performance curves defined by Eqns. 4.13 and 4.15 at the equilibrium flow rate. This pressure drop can be seen graphically in Figure 4.4.

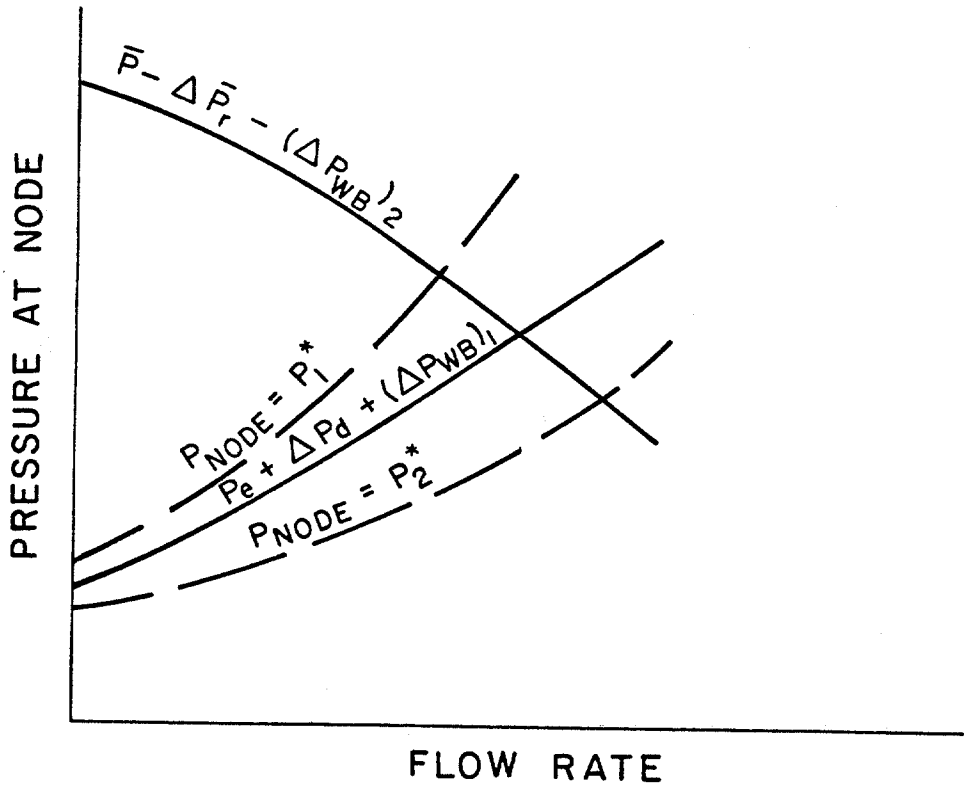

Figure 4.4 Graphical Solution to Complex Geometry Systems Analysis

Although flow is critical downhole, it can also remain critical at the diverter exit. In that case, flow at the exit would not control the flow rate of the well, but would affect the pressure profile of the well.

4.3 Applications to Design

Use of systems analysis on a diverter/wellbore/reservoir system results in immediate design applications. If the systems analysis is performed with the node at the wellhead, the resulting flowing wellhead pressure provides a basis for determining the operating pressure of the system. The working pressure of the annular preventer and valve system can be chosen to insure that these components maintain their integrity under the conditions imposed by diverter operations.

The equilibrium flow rate and pressure found from the systems analysis can be used to initiate a pressure traverse, which will then be used to determine the pressure profile in the well during diverter operations. This pressure profile can be compared to the fracture pressures of the exposed formations to determine the fracture load placed on the formations by the diverter system. If the pressure at a point in the well, opposite exposed formation, is greater than the fracture pressure, the formation is in danger of fracturing and broaching back to the surface. Steps can be taken to either decrease the backpressure on the well, thereby relieving the load on the formation, or to protect the exposed formation by increasing the setting depth of the conductor casing. Systems analysis allows the design of the diverter system, in terms of backpressure, to be coupled

with the design of the well, which is in terms of conductor depth. This method provides a means of designing the conductor casing which to date has not been recognized.

CHAPTER V

A COMPUTER PROGRAM FOR DIVERTER SYSTEMS ANALYSIS

5.1 Introduction

The procedures presented in Chapter IV require numerous calculations and numerical methods that are best performed on a digital computer.

A computer program was written in FORTRAN to perform the systems analysis. The program can be used in the design of a specific well/diverter system or to investigate a wide variety of parameters that affect diverter system design or performance.

The theoretical methods previously presented have been incorporated into the program, and are summarized as follows.

5.2 Description of Computer Program

5.2.1 General Description

The systems analysis solution for the node position within the wellbore, presented in section 4.2.8, has been adopted for use by the program. The "node" can be placed at any position in the wellbore, from the wellhead to bottom hole, inclusive. This is accomplished by dividing the wellbore into two sections, one above the node ("upper section") and one below ("lower section"). The program automatically places the node at the top of the lower section of the wellbore.

As stated earlier, vertical two-phase flow correlations are suspected of underpredicting pressure losses at low gas-liquid ratios and high flow rates. To account for this behavior, both

no-slip and correlation calculations are performed for vertical two-phase flow. The method resulting in the largest pressure loss is selected by the program.

5.2.2 Flow Diagram and Description of Subroutines

A flow diagram of the main computer program is presented in Figure 5.1. The program is in modular form, calling main subroutines to generate specific parameters. The main subroutines are described below.

Subroutine "DIVPER"

Subroutine DIVPER calculates the performance curve for the diverter/upper wellbore. This subroutine calls the following subroutines.

Subroutine CRITQ - Critical flow rate (single or two-phase) is calculated from equations 3.11 and 3.12 for a given value of exit pressure.

Subroutine HDRYGA - A horizontal dry gas pressure traverse subroutine. Flowing wellhead pressure is calculated from values of exit pressure and flow rate provided by subroutine CRITQ. Equations 3.16 and 3.19 are used to calculate friction and acceleration losses, respectively.

Subroutine FWHPH - The two-phase version of HDRYGA. "FWHPH" uses the Dukler correlation to calculate frictional losses and equation 3.19 to calculate the acceleration losses.

Subroutine DGBHPV - A vertical dry gas pressure traverse subroutine. Flowing bottomhole pressure is calculated from

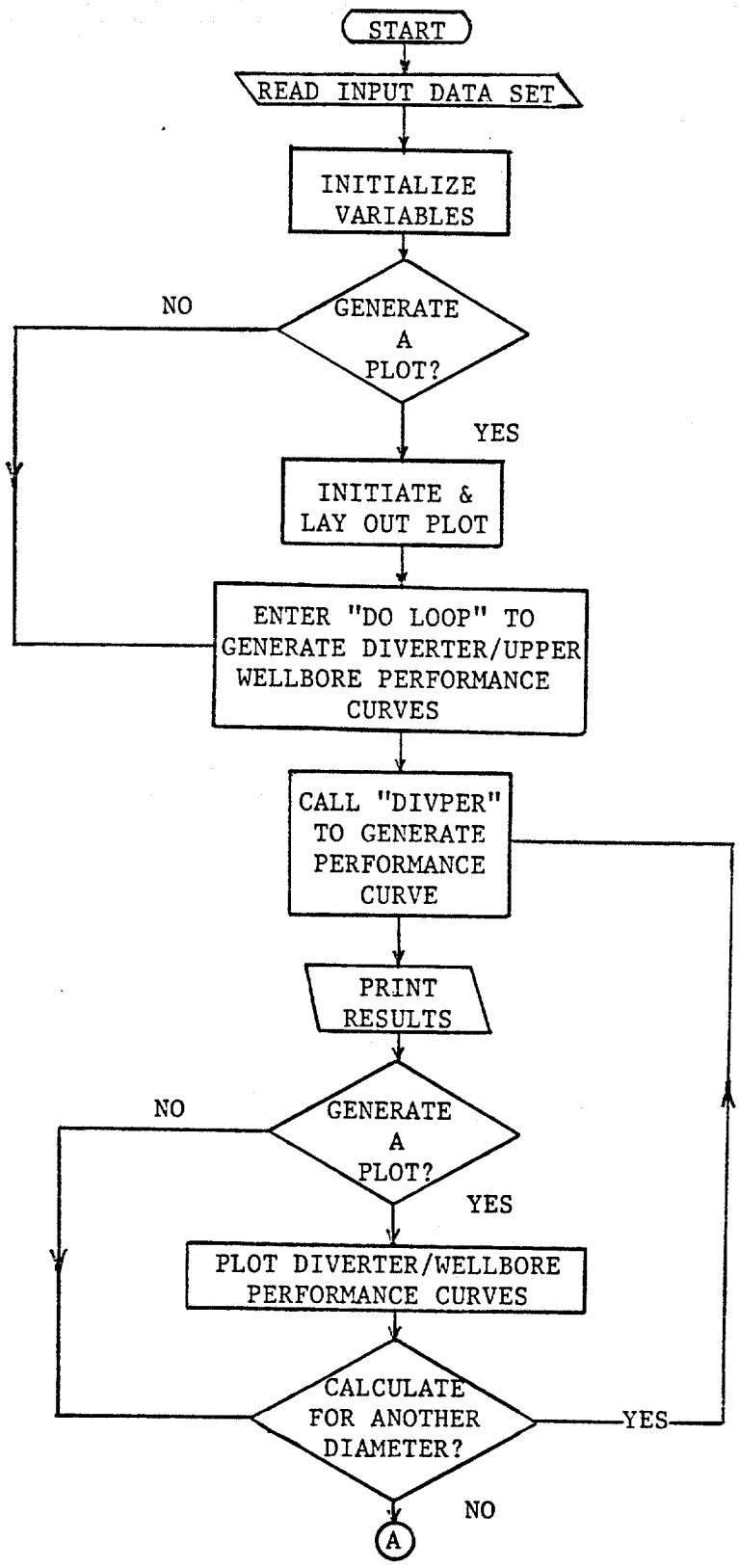

Figure 5.1 Flow Diagram of Main Computer Program

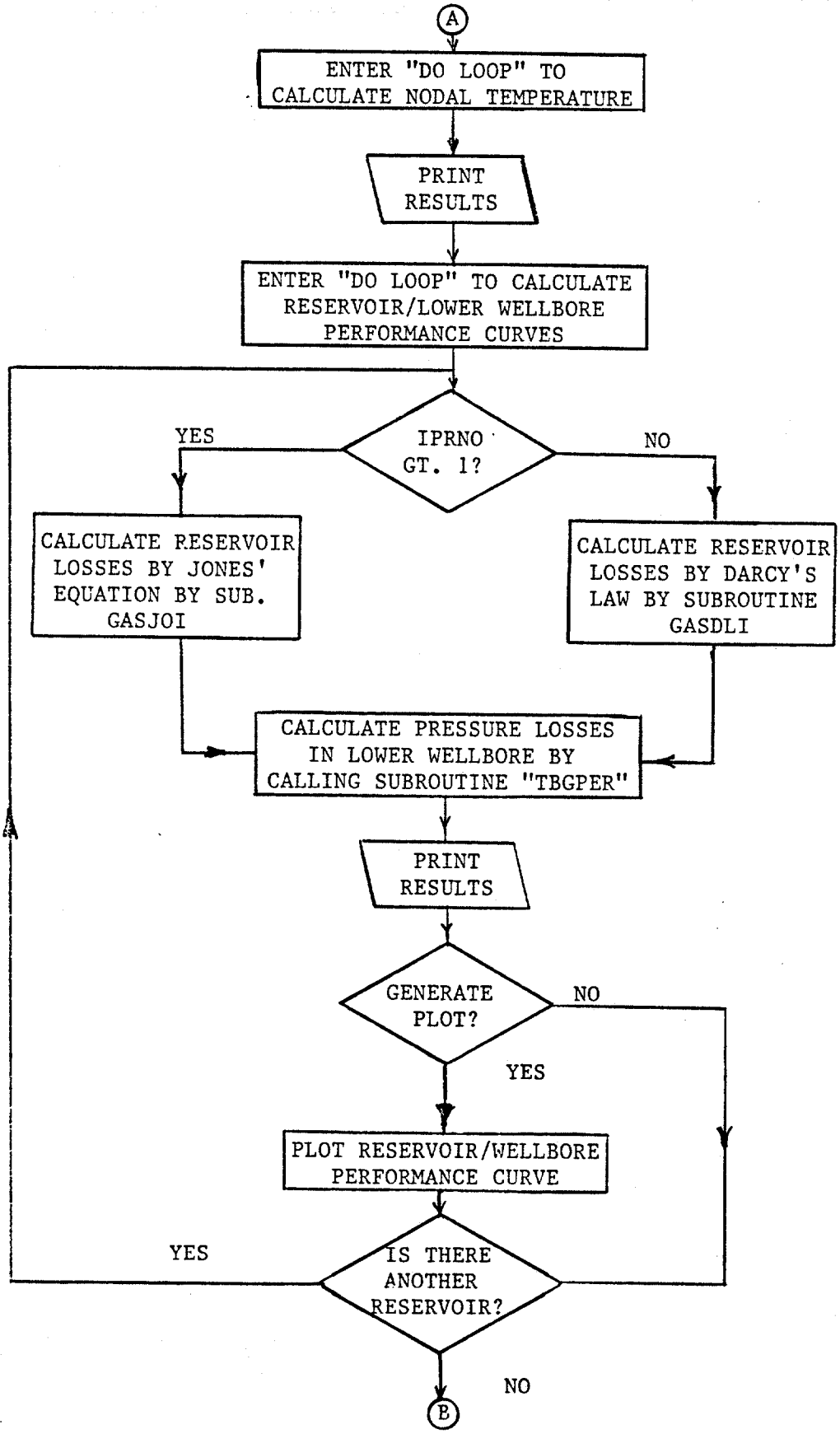
A
ENTER "DO LOOP" TO CALCULATE NODAL TEMPERATURE
PRINT RESULTS
ENTER "DO LOOP" TO CALCULATE RESERVOIR/LOWER WELLBORE PERFORMANCE CURVES
IPRNO GT. 1?
YES
NO
CALCULATE RESERVOIR LOSSES BY JONES' EQUATION BY SUB. GASJOI
CALCULATE RESERVOIR LOSSES BY DARCY'S LAW BY SUBROUTINE GASDLI
CALCULATE PRESSURE LOSSES IN LOWER WELLBORE BY CALLING SUBROUTINE "TBGPER"
PRINT RESULTS
GENERATE PLOT?
NO
YES
PLOT RESERVOIR/WELLBORE PERFORMANCE CURVE
IS THERE ANOTHER RESERVOIR?
YES
NO
B

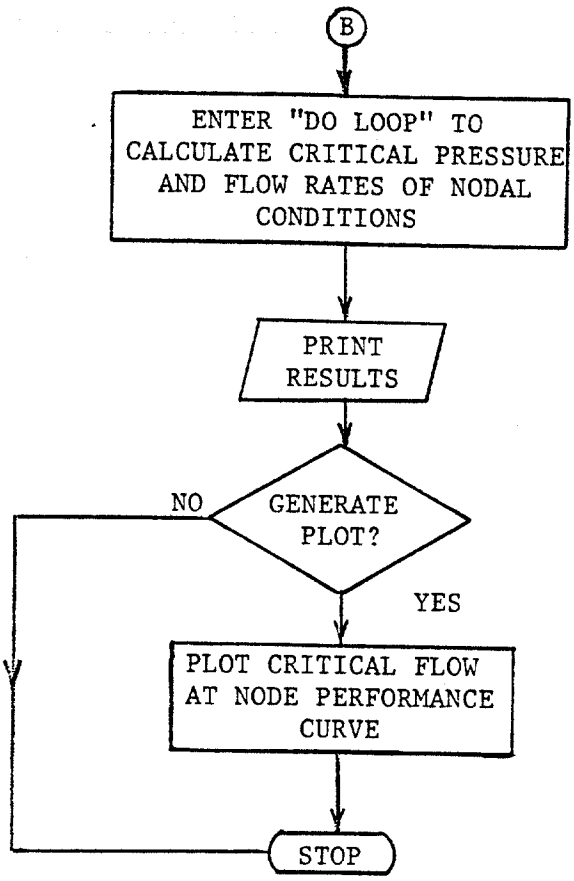
B
ENTER "DO LOOP" TO CALCULATE CRITICAL PRESSURE AND FLOW RATES OF NODAL CONDITIONS
PRINT RESULTS
GENERATE PLOT?
NO
YES
PLOT CRITICAL FLOW AT NODE PERFORMANCE CURVE
STOP

the value of flowing wellhead pressure provided by subroutine HDRYGA. Equations 3.16, 3.19, and 4.7 are applied to calculate frictional, acceleration, and hydrostatic pressure losses. DGBHPV is also capable of performing no-slip two-phase flow calculations.

Subroutine FBHP - The two-phase version of DGBHPV. The Hagedorn and Brown correlation is used to calculate frictional pressure loss gradients. The subroutine HAGBR provided by Beggs and Brill (1978) was slightly modified to allow calculations to continue near critical conditions. Equation 3.19 is used to calculate acceleration losses.

Subroutines GASDLI and GASJOI

These subroutines calculate pressure losses in the reservoir. GASDLI applies Darcy's law (equation 4.9) and GASJOI Jones' equation (equation 4.10). They were provided by David S. Sutton, Ph.D. candidate in the Department of Petroleum Engineering at Louisiana State University. Values of flow rate and flowing bottomhole pressure are saved for use in subroutine TBGPER.

Subroutine TBGPER

This subroutine combines reservoir pressure losses with pressure losses in the lower wellbore section, generating a performance curve for the reservoir/lower wellbore. The following subroutines are used.

Subroutine DRYGAS - A vertical dry gas pressure traverse. Calculates flowing surface pressure from a value of flowing bottomhole pressure calculated by GASDLI or GASJOI. Applies equations 3.16, 3.19, and 4.7 to calculate frictional, acceleration, and hydrostatic pressure losses. A second version, DRYGA2, performs the same functions for no-slip two-phase flow.

Subroutine FSPV - The two-phase version of DRYGAS. Uses the Hagedorn and Brown correlation to calculate frictional pressure loss gradients and equation 3.19 to calculate acceleration gradients.

5.2.3 Program Input

In addition to allowing the theory developed in this dissertation to be applied to a specific design problem, the program was written to provide a means of investigating the many parameters affecting the design and performance of a diverter system. Parameters that can be varied in the program include diverter and wellbore length and diameter, gas-liquid ratio, and reservoir parameters such as depth, pressure, thickness, and permeability. An input data set is used to specify these parameters, as well as to initialize many of the variables. The following is a description of the data required to run the program, presented in the order of occurence.

TSEP - Standard temperature in degrees Fahrenheit.

PSEP - Standard pressure in PSIA.

SGPG - Specific gravity of natural gas (air = 1.0).

SGW - Specific gravity of water (density, g/cc).

ANG - The angle of inclination (in degrees) of the diverter line (0 degrees for horizontal).

INC - The number of finite elements in to be used in the diverter calculations. A minimum of 1 foot increments are recommended.

YWAT - The water yield of the gas, or inverse GLR, in BBL/MMSCF.

JJJ - Flow type indicator. 0 for two-phase flow, 1 for dry gas flow.

ST - Surface flowing temperature, deg. Fahrenheit.

BHT - Flowing bottom hole temperature, deg. Fahrenheit.

TVD - The true vertical depth of the well, in feet.

VANG - The inclination angle of the wellbore, in degrees. (Vertical is 90 degrees.)

NSU - The number of geometrical sections in the upper wellbore. This allows the wellbore geometry to change. A maximum value of 5.

NSL - The number of geometrical sections in the lower wellbore. Analogous to NSU. A maximum value of 5.

NUMPNC - The number of points to be calculated for the critical node pressure performance curve.

XMIN - A plotting parameter. Defines the minimum value on the x-axis. Usually taken as 0.

YMIN - Same as XMIN, but applies to the y-axis.

XL - A plotting parameter. The length of the x-axis, in inches.

YL - A plotting parameter. The length of the y-axis, in inches.

XAINC - This variable determines the number of points calculated in the diverter/upper wellbore performance curve. It is defined by:

# of points - QMAX*10/XAINC

set not to exceed 600.

NUMDEX - The number of diverter lines to be investigated. A maximum value of 20 is allowed.

NUMREX - The number of reservoirs to be investigated. A maximum value of 6 is allowed.

DEH - Reservoir thickness, in feet.

RPERMG - The relative permeability to gas of the formation.

TRES - Reservoir temperature, degrees Fahrenheit.

RE - Reservoir radius, in feet.

RW - Wellbore radius, in feet.

SKN - The skin factor in the reservoir. Usually taken as 0.

DEHP - Depth drilled into the reservoir, in feet.

PMAX - A plotting parameter. It is a rough estimate of the maximum pressure value expected. (1000, 2000 psia is usually used.)

QMAX - A plotting parameter. Analogous to PMAX. (100, 200, 400 MMSCFD are usually sufficient.)

ISHAPE - Reservoir shape factor, after Odeh (1978).

ISHAPE	RESERVOIR SHAPE
1	circle
2	square
3	hexagon
4	triange

SAREA - The surface area of the reservoir, in acres.

AINC - This variable determines the number of points calculated for the reservoir/lower wellbore performance curve. It is defined by:

# of points = QMAX*10/AINC

set AINC so that # of points does not exceed 600.

NPPRT - The number of points on the reservoir/lower wellbore performance curve to be printed out.

IPLOT - This variables chooses whether or not to create plotted output. If IPLOT is not equal to 1, a plot will not be generated.

IPRNO - Determines the reservoir equation used to calculate pressure losses. If IPRNO equals 1, Darcy's law will be applied. To use Jones' equation, set IPRNO greater than 1.

DO - The outer diameter of the diverter, inches. Must be read in NUMDEX times.

DI - The inner diameter of the diverter, inches. Usually taken as 0. Must be read in NUMDEX times.

T - The flowing temperature of the diverter line, deg. Fahrenheit. Must be read in NUMDEX times.

XLEN - Diverter line length, feet. Must be read in NUMDEX times.

DOVU - The outer diameter of the upper wellbore, in inches. Must be read in NSU times.

DIVU - Inner diameter of th upper wellbore, in inches. Must be read in NSU times.

INCRU - The number of finite elements in the upper wellbore section. Must be read in NSU times.

XLENSU - The length of the upper wellbore section, in feet. Must be read in NSU times.

DOVL, DIVL, INCRL, XLENSL - Lower wellbore geometry terms perfectly analogous to upper geometry terms.

PERMR - Reservoir permeability, millidarcies. This value must be read in NUMREX times.

PRES - Initial reservoir pressure, PSIA of maximum value of 6 is allowed, and NUMRES values must be read in.

Data is input into the program via a data set. The data is read into the program in the following order:

```
TSEP,PSEP,SGPG,SGW
ANG,INC,YWAT,JJJ
ST,BHT,TVD,VANG,NSU,NSL,NUMPNC
XMIN,YMIN,XL,YL,XAINC,NUMDEX,NUMREX
DEH,RPERMG,TRES,RE,RW,SKN,DEHP,PMAX
QMAX,ISHAPE,SAREA,AINC,NPPRT
IPLOT,IPRNO
```

The following diverter geometry data is read in within a "DO LOOP". NUMDEX lines must be read in.

DO,DI,T,XLEN

The following wellbore geometry terms are also read in via a "DO LOOP". NSU lines are required for the upper wellbore data, and NSL lines for the lower wellbore data.

DOVU,DIVU,INCRU,XLENSU

DOVL,DIVL,INCRL,XLENSL

Reservoir permeability and pressure are read in with a "DO LOOP", requiring NUMREX lines.

PERMR PRES

PERMR and PRES are the last of the input data.

Node Position

The position of the node is determined by the geometry terms for the upper and lower wellbore. The node is automatically positioned at the top of the lower wellbore section. Section lengths less than 10 feet are ignored by the program. Therefore, to place the node at the bottom of the well, set NSL = 1, and XLENSL less than 10 feet. To place the node at the wellhead, set NSU = 1 and XLENSU less than 10 feet. The position of the node within the well is determined by the combination of upper and lower geometry terms.

If multiple sections are used within either the upper or lower wellbore, the order of entry of the gometry terms is important. Upper wellbore geometry is entered from the upper section (larger diameter) to lower section (smaller diameter). Lower wellbore geometry is entered from the lower section (smaller diameter) to the upper section (larger diameter).

5.2.4 Program Output

Graphical

The program provides optional output to the Benson plotter. An example of the plotted output of the program is provided in Figure 5.2. In this example, the wellhead served as the node, and the performance curves represent eqns. 4.1 and 4.2. As can be seen on the figure, an equilibrium flow rate of 151 mmscfd and flowing wellhead pressure of 120 psia is predicted for the particular set of input conditions used.

Printed

Printed output is provided by the program. Individual values of flow rate and pressure are printed for each performance curve. An example of the printed output is presented in Figure 5.3.

5.3 Exploitation Program

A second program was developed to exploit the information gained from the first program. This program is nearly identical to the first program; the output has been changed to show wellbore pressure profiles. This program calculates the pressure profile in the well from the flow rate and flowing pressure obtained form the systems analysis, and compares the profile to the fracture pressure of the formations. The fracture pressure is determined by the method suggested for offshore areas by Constant and Bourgoyne (1986). Figure

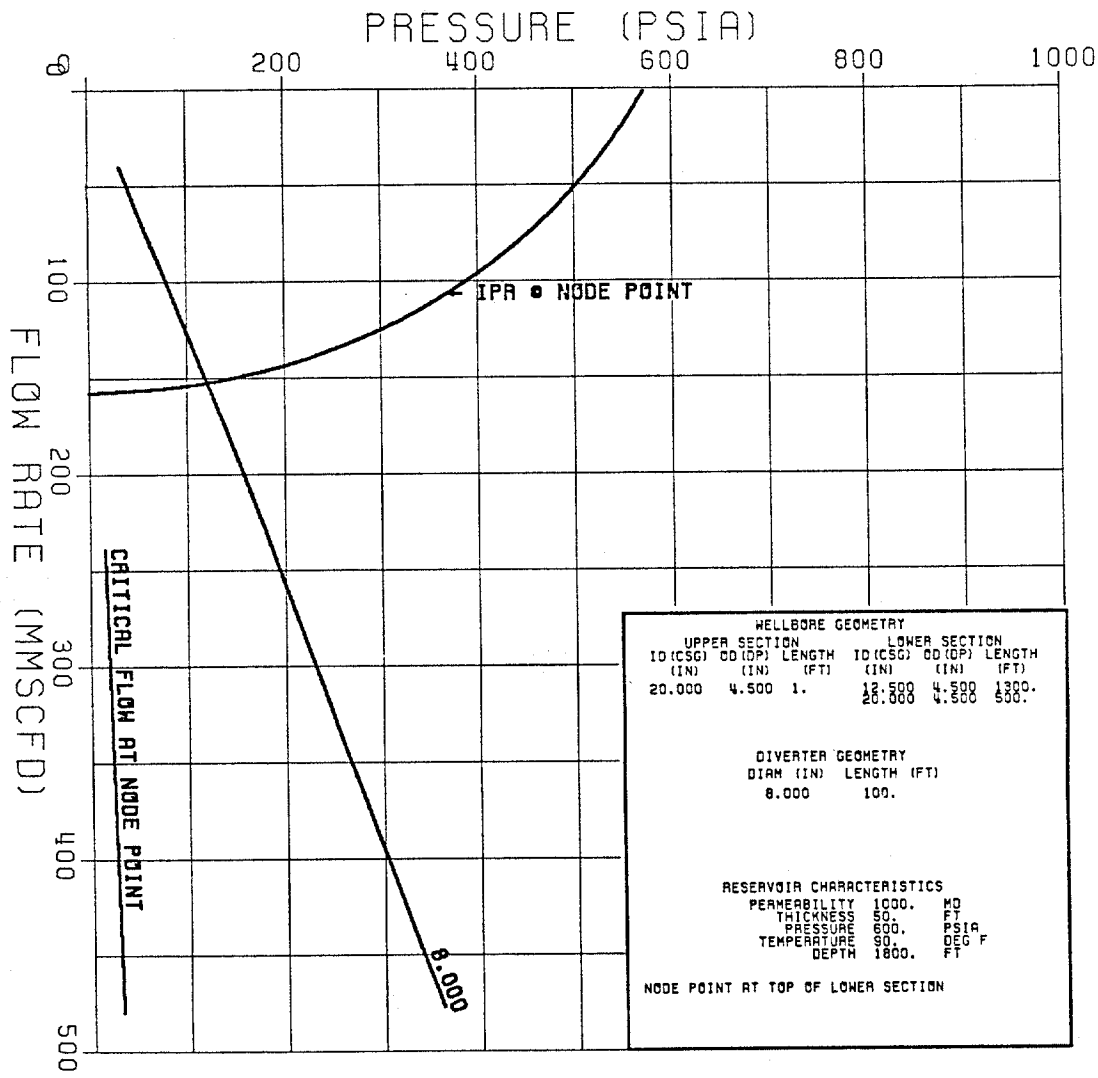

Figure 5.2. Example of Main Program Output to Benson Plotter

```
INPUT DATA SET IS:

 60.  14.7  .65  1.07
 0. 100  .0001    1
 80.  90.  1150.  90.  1 2  500
 0.  0.  10.  10.  10.  1  1
 600.  50.  1.  90.  3000.  .5  0.   50.  1000.
 200.  1  650.  10  5
  1   2
 6.  0.  80.  100.
 28.   4.5  20 1.
 9.875 4.5   20   660.
 28.0  4.5   20   490.
 1000.

 VALUES OF DIVERTER PERFORMANCE CURVE

        DIVERTER DIAMETER =  6.000

    PEXIT      PNODE       Q
      15.        35.      -23.
      25.        59.      -38.
      35.        82.      -53.
      45.       105.      -68.
      55.       129.      -84.
      65.       152.      -99.
      75.       175.     -114.
      85.       197.     -129.
      95.       219.     -145.
     105.       241.     -160.
     115.       264.     -176.
     125.       286.     -191.

 VALUES OF LOWER WELLBORE/RESERVOIR PERFORMANCE CURVE

 PERMEABILITY =  1000.

     FLOW RATE    BHP     NODE P

         0.0      600.     582.
       -10.0      588.     570.
       -20.0      575.     557.
       -30.0      561.     542.
       -40.0      545.     525.
       -50.0      529.     507.
       -60.0      510.     487.
       -70.0      491.     464.
       -80.0      469.     438.
       -90.0      445.     410.
      -100.0      418.     377.
      -110.0      389.     339.
      -120.0      356.     294.
      -130.0      318.     237.
      -140.0      273.     155.
```

Figure 5.3 Example of Main Program Printed Output

5.4 is an example of the output of this program, and shows that the setting depth of the conductor can be chosen based on the intersection of the fracture pressure curve with the pressure profile of the well.

Data Input

Additional data is required to run this program. Solutions to the systems analysis for the first run of the program result in flowing pressures and flow rates. These values must be input into the exploitation program. Information used to calculate formation fracture pressures must also be input. Input variables not previously described as as follows.

NUMEX - The number of solutions to the systems analysis that will be investigated by the program. NUMEX pairs of flow rate and pressure will be required by the program.

ECDMAX - A rough estimate of the maximum value of equivalent density (in ppg) that will occur in the well. Used as a plotting parameter.

DMAX - The maximum depth (in feet) of the well. Usually taken as some value larger than total depth. Used as a plotting parameter.

DAIR - The depth or length (in feet) of the air gap between the water surface and the mud level in the well.

DW - The depth of the water (in feet) at the well.

GP - Formation pore pressure gradient (ppg).

PR - The porosity of the sediments at the surface.

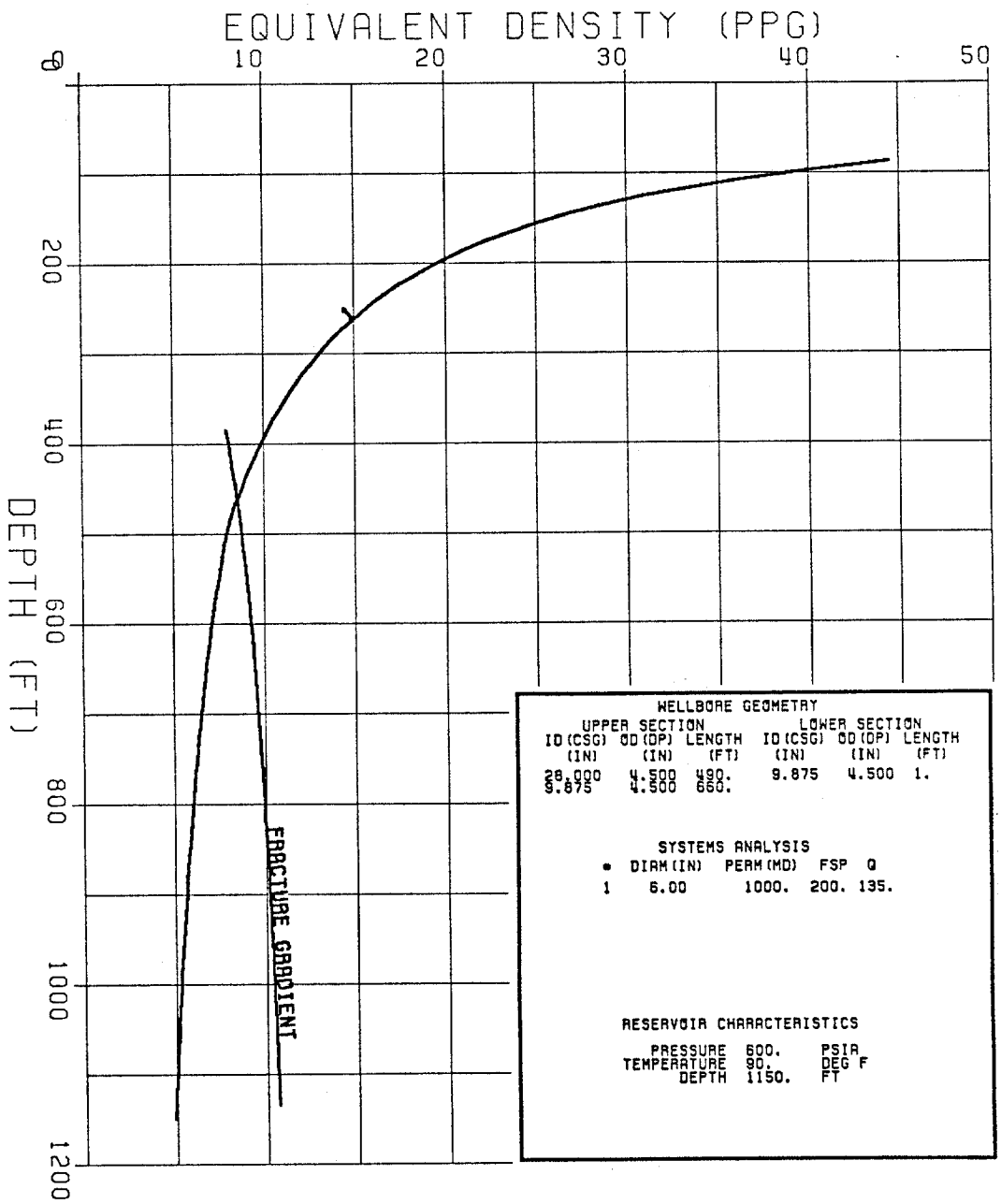

Figure 5.4 Example of Output of Exploitation Program

XK - The porosity decline constant for the formations. Units are FT^{-1}

NDEP - The maximum number of points to be calculated in the formation fracture pressure calcultions.

Q1 - The value of flow rate (MMSCF) taken from the systems analysis obtained from the original program.

PE - The pressure (psia) value of the systems analysis. This value does not have to be exit pressure.

Data Sets

The data set required to run this program must be of the following form.

```
TSEP,PSEP,SGPG,SGW
ANG,INC,YWAT,JJJ
ST,BHT,TVD,VANG,NSU,NSL
XMIN,YMIN,XL,YL,NUMEX
DEH,RPERMG,RE,RW,SKN,DEHP,ECDMAX
DMAX,ISHAPE,SAREA,DAIR,DW,GP
PR,XK,NDEP
IPLOT,IPRNO
```

The following diverter geometry and systems analysis data is read in within a "DO LOOP". NUMEX lines must be read in.

```
DO,DI,T,XLEN,Q1,PE,PERMR,PRES,TRES
```

The remainder of the data set description is identical to that of the original data set.

This program requires results from a systems analysis based on the node at either the wellhead or the bottom hole. Execution

time can be shortened by providing flowing wellhead pressure to the well, as opposed to exit pressure, and using diverter lengths or 1 foot. The program will run with identical wellbore geometry data sets as the original program.

5.4 Summary

The two programs described in this chapter incorporate the theoretical principles discussed in Chapters III and IV. By using these programs in combination, a proposed well plan can be evaluated in terms of diverter system and conductor casing requirements. In addition, a variety of conditions encountered during diverter operations can be investigated.

Chapter VI will apply the programs to investigate the possible causes of an actual diverter failure incident. The programs will be used to evaluate the cause of failure in the incident, as well as to investigate designs that would possibly correct the cause of failure.

CHAPTER VI

APPLICATION OF THEORY TO FIELD EXAMPLE

6.1 Introduction

The theoretical procedures outlined in Chapter IV and the computer programs described in Chapter V provide a means of designing both the diverter system, primarily in terms of vent line diameter, and the conductor casing, in terms of setting depth. Systems analysis can be used to perform case studies of diverter system failure to analyze failure modes and provide solutions to design flaws. This chapter will present an analysis of an actual incident of diverter failure, identifying the apparent cause of failure and presenting design improvements.

6.2 Description of Incident

The diverter accident analyzed occurred in the Gulf of Mexico offshore Texas in approximately 300 ft. of water. The diverter system was attached to 30 in. (1 in. wall thickness) drive pipe, which was set to 490 ft. The drive pipe thus functioned as conductor pipe. The diverter system consisted of two 6 in. vent lines. A 9.875 in. pilot hole was drilled to 1150 feet. The well plan called for enlarging the hole to 20 in. to set the conductor casing. However, gas was encountered at 1150 ft., and a kick was taken while pulling drill pipe out of the hole, causing the well to blow out. The diverter system was actuated and both 6 in. vent lines were opened. The rig was evacuated, and was lost shortly thereafter when the foundation of the rig failed and the rig sank. The well flowed until finally bridging over six days later.

This incident apparently resulted in formations fracturing and weakening the rig foundation to the point of collapse. The computer programs previously discussed were used to determine the pressure in the well during the blowout to evaluate the performance of the diverter system and the effectiveness of the conductor pipe. Design considerations investigated include the presence and magnitude of two-phase flow, formation capacity, flowing surface pressure, flow rate, fracture pressure, and casing setting depth.

6.3 Systems Analysis

The diverter incident in question presents a different form of the previously discussed systems analysis in that both diverter lines were functioning during the blowout. By placing the node at the wellhead, the systems analysis of two vent lines of equal diameter and length is given as the simultaneous solution of the following equations:

$$P_{node} = P_e(Q1) + \Delta P_d(Q1) \tag{6.1}$$

$$P_{node} = \bar{P}_r - \Delta P_r(Q2) - \Delta P_{wb}(Q2) \tag{6.2}$$

$$Q2 = 2\ Q1 \tag{6.3}$$

where Q1 is the flow rate in a single vent line, and Q2 the total flow rate of the well.

These equations recognize that the flow in the well will be equally divided into each identical vent line. The solution to these equations is identical to that previously discussed, except the diverter performance, determined in terms of Q1, must be expressed in terms of Q2, or twice that of Q1. For example, if a single 6 in. diverter line requires 150 psi to flow 50 MMSCFD, two lines will flow

twice the rate, or 100 MMSCFD, at the same 150 psi pressure requirement. The systems analysis of dual vent lines is performed by doubling the flow rate of the diverter performance curves. The computer program was thus altered to perform the systems analysis.

6.4 Systems Analysis Results

The reason for this analysis was to show that, under acceptable design assumptions, the pressure in the wellbore exceeded the fracture pressure of the exposed formations. Diverter and wellbore geometries were known; however, reservoir properties must be estimated, and the effects of two-phase flow determined. The systems analysis was performed under a wide range of permeabilities and gas-liquid ratios to determine the assumed conditions under which the formations would fracture. The results of the systems analysis are thus presented in terms of varying gas-liquid ratios and reservoir permeabilities.

6.4.1. Surface Pressure

There were no indications of failure in the surface equipment, indicating that surface pressures were below the operating pressure of the annular preventer. The results of this analysis support this observation. Figure 6.1 presents the results of the systems analysis in terms of flowing surface pressure and liquid yield (inverse GLR) at various assumed values of permeability. At the lower values of permeability, surface pressure increases with increasing liquid yield. However, at the higher values of permeability, surface pressure reaches a maximum

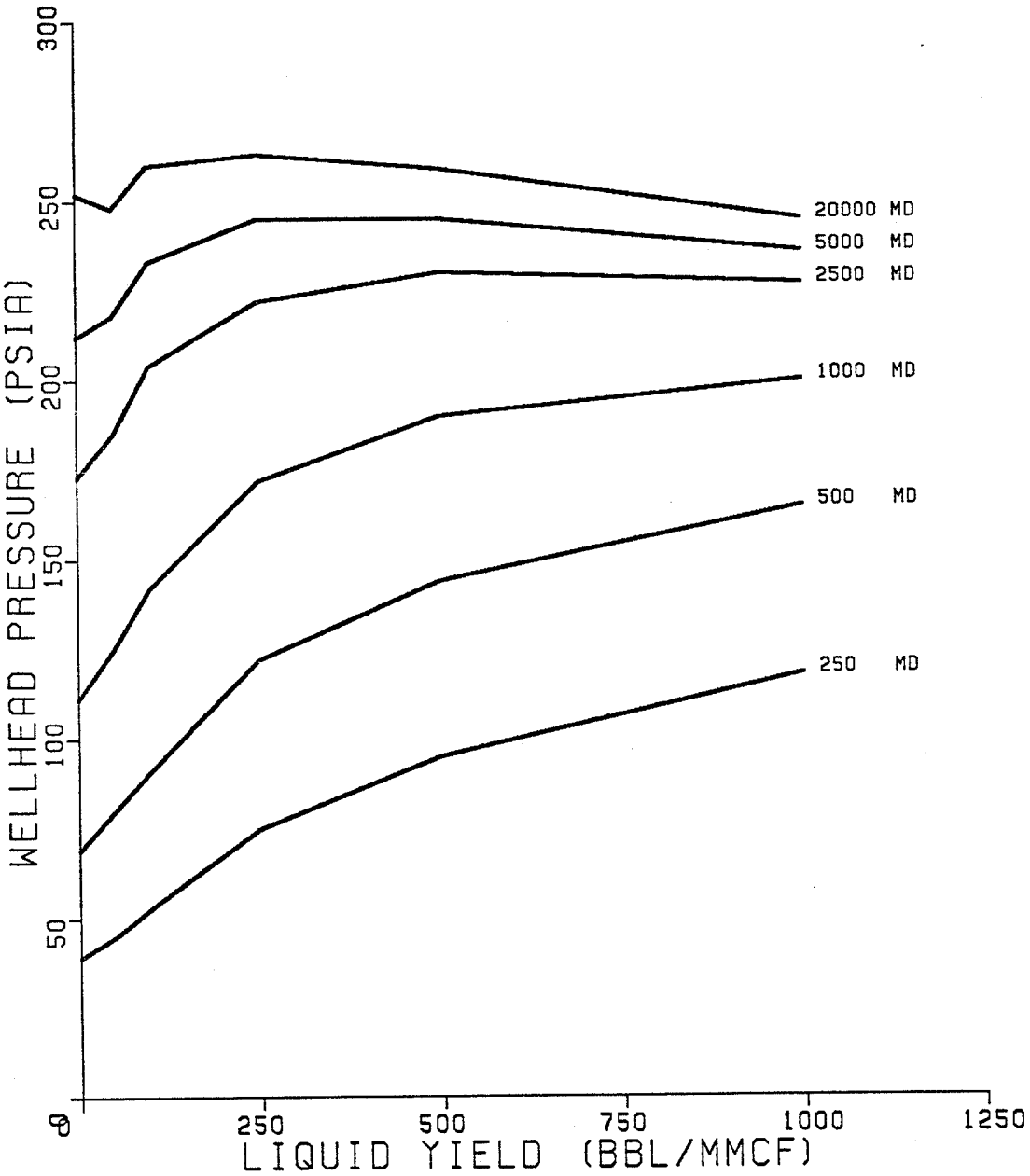

Figure 6.1 Flowing Wellhead Pressure as a Function of Liquid Yield and Permeability

at the intermediate values of liquid yield. Shallow gas sand permeabilities would be expected to exceed 5 darcy, resulting in maximum pressures at the intermediate values of liquid yield. This figure also shows a maximum pressure, at very high permeability, to be only about 265 psia, well below the working pressure of the annular preventer. Another point of interest is that dry gas flow, at higher permeabilities, results in flowing surface pressures only about 5 percent below the maximum predicted value. This fact is important because dry gas flow calculations are performed much more efficiently than are two-phase flow calculations, resulting in a savings in computer time needed to perform the systems analysis.

6.4.2. Flow Rate

The expected flow rate of the well, as determined from the systems anlaysis performed for various permeabilities and liquid yields, varies considerably with both liquid yield and permeability. Flow rate will be controlled by critical velocity, whcih is strongly dependent on liquid yield. The deliverability of the reservoir will also control the flow rate of the well, and is strongly dependent on reservoir permeability. Figure 6.2 presents flow rate as a function of liquid yield and permeability. The figure shows a strong dependence of flow rate on liquid yield. Dry gas flow, at higher permeabilities, results in approximately three times the flow rate of the maximum liquid yield studied.

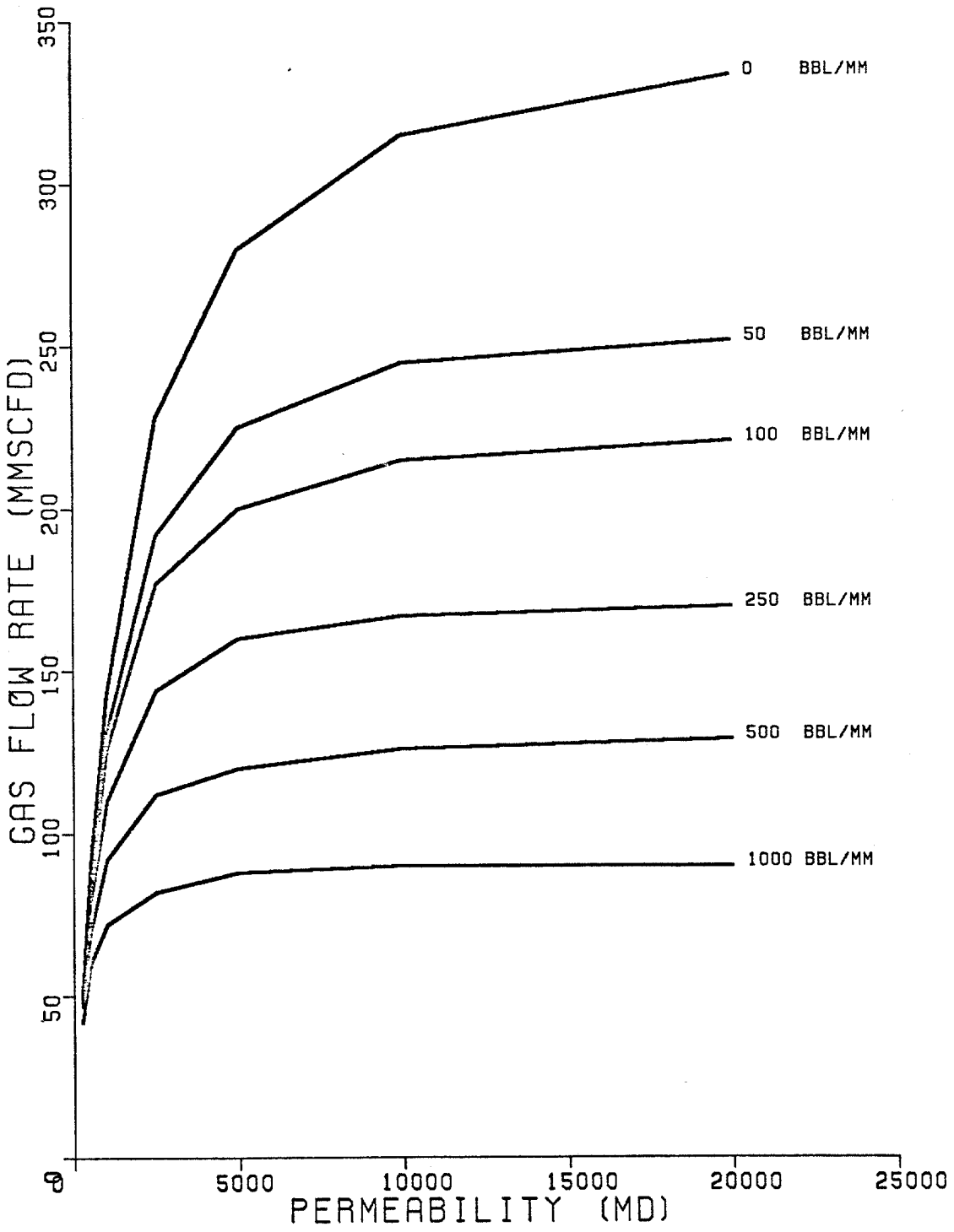

Figure 6.2 Flow Rate as a Function of Liquid Yield and Permeability

The wellbore apparently begins to restrict the flow rate at permeabilities greater than about 5 darcy, as a doubling of the permeability results in only a small increase in flow rate. A permeability assumption of about 10 darcy would then represent the highest permeability reservoir that could be encountered by this particular wellbore, as the well would perform essentially the same even if it were to encounter a more permeable reservoir.

6.4.3. Depth at Which Formation Fractures

Fracture depths, as obtained from the exploitation program, are shown in Figures 6.3a and 6.3b. Figure 6.3a presents fracture depth against liquid yield at various permeability assumptions. This figure shows two important features. First, at very high permeability values, dry gas presents the deepest depth of fracturing within the wellbore, with little or no change in fracture depth for various liquid yield assumptions. At an assumed permeability of 20 darcy, the well would first fracture at approximately 900 ft., or over 400 ft. below the drive pipe shoe. This figure also shows that, for extremely low assumed permeabilities, there is no casing depth requirement for the diverter system. These values of permeability, however, are far below those expected at the depth of the example reservoir.

Figure 6.3b represents the results of the systems analysis as fracture depth versus permeability, at various liquid yield rates. This figure also shows two important features. A minimum permeability of three darcy will fracture the formation at the drive pipe shoe (or deeper) at any assumed liquid yield.

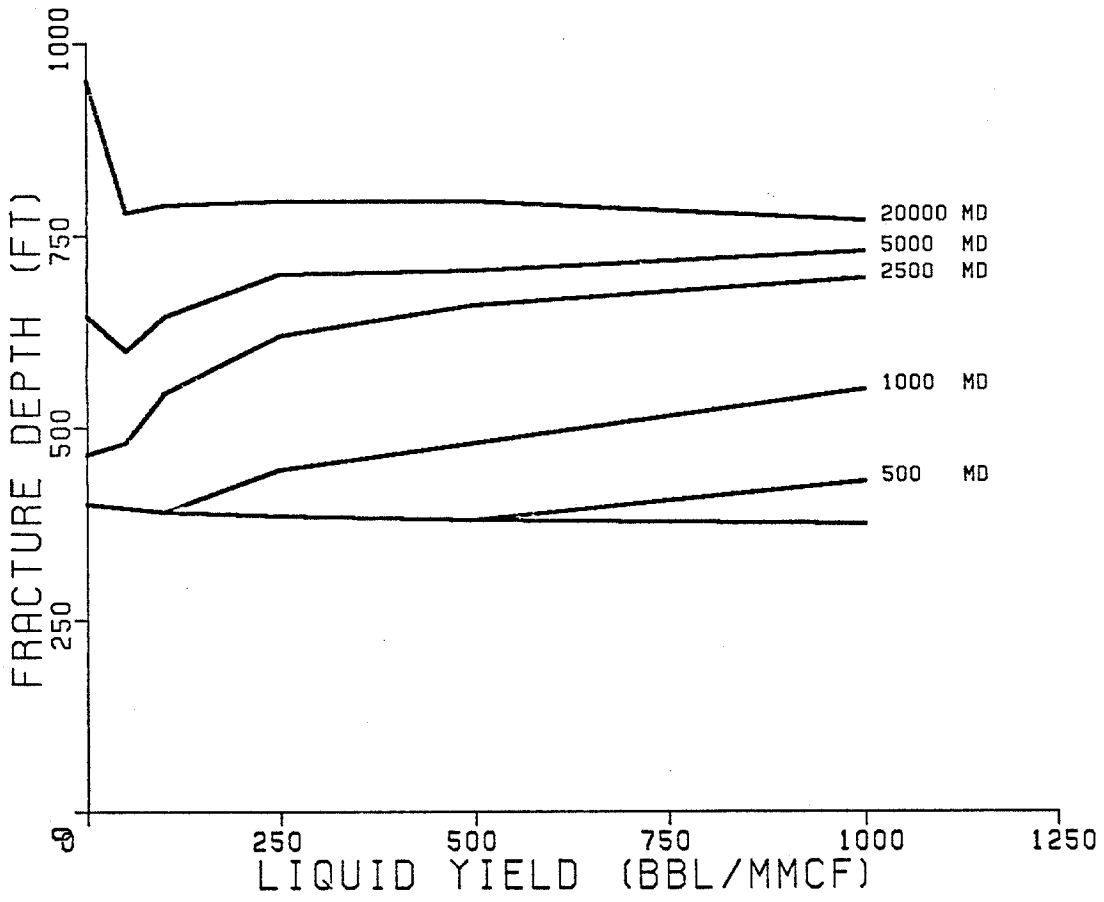

Figure 6.3.a. Depth of Fracture as a Function of Liquid Yield and Permeability

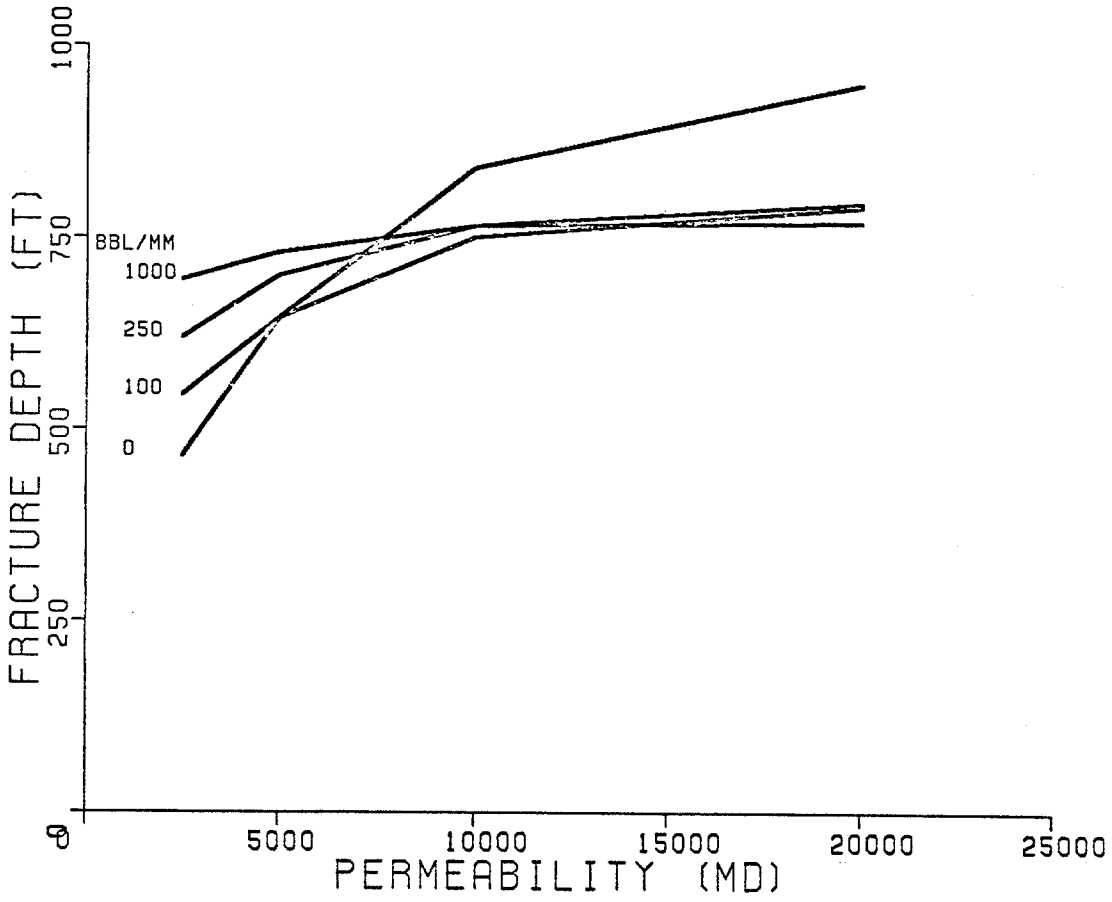

Figure 6.3.b. Depth of Fracture as a Function of Permeability and Liquid Yield

It is the opinion of the author that three darcy permeability would be a reasonable minimum value in a shallow offshore gas sand. The figure also shows that, at lower permeabilities, higher values of liquid yield cause the deepest occurence of fractures, whereas at higher permeabilities the dry gas assumption results in the deepest fracture depth.

6.4.4. Gas/Water Versus Dry Gas Flow

Based on the evaluation of flowing surface pressures and fracture depths, the dry gas flow assumption is suitable for use in the systems analysis. Dry gas flow presents the worst case for formation fracture, and is within 5 percent of the worst case for flowing surface pressures. As mentioned earlier, dry gas flow is also much more convenient for use in terms of computer time, as dry gas calculations can reduce computer time by an order of magnitude.

6.4.5. Applicability of Systems Analysis

The apparent cause of the failure of the diverter system, formation failure, is predicted by the systems analysis. The following facts and results of the systems analysis support this conclusion:

1) There was no indication of failure in the surface diverter equipment.

2) Surface pressures predicted by the systems analysis under all assumptions were below the operating pressures of the annular preventer. Therefore, this analysis predicts the

successful performance of the diverter systems' surface equipment.

3) The rig collapsed and sank, indicating formation failure.

4) Formation failure is predicted by the systems analysis at a minimum permeability assumption of 3 darcy. An assumption of two-phase flow is not required to indicate failure, even though some liquid is expected in the flow.

The systems analysis has therefore correctly predicted the results of the diverter operations. It can also be used to imply design improvements that may have prevented the disaster.

6.5 Design Considerations to Improve Performance

The most important factors controlling diverter system performance are:

1) surface operating pressure

2) conductor depth

3) diverter vent line diameter

The surface equipment was apparently sufficient to divert the well. The working pressures of annular preventers are generally sufficiently high (2000 psi) too shift the design burden to the wellbore. In this case, the surface equipment needs no further investigation.

Conductor pipe was to be set to 1100 ft., presumably to protect the well from the gas zone which caused the blowout, as this zone had been identified by seismic methods. The conductor was to be set to a depth conducive to deeper drilling, not to diverter operations.

The diverter vent line diameter is the one parameter that could have been designed into this particular system. It should thus be investigated as to whether a larger vent line could have resulted in successful operations.

Systems analysis was performed assuming 8 in. and 10 in. vent line diameters. The results of the systems analysis are shown in figure 6.4 as a plot of equivalent density versus fracture gradient. This figure shows that, for the assumptions of dry gas flow and 20 darcy permeability, the 8 in. vent line would cause formations to fracture at or below the drive pipe shoe. However, it appears in this case that a 10 in. diameter line would result in a fracture depth above the drive pipe shoe, indicating a successful design. Although the pressure in the well approaches the formation fracture pressure, fracture pressure is not exceeded. Also, a slightly lower assumed permeability would result in a slightly higher safety margin. It is assumed in this analysis, as in the others, that both 10 in. lines would be opened. The use of 10 in. vent lines, as opposed to either 8 in. or 6 in. lines, would probably have resulted in successful operations, or at least a higher probability of successful operation.

6.5.1. Conductor Depth Requirements

The diverter example presented resulted in failure because drive pipe was set to an insufficient depth to protect against the pressure load placed on the well by the diverter system. The diverter vent line diameter and the depth of the conductor (or drive) pipe interact to determine a safe interval over which the well may be drilled and safely diverted. Figure 6.5 shows an example of the relationship between conductor setting depth,

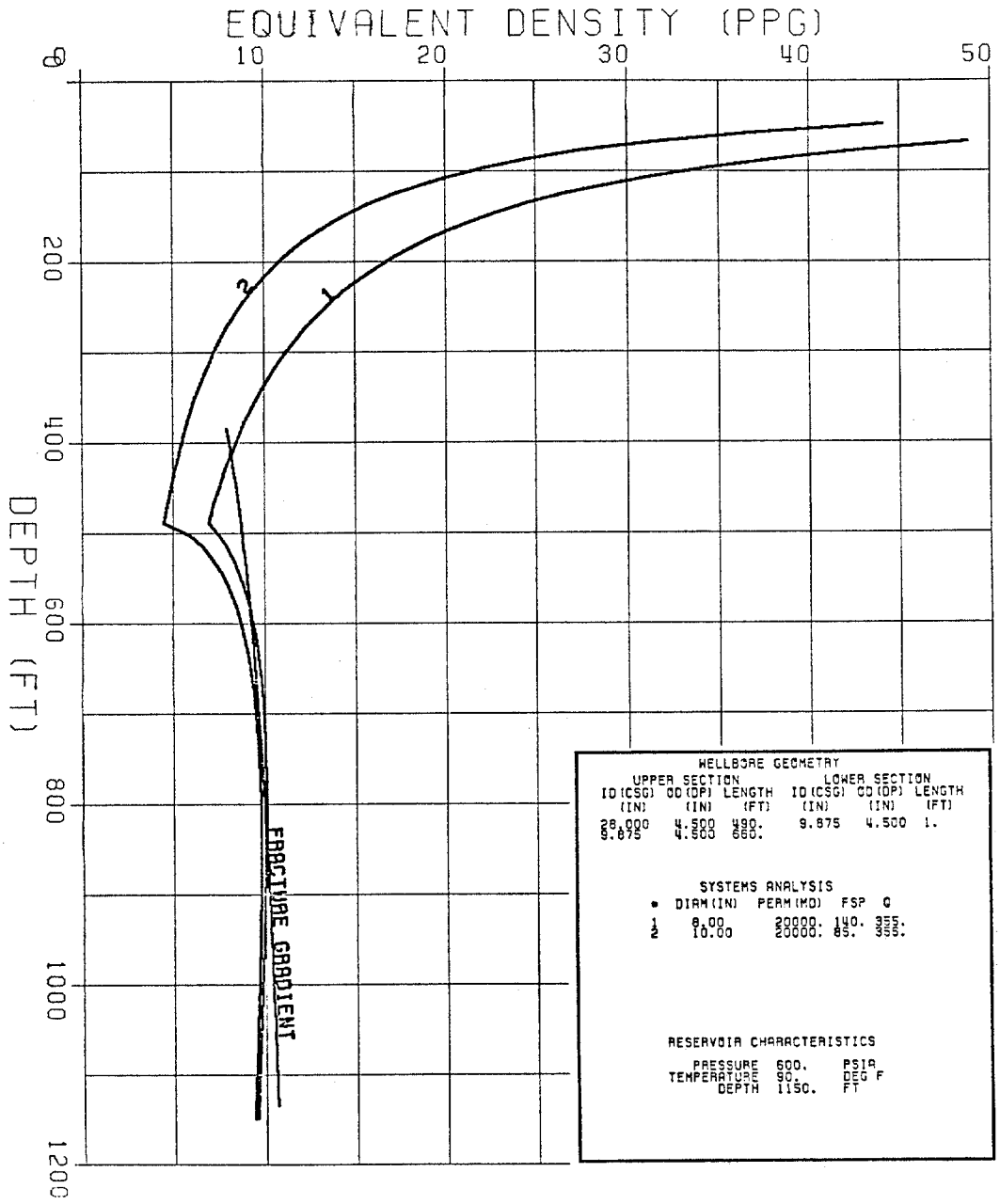

Figure 6.4 Performance of 8 in. and 10 in. Diameter Vent Lines

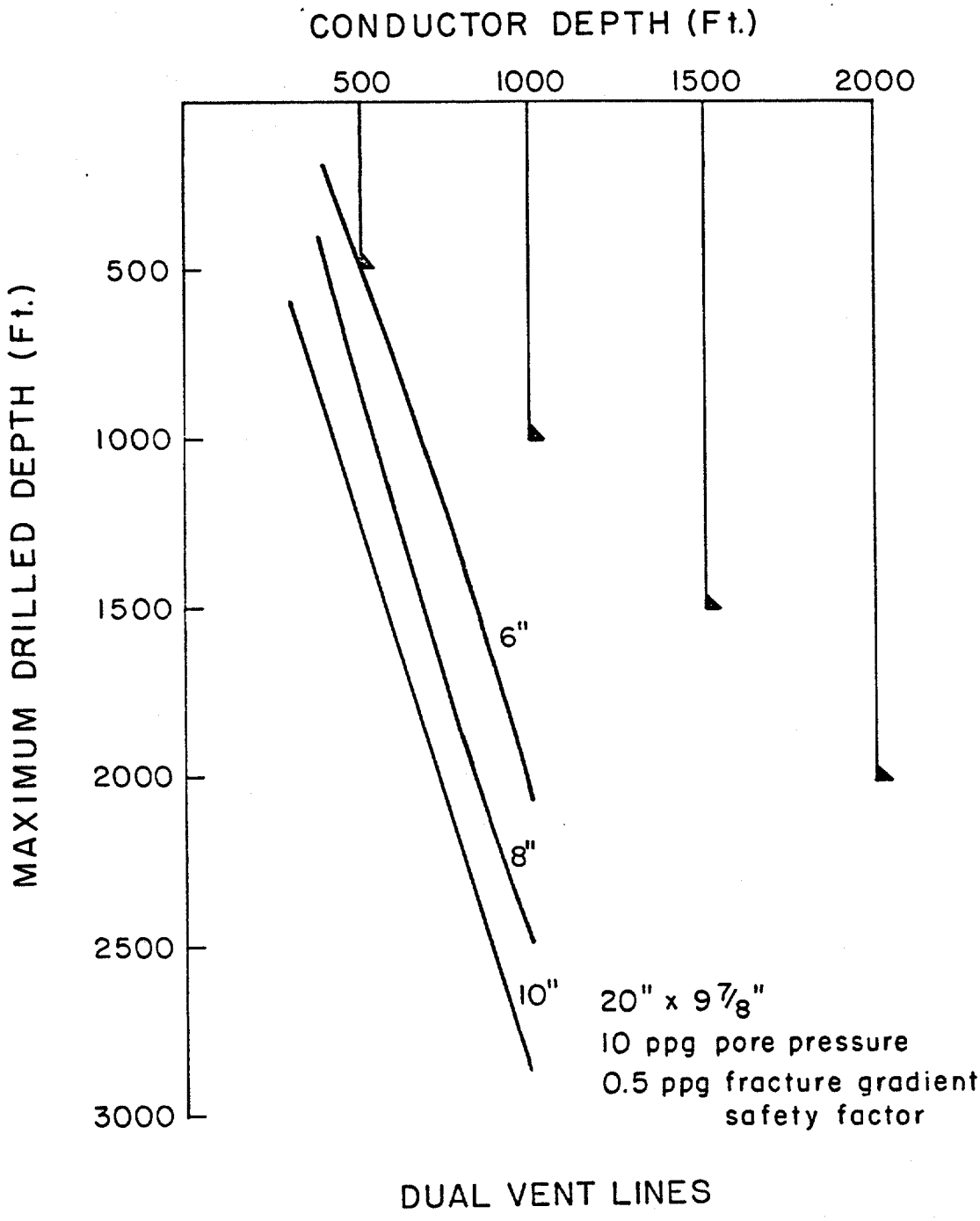

Figure 6.5 Maximum Safe Drilling Depth as a Function of Conductor Depth and Diverter Diameter

maximum safe drilling depth, and diverter diameter. To generate this figure, systems analyses were performed for a specific conductor depth at various drilling depths. The drilling depth at which the fracture pressure of the formation equaled the pressure in the wellbore at the casing depth was then determined as the maximum depth that can be safely drilled by the assumed conductor depth. Various diverter vent line diameters and casing depths were evaluated to generate figure 6.5.

Figure 6.5, or a similar graph, when calculated for a specific well geometry and maximum expected reservoir conditions, provides a means of determining shallow hole casing depth and diverter vent line diameter requirements. The determination of casing depth and vent line diameter from a graph such as this would then result in identifying a safe zone over which to operate the diverter system without risk of fracturing the formations at the casing shoe. If sufficiently high operating pressures are designed into the surface equipment, as is usually the case, this type of graph provides a powerful design tool that can be used to help insure successful diverter operations, if the need should arise.

6.6 Other Design Considerations

6.6.1. Single Line Design

The analysis performed in the previous sections assumed the use of two vent lines, as dictated by the actions of the operator of the rig. However, it is suggested that design work be performed on the assumption of a single operative vent line.

This suggestion is based on three considerations. First, diversion upwind is not recommended, due to obvious safety reasons. There is always the likelihood that only one vent line will be oriented downwind, precluding the use of a second line. Secondly, vent lines are sometimes plugged by large fragments of formation. If both lines are operating and one is plugged, the system should maintain its integrity with only the remaining line functioning. Finally, the loss of a vent line due to erosion is always a possibility, necessitating a design based on a single functioning line. The worst case would thus always be a single line in operating condition.

6.6.2. Parameters Affecting Diverter Performance

Many factors unique to individual drilling conditions may affect diverter performance. These include water depth, well geometry, pore pressure gradient, fracture pressure gradient, and the diverter geometry requirements imposed by a specific rig. Of these parameters, the engineer can control both well geometry and diverter geometry to enhance the chances of successful well control operations.

Well Geometry

One common drilling practice is to drill a smaller diameter wellbore, or pilot hole, to a casing point, and then later enlarge the hole. Systems analysis can be used to analyse the performance of a pilot hole in diverter operations.

Figure 6.6 presents a theoretical systems analysis of various diameter wellbores. As seen on the figure, a decrease in wellbore diameter causes the solution point of the analysis to move to lower pressures and flow rates, thus decreasing the load on the well. The practice of drilling a pilot hole thus appears to be beneficial to diverter operations.

Diverter Geometry

The diameter and length of the vent lines are the geometrical parameters of the diverter system that may be varied to improve diverter performance. The performance of a diverter system is greatly dependent upon the diameter of the vent line, and only slightly dependent upon the length of the vent line.

The effects of vent line diameter have been addressed in section 6.5.1 in terms of the pressure load on the wellbore. Figure 6.7 presents the typical sensitivites of flow rate, surface pressure, and exit pressure to vent line diameter. Flow rate will increase with increasing diameter until the combined pressure losses in the reservoir and wellbore begin to restrict the flow rate. Once the flow rate becomes wellbore or reservoir limited, an increase in diverter vent line diameter will have little to no effect on the flow rate of the well.

Flowing surface pressure will decrease with increasing vent diameter, with the most drastic and substantial decreases occurring by increasing diameter from 6-in. to 108inches. There is only a nominal decrease in pressure for diameters greater than 10-inches. Exit pressure responds to vent line diameter in a

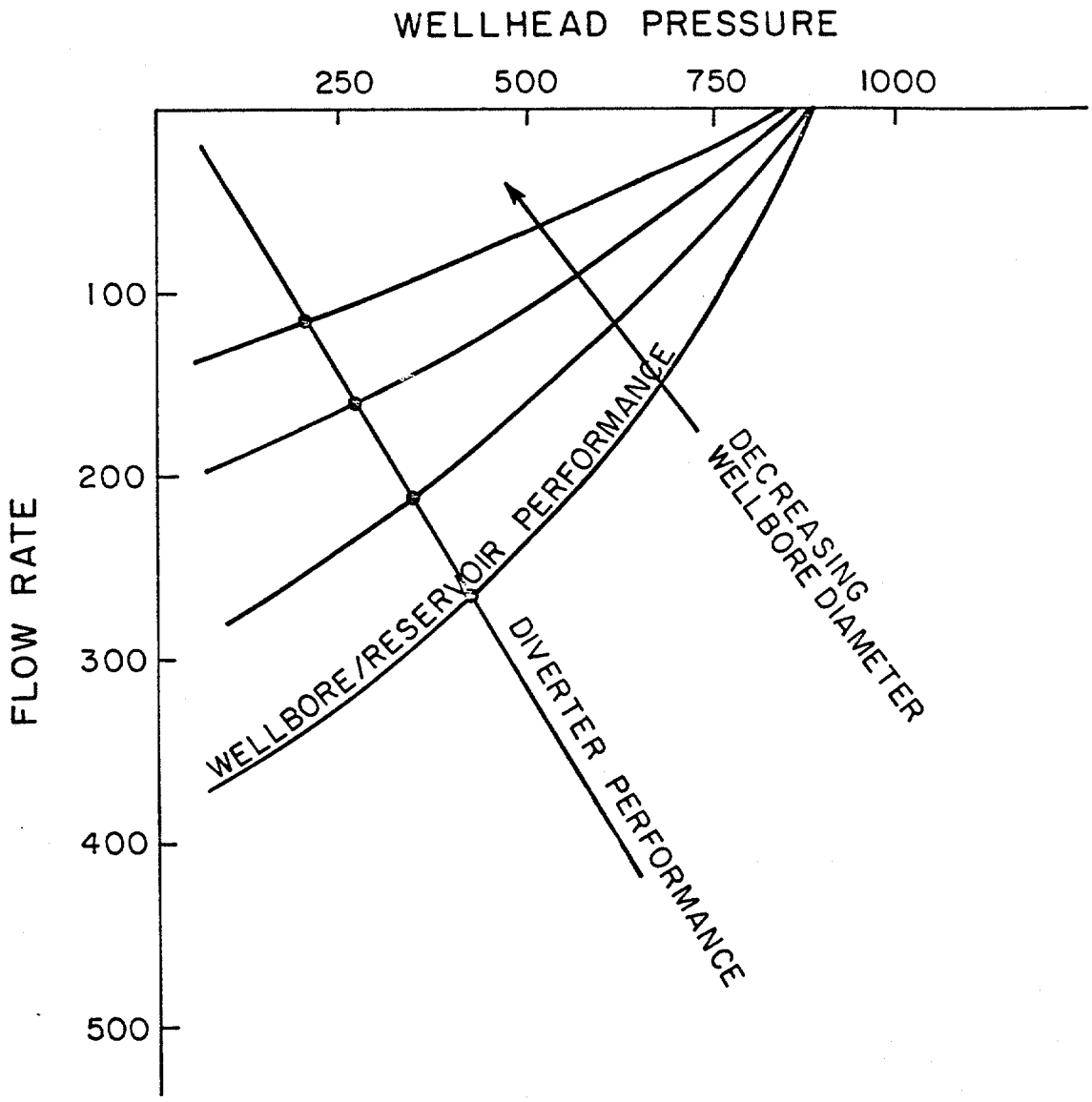

Figure 6.6 The Effect of Wellbore Diameter on Systems Analysis Results

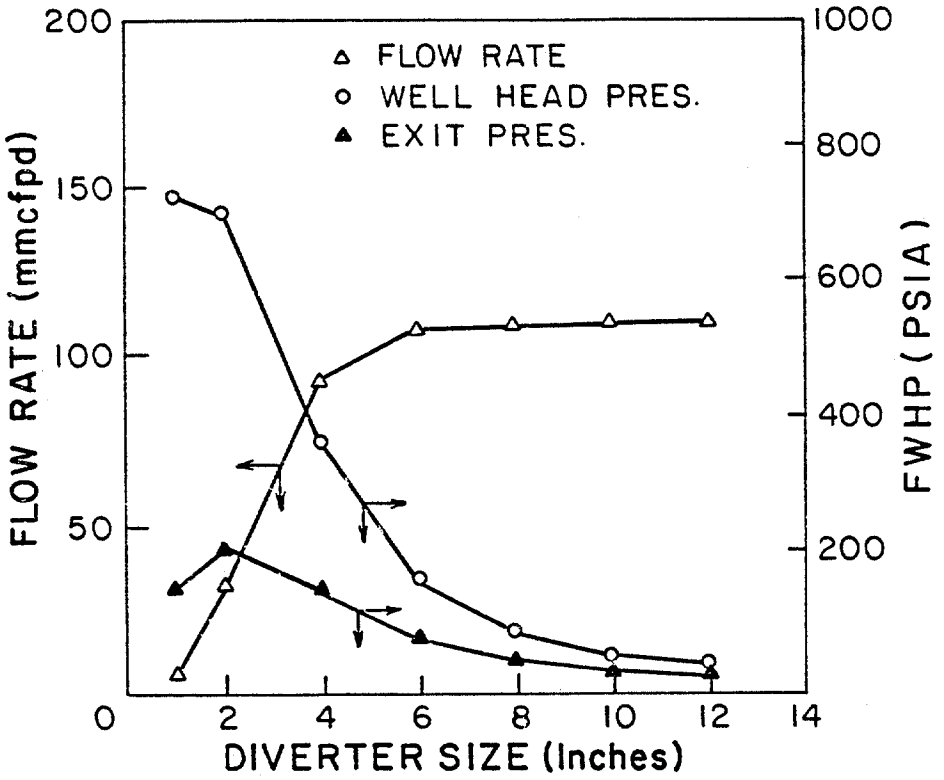

Figure 6.7 The Effect of Diverter Vent Diameter on Flow Rate, Flowing Wellhead Pressure, and Exit Pressure

manner similar to the response of flowing surface pressure to diameter.

In general, Figure 6.7 shows well response to be most affected by increases in vent diameter from 6-in. to 10-inches. Vent line diameters greater than 10-inches have a very small effect on the performance of the system, but may minimize the risk of plugging the vent line during operations.

Figure 6.8 presents the effects of diverter line length on flowing surface pressure. Length changes on the order of 10 feet result in relatively small changes in surface pressure. However, length changes approaching 50 feet or more can present substantial increases in backpressure, and should not be neglected. The effect of length on surface pressure in the larger diameter lines is less pronounced.

Other Design Parameters

Although pore pressure, fracture gradient, and water depth may show systematic effects on diverter performance, these factors must always be considered in unison, and a unqiue relationship between conductor depth, safe drilling depth, and diverter diameter exists for each individual well. Graphs similar to figure 6.5 should customarily be generated for each well or field area.

6.7 Summary

This chapter has shown the applicability of systems analysis in the design and evaluation of the performance of a diverter system.

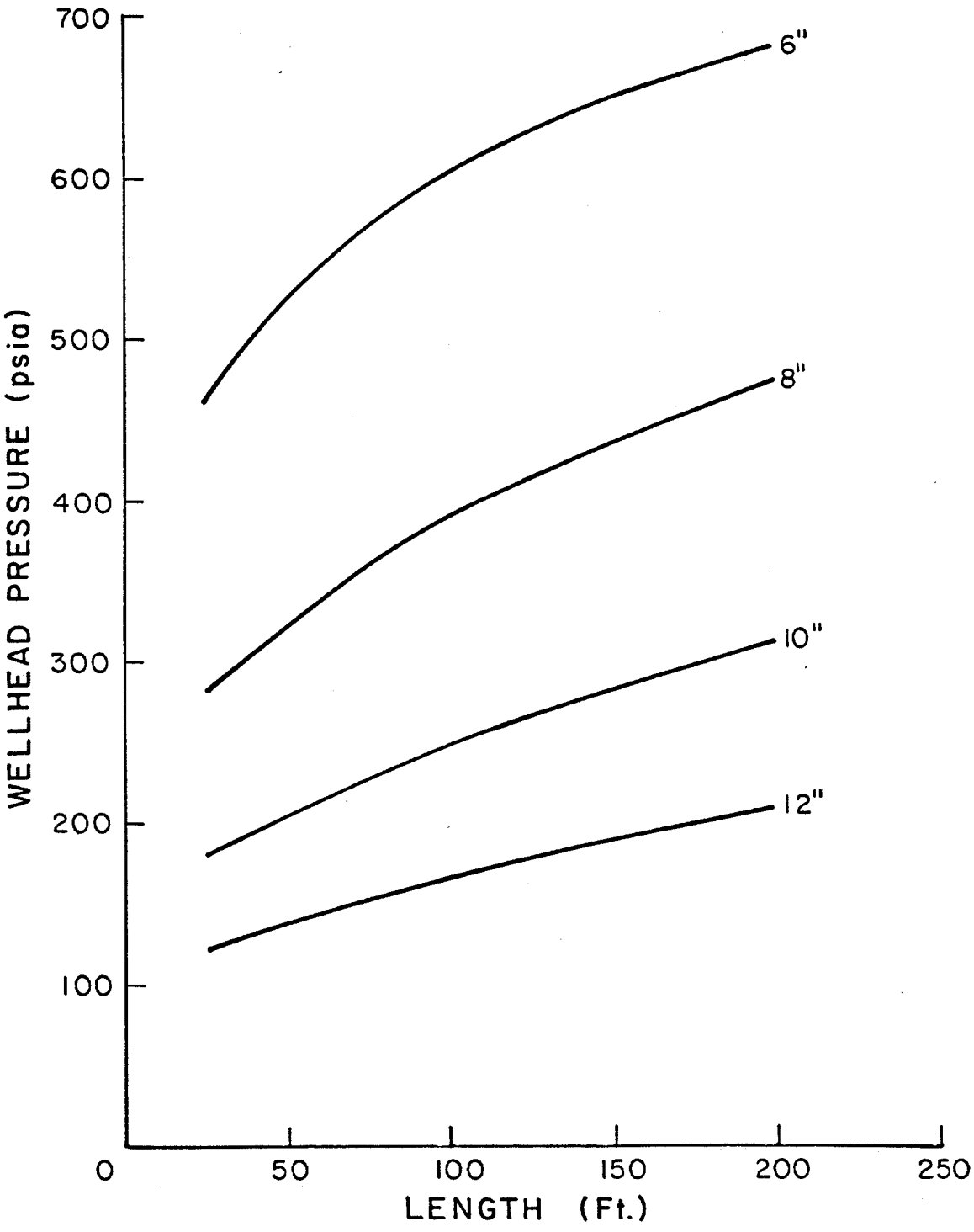

Figure 6.8 The Effect of Diverter Vent Line Length on Flowing Wellhead Pressure for Various Vent Line Diameters

Systems analysis successfully predicted conditions that would, and did, result in failure. In addition, it was shown how to incorporate the systems analysis into a simple set of design curves that allow the engineer to choose a combination of diverter vent line diameter and conductor depth that should maintain wellbore integrity during diverter operations.

CHAPTER VII

CONCLUSIONS AND RECOMMENDATIONS

7.1 Conclusions

1) Critical flow effects are significant in diverter operations and should not be neglected. Experimentally based methods of quantifying critical flow in small diameter pipes have been presented for both gas and gas/water mixtures.

2) Fluid acceleration effects should not be neglected in diverter backpressure calculations, as was proven by experimentation and theoretical modeling.

3) "Systems analysis" has been developed and proven effective as a method of estimating design loads on the diverter system and the wellbore during diverter operations. This method predicts the flow rate and flowing pressures within the well during diverter operations for steady state conditions.

4) Successful diverter operations depend upon sufficient casing being in place during diverter operations. Required setting depths are significantly reduced by increasing the diverter vent line diameter.

5) The effect of increasing vent line diameters is most pronounced by increasing from 4-in. to 10-in. diameter lines; vent line diameters greater than 10-inches generally have very little effect on backpressure and required conductor depth.

6) A method has been presented by which to estimate the proper combination of diverter vent line diameter and conductor setting

depth, therefore identifying a safe interval over which to operate the diverter system.

7.2. Recommendations

1) The experimental work should be extended to larger diameter pipe.
2) Critical flow phenomena associated with two-phase flow warrants further investigation.
3) The methods presented assume steady state flow. Similar work should investigate the transient pressure effects of unloading the wellbore during a blowout to determine the maximum load placed on the well during diverter operations.
4) Diverter operational procedures should be thoroughly investigated, with emphasis on dynamic kill operations. The software generated during this research should prove useful.
5) A study estimating the duration of pressures and flow rates during diverter operations should be performed. System designs based on time dependency may result.

BIBLIOGRAPHY

Baird, Ralph W.: "Explanation of Shallow Blowouts and Lost Time Incidents with Some Recommendations," SPE 6306, presented at the 8th Offshore Tech. Conf., Houston, TX, May 3-6, 1976, pp. 925-930.

Bourgoyne, A.T., Jr., Milheim, K.K., Chenevert, M.E., and Young, F.S.: Applied Drilling Engineering, SPE Textbook Series, Vol. 2 (1986).

Brill, J.P., and Beggs, H.D.: Two-Phase Flow in Pipes, U. Tulsa, (March 1978).

Brown, K.E., and Beggs, H.D.: The Technology of Artificial Lift-Volume I - Methods, Penn Well Books, Tulsa, OK (1977).

Browne, E.J.P.: "Practical Aspects of Predicting Errors in Two-Phase Pressure Loss Calculations," J. Pet. Tech., April 1975, pp. 515-522.

Clark, A.R., and Perkins, T.K.: "Wellbore and Near-Surface Hydraulics of a Blown-Out Oil Well," SPE 9257, presented at 55th Fall Tech. Conf., Society of Petroleum Eng., Dallas, TX, Sept. 21-24, 1980, pp. 1-6.

Constant, W.D. and Bourgoyne, A.T., Jr.: "Fracture Gradient Prediction for Offshore Wells," SPE 15105, presented at the California Regional Meeting, Society of Petroleum Eng., Oakland, CA, April 3-5, 1986, pp. 1-4.

Crouch, E.C., and Pack, K.J.: "'Systems Analysis' Use for the Design and Evaluation of High Rate Gas Wells," SPE 9424, presented at the 55th Annual Fall Tech. Conf., Society of Petroleum Eng., Dallas, TX, Sept. 21-24, 1980, pp. 1-4.

Dukler, A.E., Wicks, Moye III, and Cleveland, R.G.: "Frictional Pressure Drop in Two-Phase Flow: B: An Approach Through Similarity Analysis," AIChE Jour., Jan. 1964, pp. 44-51.

Elfaghi, F., Langlinais, J., Bourgoyne, A.T., Jr., and Holden, W.: "Frictional Pressure Losses for Single-Phase and Two-Phase Flow of Drilling Muds," Trans. ASME, V. 105 (1983), pp. 372.

Fortunati, F., "Two-Phase Flow Through Wellhead Chokes," AIME SPE 3742, presented at the SPE European Meeting, Amsterdam, The Netherlands, May 16-18, 1972, pp.1-8.

Goins, W.C., Jr.: Blowout Prevention, Gulf Publishing, Houston, TX (1969).

Jones, L.G., and Blount, E.M.: "Use of Short Term Multiple Flow Tests to Predict Performance of Wells Having Turbulence," SPE 6133, presented at the 51st Annual Fall Tech. Conf., Society of Petroleum Engineers, New Orleans, LA, Oct. 3-6, 1976, pp. 1-8.

Hagedorn, A.R., and Brown, K.E.: "Experimental Study of Pressure Gradients Occuring During Continuous Two-Phase Flow in Small-Diameter Conduits," J. Pet. Tech., April 1965, pp. 475-483.

Lawson, J.D., and Brill, J.P.: "A Statistical Evaluation of Methods Used to Predict Pressure Losses for Multiphase Flow in Vertical Oilwell Tubing," J. Pet. Tech., August 1974, pp. 903-913.

Lazayres, M.: Blowout Prevention and Well Control, (Editions Technip), Imprimerie Nouvelle, France (1981).

Lukkien, Harry B.: "Subsea Shallow Gas Presents Unique Problems - And Solutions," Oil and Gas Jour., Aug. 2, 1982, pp. 120.

Mach, J., Proano, E.A., and Brown, K.E.: "Application of Production Systems Analysis to Determine Completion Sensitivity on Gas Well Production," Journal of Energy Resources Technology, 104, June 1982, pp. 162-69.

Moody, L.F.: "Friction Factors for Pipe Flow," Trans. ASME, V. 66, 1944, pp. 671.

Odeh, A.S.: "Pseudo-Steady State Flow Equation and Productivity Index for a Well with Non-Circular Drainage Area", J. Pet. Tech., Nov. 1978, pp. 1630.

Rohleder, Stephen: Erosional Aspects of Diverter Design, M.S. Thesis, Louisiana State University (1985).

Ros, N.C.J.: "An Analysis of Critical Simultaneous Gas/Liquid Flow Through a Restriction and its Application to Flow Metering," Appl. Sci. Res. (1960) 9, Section A, pp. 374.

Schuh, F.: "Conductor and Surface Casing Depth Requirements," SPE 8316, presented at the 54th Annual Fall Tech. Conf., Society of Petroleum Eng., Las Vegas, Nevada, Sept. 23-26, 1979, pp. 1-2.

Smith, J.M., and Van Ness, H.C.: Introduction to Chemical Engineering Thermodynamics, Third Ed., McGraw-Hill (1959).

Thomas, L.K., Hankinson, R.W., and Phillips, K.A.: "Determination of Acoustic Velocities for Natural Gas," J. Pet. Tech., July 1970, pp. 889-895.

Vohra, I.R., Robinson, J.R., and Brill, J.P.: "Evaluation of Three New Methods for Predicting Pressure Losses in Vertical Oil Well Tubing," J. Pet. Tech., August 1974, pp. 829-832.

Wallis, G.B.: One Dimensional Two-Phase Flow, McGraw-Hill Book Co., Inc., New York (1969).

NOMENCLATURE

A = cross sectional pipe area, ft^2

BBL = Barrel of fluid, 5.615 ft^3

C_v = specific heat at constant volume, BTU/lb-mole/°R

C_p = specific heat at constant pressure, BTU/lb-mole/°R

c = compressibility, psi^{-1}

D = pipe diameter, in.

d = pipe diameter, ft.

dq = differential heat added to fluid

dv = differential volume

dW = differential work on the fluid

dZ = differential height of fluid

FBHP = Flowing bottom-hole pressure, psia

FNP = Flowing nodal pressure, psia

FWHP = Flowing wellhead pressure, psia

f = Moody friction factor, d'less

GLR = Gas-Liquid Ratio, SCF-STB

g = acceleration due to gravity, ft/sec^2

g_c = units maintenance constant, 32.2 $\frac{lbm\text{-}ft}{lbf\text{-}sec^2}$

H = formation thickness, ft.

K = permeability, md

k = ratio of specific heats, $\frac{Cv}{Cp}$

L = Length, ft.

MMSCFD = Million Standard Cubic Feet per Day

m = two-phase expansion coefficient, d'less

N_r = Reynold's Number, d'less

n = moles of gas

P = pressure, psia

Q = gas flow rate, MMSCFD

q = in situ volumetric flow rate, ft^3/sec

R = Real Gas Constant, 10.73 $\frac{psia\text{-}ft^3}{lb\text{-}mole\text{-}^\circ R}$

r_e = external radius of the reservoir, ft.

r_w = radius of the wellbore, ft.

S = Reservoir Skin Factor, d'less

T = Temperature, °R

V = Velocity, ft/sec

v = volume, ft^3

x = mass fraction of gas in flow, d'less

Y_w = Liquid Yield, BBL/MMSCF

z = gas compressibility factor, d'less

Greek Symbols

ε = pipe roughness, in.

γ = specific gravity

ρ = density, lbm/ft^3

λ = holdup

μ = viscosity, cp

β = Gas turbulence factor, ft^{-1}

Δ = "change in"

Subscripts and Superscripts

g = gas

e = exit

l	=	liquid
w	=	water
t.p.	=	two-phase
STD	=	Standard Conditions
d	=	diverter
r	=	reservoir
wb	=	wellbore
*	=	critical conditions
NODE	=	Nodal Conditions

APPENDIX A

FRICTION FACTOR AND PIPE ROUGHNESS CALCULATIONS

A friction factor can be obtained from recorded pressure loss information for water flow tests or for gas flow tests. In gas flow, pressure losses due to acceleration must be accounted for. The pressure traverses presented in Chapter 2 for dry gas flow were evaluated to determine a friction factor, from which pipe roughness can be calculated.

By the Darcy-Weisbach equation

$$\left(\frac{DP}{DL}\right)_{friction} = \frac{f\ v^2}{2g_c d}$$

a friction factor can be calculated from the measured value of DP/DL.

$$f = \frac{\Delta P\ 2\ g_c\ d}{\Delta L\ \rho\ v^2}$$

For gas flow, the value of DP/DL must be corrected for acceleration pressure losses. The pressure drop due to acceleration is given as

$$\Delta P_{acc} = \frac{\Delta(\rho v^2)}{2g_c}$$

To calculate a friction factor, the recorded value of DP/DL (from the pressure traverse) is corrected for acceleration.

$$(\Delta P)_{corr} = (\Delta P)_{meas} - (\Delta P)_{acc}$$

and $(\Delta P)_{corr}$ used to calculate a friction factor.

Once a friction factor is determined, pipe roughness can be calculated from the Colebrook equation

$$\varepsilon = 10\ [((\ 1.74 - \frac{2.}{\sqrt{f}}\ ) - (\ \frac{18.7\ D}{2\ N_r\ \sqrt{f}}))]$$

The following FORTRAN program calculates pipe roughness from the recorded value of ΔP over a given ΔL.

```
C PROGRAM TO CALCULATE PIPE ROUGHNESS AND FRICTION FACTOR FROM
C EXPERIMENTAL PRESSURE TRAVERSES.
CC
C PROGRAMMED BY F. E. BECK
C
C DEFINITION OF INPUT VARIABLES
C
C PSEP, TSEP ..... STANDARD PRESSURE (PSIA) AND TEMPERATURE (F)
C SGPG ..... GAS SPECIFIC GRAVITY (AIR = 1.0)
C D ..... DIAMETER OF PIPE (IN.)
C TU, TD .....UPSTREAM AND DOWNSTREAM FLOWING TEMPERATUES (F)
C DL ..... PIPE LENGTH BETWEEN DATA POINTS (FT.)
C
C INPUT DATA VIA DATA STATEMENTS
      DATA PSEP,TSEP,SGPG,D,TU,TD/14.7,60.,.70,0.918,100.,100./
      DATA DL/28.31/
   2  CONTINUE
C ENTER PRESSURES FROM TRAVERSE INTERACTIVELY
      WRITE(6,1)
   1  FORMAT(1X,'ENTER 1ST AND 2ND PRESSURES, FLOW RATE(MMSCFD)')
      READ(5,*)PU,PD,Q
C CALCULATE AVERAGE PRESSURE AND TEMPERATURE FOR USE IN CALCULATIONS
      PAVG=(PU+PD)/2.
      TAVG=(TU+TD)/2.
C GENERATE Z-FACTORS AT AVERAGE, UPSTREAM, AND DOWNSTREAM PRESSURES AND
C TEMPERATURES BY CALLING SUBROUTINE ZFACHY.
      CALL ZFACHY(TAVG,PAVG,SGPG,ZAVG)
      CALL ZFACHY(TU,PU,SGPG,ZU)
      CALL ZFACHY(TD,PD,SGPG,ZD)
C GENERATE GAS VISCOSITY (GVIS) AT AVERAGE PRESSURE AND TEMPERATURE
C BY CALLING SUBROUTINE GASVIS.
      CALL GASVIS(TAVG,SGPG,PAVG,GVIS)
C CALCULATE GAS DENSITIES AT UPSTREAM, DOWNSTREAM, AND AVERAGE VALUES
C OF PRESSURE AND TEMPERATURE.
      RHOU=2.70*PU*SGPG/ZU/(TU+460.)
      RHOD=2.70*PD*SGPG/ZD/(TD+460.)
      RHOGAS=2.70*PAVG*SGPG/ZAVG/(TAVG+460.)
C CALCULATE UPSTREAM, DOWNSTREAM, AND AVERAGE FLUID VELOCITIES
      VU=2122.*Q*ZU*PSEP*(TU+460.)/D**2/PU/(TSEP+460.)
      VD=2122.*PSEP*ZD*(TD+460.)*Q/D**2/(TSEP+460.)/PD
      VAVG=(VU+VD)/2.
C CALCULATE REYNOLD'S NUMBER AT AVERAGE TEMPERATURE AND PRESSURE
      REY=1488.*RHOGAS*VAVG*D/GVIS
C CALCULATE THE PRESSURE DROP DUE TO FLUID ACCELERATION.
      ACC=(VD**2*RHOD-VU**2*RHOU)/64.4/144.
C CALCULATE THE PRESSURE DROP DUE TO FRICTION
      DPFRIC=PU-PD-ACC
C CALCULATE THE FRICTION FACTOR FROM THE DARCY-WEISBACH EQUATION
      FF=DPFRIC*D*64.4*144./(DL*RHOGAS*VAVG**2*12.)
C CALCULATE THE PIPE ROUGHNESS FROM THE COLEBROOK EQUATION.
      SIGMA=(10.**((1.74-1./SQRT(FF))/2.)-(18.7/REY/SQRT(FF)))*D/2.
```

```
C WRITE RESULTS
      WRITE(6,*) FF,SIGMA,REY
C INTERACTIVELY CONTINUE OR END PROGRAM
      WRITE(6,3)
    3 FORMAT(1X,'ENTER 1 TO CONTINUE, 2 TO STOP')
      READ(5,*)II
      IF(II.EQ.1) GO TO 2
      STOP
      END
```

APPENDIX B

ESTIMATION OF "K" FROM GAS PROPERTIES

Thomas (1970) presented a method of estimating the ratio of specific heats, K, from gas gravity and temperature. Specific heat at constant pressure at base pressure of 14.7, C_p°, was found by regression analysis to be

$$C_p^\circ = A + BT + CG + DG^2 + E\,(TG) + FT^2$$

where

$A = 4.6435$ $\qquad$ $D = 1.1533$

$B = -0.0079997$ $\qquad$ $E = 0.020603$

$C = 5.8425$ $\qquad$ $F = 9.849 \times 10^{-6}$

Units are BTU/# mole °R.

Specific heat at constant pressure at 14.7 psia is found from the fundamental thermodynamic relationship

$$C_v^\circ = C_p^\circ - R$$

The ratio of specific heats, at 14.7 psia, is thus

$$K^\circ = \frac{C_p^\circ}{C_v}$$

The ratio of specific heats at a pressure of interest is found by:

$$K = \frac{K^\circ}{Z} \ .$$

The equation of gas critical velocity thus becomes

$$V_g^* = 41.4 \sqrt{\frac{K^\circ T}{\gamma_g}}$$

APPENDIX C

DERIVATION OF A CRITICAL FLOW RATE EQUATION FOR TWO-PHASE FLOW

An expression can be derived for a critical gas flow rate that is dependant on a constant value of GLR or, inversely, yield. Critical two-phase velocity is based on the total mixture flow rate

$$q_t^* = V^*A \quad ft^3/sec \tag{1}$$

The total volumetric flow rate is also the sum of the individual volumetric rates.

$$q_t = q_g + q_w \quad ft^3/sec \tag{2}$$

Gas and water flow rates, q_g and q_w, are related by the yield, or inverse GLR, in terms of bbls/MMSCF.

$$q_w = Q_g^* \frac{MMSCF}{day} * Y_w \frac{bbl}{MMSCF} * \frac{1\ day}{86400\ sec} * \frac{5.615\ ft^3}{bbl}\ ft^3/sec \tag{3}$$

In situ gas flow rate is given as

$$q_g = Q_g^* \frac{MMSCF}{day} \times B_g \frac{ft^3}{SCF} \times 1{,}000{,}000 \frac{SCF}{MMSCF} * \frac{1\ day}{86400\ sec}\ ft^3/sec$$

or

$$q_g = 11.574\ Q_g^*\ B_g\ ft^3/sec \tag{4}$$

Combining equations 1, 2, 3, and 4 results in

$$V^*A = 11.574\ Q_g^* B_g + \frac{Q_g\ Y_w}{15387.4} \tag{5}$$

or

$$V^*A = Q_g^* \left[11.574\ B_g + \frac{Y_w}{15387.4}\right] \tag{6}$$

solving for Q_g^* yields:

$$Q_{gas}^* \frac{MMSCF}{day} = \frac{V^*\ A}{11.574\ B_g + \frac{Y_w}{15387.4}} \tag{7}$$

The gas formation volume factor, B_g, is given as:

$$B_g = Z \frac{T}{P} \frac{P_{sc}}{T_{sc}} \frac{ft^3}{SCF} \tag{8}$$

Pipe area, where diameter is in inches is:

$$A = \frac{\pi d^2}{4} = \frac{\pi}{4} \left(\frac{D^2}{144} \frac{ft^2}{in^2} \right) \tag{9}$$

Making these substitutions into eqn. (7) results in

$$Q_g^* = \frac{V^* D^2}{\frac{2122.1 \; Z \; TP_{sc}}{P \; T_{sc}} + \frac{Y_w}{83.9}} \tag{10}$$

which is an equation for critical gas flow rate for a given gas-liquid ratio.

APPENDIX D

DERIVATION OF ACCELERATION PRESSURE LOSS EQUATION

The general energy balance results in a kinetic energy loss term in the form

$$dP = \frac{1}{g_c} (\rho V)\, dV$$

where velocity and density are both functions of pressure, and cannot be separated in order to perform an integration. Attempting to integrate yields:

$$\Delta P = \frac{1}{g_c} \int (\rho V)\, dV$$

This integral can be numerically integrated during the finite element calculations of a pressure traverse, where $\rho_u V_u$ and $\rho_d V_d$ are either known or assumed. By the trapezoidal rule, $\int(\rho v)dv$ becomes

$$\left(\frac{\rho_u V_u + \rho_D V_D}{2} \right)(V_d - V_u)$$

or

$$\tfrac{1}{2}(\rho_d V_d^{\,2} - \rho_u V_u^{\,2} + \rho_u V_u V_d - \rho_d V_d V_u)$$

By neglecting the final two terms, $\int \rho v dv \simeq \rho_d V_d^{\,2} - \rho_u V_u^{\,2}$

and

$$\Delta P_{acc} \simeq \frac{\Delta(\rho V^2)}{2g_c}$$

APPENDIX E

FORTRAN LISTING OF PROGRAM TO MODEL EXPERIMENTAL PRESSURE TRAVERSES

```
CC PROGRAM TO ANALYSE PRESSURE LOSSES FOR HORIZONTAL FLOW
CC
CC PROGRAMMED BY F.E. BECK
CC
CC THIS PROGRAM IS USED TO MODEL EXPERIMENTAL PRESSURE TRAVERSES.
CC THE MAIN FEATURES OF THE PROGRAM ARE:
CC
CC  1) GRAPHICAL OUTPUT COMPARING MEASURED TRAVERSE TO CALCULATED
CC     TRAVERSE.
CC
CC  2) SINGLE OR TWO-PHASE CAPABILITIES
CC
CC  3) TWO MAIN SUBROUTINES FORM THE BULK OF THE PROGRAMMING; BOTH
CC     PERFORM A HORIZONTAL PRESSURE TRAVERSE.
CC       SUBROUTINE "HDRYGA" IS FOR GAS FLOW, "FWHPH" FOR TWO-PHASE FLOW
CC       EACH TRAVERSE SUBROUTINE RUNS UPSTREAM, AND MUST BE PROVIDED
CC       AN EXIT PRESSURE AND FLOW RATE.
CC
CC
CC
CC
CC
CC
CC
CC
CC
CC
CC
CC  THE DATA REQUIRED TO EXECUTE THE PROGRAM ARE AS FOLLOWS:
CC
CC    TSEP.............. STANDARD TEMPERATURE (DEG F)
CC    PSEP.............. STANDARD PRESSURE (PSIA)
CC    SGPG.............. GAS SPECIFIC GRAVITY (AIR = 1.0)
CC    SGW............... WATER SPECIFIC GRAVITY (FRESH WATER = 1.)
CC    ANG............... INCLINATION ANGLE OF PIPE (0. FOR HORIZONTAL)
CC    INC............... # OF INCREMENTS IN FINITE ELEMENT ANALYSIS
CC                       (USE 1 FT. INCREMENTS MINIMUM)
CC    E................. PIPE ROUGHNESS (IN.)
CC    XLEN.............. LENGTH OF PIPE (FT)
CC    DO................ OUTER DIAMETER OF PIPE (IN.)
CC    DI................ INNER DIAMETER OF PIPE (IN., 0. FOR PIPE FLOW)
CC    YWAT.............. WATER YIELD (BBL/MMSCF)
CC    QGAS.............. GAS FLOW RATE (MMSCFD)
CC    PE................ EXIT PRESSURE (PSIA) - USUALLY MEASURED
CC    JJJ............... FLOW TYPE INDICATOR - 0 FOR TWO-PHASE
CC                                             1 FOR DRY GAS
CC    NUMT.............. NUMBER OF TEMPERATURE READINGS
CC    XLENA............. LENGTH OF X-AXIS (IN.) PLOTTING PURPOSES
CC    XMIN.............. MINIMUM VALUE OF X-AXIS
CC    XINC.............. SCALE OF X-AXIS
CC    YLENA............. LENGTH OF Y-AXIS (IN.) PLOTTING PURPOSES
CC    YMIN.............. MINIMUM VALUE OF Y-AXIS
```

```
CC    YINC.............. SCALE OF Y-AXIS
CC                       SEE SNCC PLOTTING MANUAL FOR DEFINITIONS
CC                       OF XINC AND YINC
CC    NUMDAT............ # OF EXPERIMENTAL DATA POINTS
CC    XPTAP............. DISTANCE OF PRESSURE READING FROM EXIT (FT)
CC    PTAP.............. PRESSURE READING (PSIA)
CC                       XPTAP AND PTAP OCCUR NUMDAT TIMES
CC    T................. TEMPERATURE READING (DEG F)
CC    TLOC.............. DISTANCE OF TEMPERATURE READIND FROM EXIT (FT)
CC                       T AND TLOC OCCUR NUMT TIMES
CC
CC   A DATA SET CAN BE CREATED WITH VALUES FOR THE ABOVE VARIABLES,
CC   IN ORDER OF APPEARANCE.
CC
CC
CC
CC  BEGIN MAIN PROGRAM
CC
CC MAKE ENTIRE PROGRAM DOUBLE PRECISION
      IMPLICIT REAL*8 (A-H,O-Z)
CC PLOTTING VARIABLES  ARE SET TO SINGLE PRECISION
      REAL*4 QQGAS,YYWAT,T1,T2,XXLEN,DDO,EE,XXPT,YYPT,XPTAP,PTAP
CC DIMENSIONING ARRAYED VARIABLES
      DIMENSION XPTAP(10),PTAP(10),XPT(3000),YPT(3000),T(5),TLOC(5),
     *XXPT(3000),YYPT(3000)
CC READ IN BASIC DATA
      READ(5,*) TSEP,PSEP,SGPG,SGW,ANG,INC,E
      READ(5,*) XLEN,DO,DI,YWAT,QGAS,PE,JJJ,NUMT
      READ(5,*) XLENA,XMIN,XINC
      READ(5,*) YLENA,YMIN,YINC
      READ(5,*) NUMDAT
CC READ IN EXPERIMENTAL PRESSURE DATA
      DO 10 I=1,NUMDAT
   10 READ(5,*) XPTAP(I),PTAP(I)
CC READ IN EXPERIMENTAL TEMPERATURE DATA
      DO 9 I=1,NUMT
    9 READ(5,*)T(I),TLOC(I)
C  SET PLOTTING VARIABLES AS 0. FT AND PE PSIA
      XPT(1)=0.
      YPT(1)=PE
CC BEGIN PLOTTING
      CALL IDENT
CC SET FACTOR AND PAPER LENGTH
      CALL FACTOR(.5)
      CALL SETMAX(15.)
CC SET ORIGIN
      CALL PLOT(1.85,1.6,-3)
CC DRAW HORIZONTAL AXIS
      CALL BAXIS(0.,0.,'LENGTH-FT',-9,XLENA,0.,XMIN,XINC,0)
CC DRAW VERTICAL AXIS
      CALL BAXIS(0.,0.,'PRESSURE-PSIA',12,YLENA,90.,YMIN,YINC,0)
CC DRAW GRID
```

```
      CALL GRID(0.,0.,2,XLENA,2.,2,YLENA,2.)
      CALL VTHICK(10)
CC SET ASIDE AREA TO PRESENT DATA
      CALL RECT(0.,5.5,1.,10.,0.,3)
CC CHECK FOR DRY GAS FLOW
      IF(JJJ.EQ.1) GOTO 5
CC IF FLOW IS NOT DRY, PERFORM TWO-PASE TRAVERSE WITH SUB FWHPH
      CALL FWHPH(TSEP,PSEP,SGPG,ST,TE,SGW,XLEN,ANG,INC,DO,DI,YWAT,PE,
     *QGAS,FWHP,DEP,PU,XPT,YPT,IC)
      CALL VTHICK(2)
CC IDENTIFY AS TWO-PHASE FLOW, PRESENT INPUT DATA ON PLOT
      CALL SYMBOL(.5,6.275,.1,'TWO-PHASE',0.,9)
      YYWAT=YWAT
      CALL NUMBER(1.5,6.275,.1,YYWAT,0.,-1)
      CALL SYMBOL(1.9,6.275,.1,'BBL/MMSCF',0.,9)
CC IF FLOW IS NOT DRY, LOOP AROUND DRY GAS SUBROUTINE
      GO TO 6
CC IF FLOW IS DRY, DETERMINE EQUIVALENT DIAMETER
CC AND CALL DRYGAS SUBROTINE
   5  D=DO-DI
      CALL HDRYGA(PSEP,TSEP,SGPG,XLEN,D,INC,QGAS,PE,FWHP,XPT,
     *YPT,IC,E,T,TLOC,NUMT)
CC IDENTIFY AS DRY GAS FLOW, PRESENT INPUT DATA ON PLOT.
      CALL VTHICK(3)
      CALL SYMBOL(.5,6.275,.1,'DRY GAS',0.,7)
   6  CONTINUE
C     WRITE(6,*) QGAS,FWHP
      QQGAS=QGAS
      CALL NUMBER(.5,6.025,.1,QQGAS,0.,2)
      CALL SYMBOL(1.1,6.025,.1,'MMSCFD',0.,6)
      CALL SYMBOL(3.,6.275,.1,'WELLHEAD TEMP',0.,13)
      T1=T(1)
      CALL NUMBER(4.4,6.275,.1,T1,0.,-1)
C     WRITE(6,*) T1
      CALL SYMBOL(4.8,6.275,.1,'DEG F',0.,5)
      CALL SYMBOL(3.,6.025,.1,'EXIT TEMP',0.,9)
      T2=T(NUMT)
      CALL NUMBER(4.,6.025,.1,T2,0.,-1)
C     WRITE(6,*) T2
      CALL SYMBOL(4.4,6.025,.1,'DEG F',0.,5)
      CALL SYMBOL(6.0,6.275,.1,'DIVERTER LENGTH',0.,15)
      XXLEN=XLEN
      CALL NUMBER(7.6,6.275,.1,XXLEN,0.,1)
      CALL SYMBOL(8.3,6.275,.1,'FT',0.,2)
      DDO=DO
      CALL NUMBER(6.0,6.025,.1,DDO,0.,3)
      CALL SYMBOL(6.6,6.025,.1,'INCH ID DIVERTER',0.,16)
      CALL SYMBOL(.5,5.775,.1,'PIPE ROUGHNESS',0.,14)
      EE=E
      CALL NUMBER(2.0,5.775,.1,EE,0.,5)
      CALL SYMBOL(2.8,5.775,.1,'IN.',0.,3)
      CALL SYMBOL(3.2,5.825,.1,1,0.,-1)
```

```
      CALL SYMBOL(3.5,5.775,.1,'EXPERIMENTAL DATA',0.,17)
      CALL VECTOR(5.5,5.775,6.0,5.775)
      CALL SYMBOL(6.2,5.775,.1,'PREDICTED PROFILE',0.,17)
C LOAD VALUES TO BE PLOTTED INTO SINGLE PRECISION ARRAY, WRITE RESULTS
      DO 11 I=1,IC
      WRITE(6,*) XPT(I),YPT(I)
      XXPT(I)=XPT(I)
  11  YYPT(I)=YPT(I)
      CALL VTHICK(2)
C PROVIDE SCALING PARAMETERS IN PROPER LOCATION OF ARRAY TO "CALL LINE"
C SEE SNCC PLOTTING MANUAL "CALL LINE"
      XXPT(IC+1)=XMIN
      XXPT(IC+2)=XINC
      YYPT(IC+1)=YMIN
      YYPT(IC+2)=YINC
      XPTAP(NUMDAT+1)=XMIN
      XPTAP(NUMDAT+2)=XINC
      PTAP(NUMDAT+1)=YMIN
      PTAP(NUMDAT+2)=YINC
C USE "CALL LINE" TO PLOT THEORY
      CALL LINE(XXPT,YYPT,IC,1,0,1)
C USE "CALL LINE" TO PLOT EXPERIMENTAL DATA
      CALL LINE(XPTAP,PTAP,NUMDAT,1,-1,1)
C END PLOTTING AND PROGRAM
      CALL EOJOB
      STOP
      END
```

APPENDIX F

A SUMMARY OF FLUID PROPERTIES USED FOR TWO-PHASE CALCULATIONS ASSUMING NO SLIPPAGE BETWEEN PHASES

The following properties can be used in place of their single phase equivalents to perform no-slip pressure traverses.

1) λ_ℓ, no-slip liquid holdup, is defined as:

$$\lambda_\ell = \frac{q_w}{q_w+q_g}$$, where rates are in situ.

2) Density of the two-phase mixture, used to calculate Reynold's number, friction factors, and friction and hydrostatic pressure losses, is defined as

$$\rho_{tp} = \rho_\ell \lambda_\ell + \rho_g (1-\lambda_\ell)$$

3) Mixture velocity, used to calculate Reynold's number, frictional pressure losses, and acceleration pressure losses, is defined as

$$V_m = \frac{q_w+q_g}{A}$$

4) Viscosity of the two-phase mixture is calculated as:

$$\mu_{tp} = \mu_w \lambda_w + \mu_g (1-\lambda_\ell)$$

VITA

Frederick Eugene Beck, born November 12, 1959, is the youngest of three children born to Charles L. Beck, Sr. and Wilda Hundley Beck. A native of Youngsville, Louisiana, he was graduated from Ovey Comeaux Senior High School, Lafayette, Louisiana, in May, 1977, and enrolled at Louisiana State University in Baton Rouge, Louisiana in August, 1977. Upon receiving a Bachelor of Science in Geology in May, 1981, he entered the Graduate School of Louisiana State University, from which he received a Master's Degree in Petroleum Engineering in May, 1984.